A Proposal to Measure the Production and Decay into Two-Body Modes of B-Quark Mesons and Baryons

E605/772 Collaboration

November 9, 1987

Contact: Daniel M. Kaplan
Northern Illinois University
(815) 753-6484, (312) 840-4605

Table I. Branching ratios of D mesons decaying into two, three, and four body channels.

	D°	D^+
$K^-\pi^+$	5.4%	
$\bar{K}^\circ\pi^+$		4.1%
$K^-\pi^+\pi^\circ$	17.3%	
$\bar{K}^\circ\pi^+\pi^-$	8.5%	
$K^-\pi^+\pi^+$		11.4%
$\bar{K}^\circ\pi^+\pi^\circ$		13.4%
$K^-\pi^+\pi^+\pi^-$	10.9%	
$K^-\pi^+\pi^\circ\pi^\circ$	8%	
$\bar{K}^\circ\pi^+\pi^\circ\pi^-$	10.9%	
$K^-\pi^+\pi^+\pi^\circ$		6.4%
$\bar{K}^\circ\pi^+\pi^+\pi^-$		15.2%
$\bar{K}^\circ\pi^+\pi^\circ\pi^\circ$		15.2%

Table II. Effective branching ratios for D-mesons to produce two pions.

Decay Channels* (n,m)	D^+D^-	$D^\circ\bar{D}^\circ$	$D^\circ D^- + \bar{D}^\circ D^+$
(2,2)	0.17%	0.29%	0.44%
(3,3)	13.1%	7.39%	18.7%
(4,4)	36.4%	21.3%	54.2%
(2,3)	1.49%	1.4%	1.95%
(3,2)	1.49%	1.4%	1.06%
(2,4)	2.4%	2.2%	3.2%
(4,2)	2.4%	2.2%	1.7%
(3,4)	21.2%	12.3%	16.4%
(4,3)	21.2%	12.3%	14.7%

*(n,m) denote the number of particles in the decay channels of the first and second D meson.

Table III. Probability in unit of 10^{-10} for pion pair from D-mesons decay to simulate B-meson decay in P789 experiment.

Decay Channels (n,m)	D^+D^-	$D^\circ\bar{D}^\circ$	$D^\circ D^- + \bar{D}^\circ D^+$
(2,2)	0.0443	0.0139	0.0337
(3,3)	0.0036	0.00074	0.0024
(4,4)	<0.0012	<0.00010	<0.00057
(2,3)	0.022	0.0048	0.0154
(3,2)	0.022	0.0048	0.012
(2,4)	<0.0021	<0.00034	<0.00116
(4,2)	<0.0021	<0.00034	<0.00116
(3,4)	<0.0015	<0.00015	<0.00074
(4,3)	<0.0015	<0.00015	<0.00064

Table IV. Efficiency of various cuts for rejecting pion pairs from D^+D^- decay.

Decay Channels (n,m)	Events thrown	$4.9 < M < 5.5$ GeV	Mass cut and Z > 5mm	Mass cut and Z > 5mm and $\gamma_{close} < 0.1mm$	Mass cut and accepted by spectrometer
(2,2)	5×10^7	5.8×10^5	3.5×10^4	1.0×10^4	6
(3,3)	5×10^7	4.5×10^5	1.3×10^4	7.8×10^3	1
(4,4)	1×10^8	8.0×10^5	1.1×10^4	9.3×10^3	0
(2,3)	5×10^7	5.1×10^5	2.2×10^4	1.3×10^4	4
(2,4)	1×10^8	9.7×10^5	2.9×10^4	4.9×10^3	0
(3,4)	1×10^8	8.5×10^5	1.7×10^4	6.1×10^3	0

Table V. Expected Number of Events Accepted by Experiment P789.

	$B \to \pi^+\pi^-$	$\pi^+\pi^-$ from D decays
Interaction/pulse	10^{10}	10^{10}
Pulse/run	10^5	10^5
σ production	9 nb	x nb
$A^{0.29}$	4.5	4.5
$1/\sigma_T$	$2.5 \times 10^{-8} nb^{-1}$	$2.5 \times 10^{-8} nb^{-1}$
Effective B.R.	$0.3 \times 5 \times 10^{-5}$	y
Acceptance	$2\% \times 35\%$	$z \times 10^{-10}$
Total Events	100	$\Sigma\, x \times y \times z \times 0.0113$ $(0.10 > counts > 0.05)$

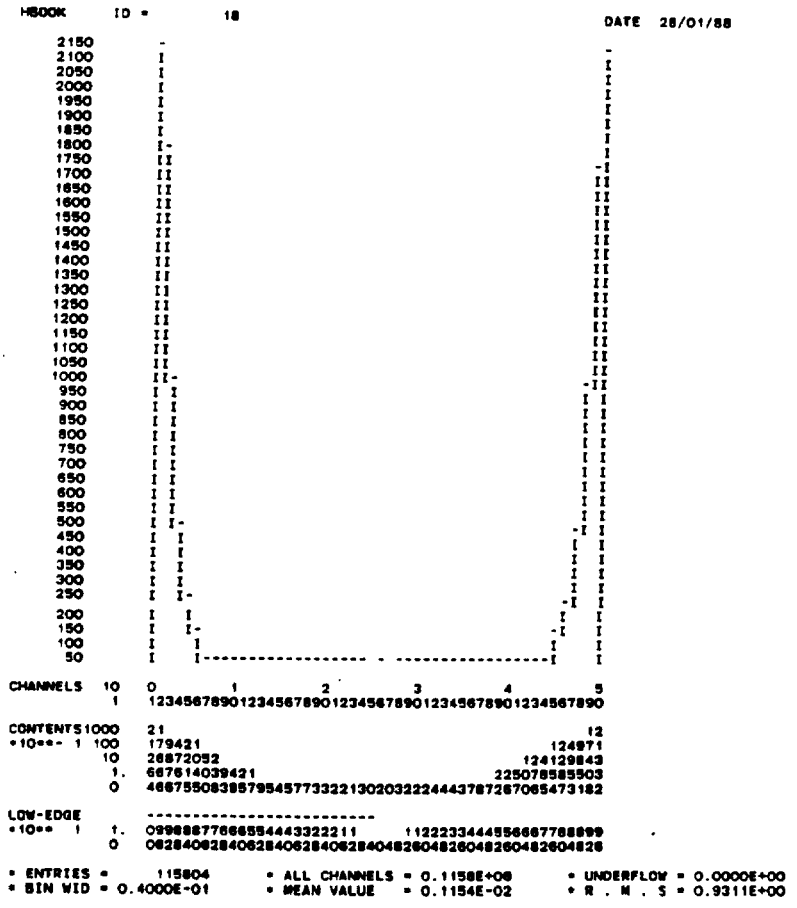

Fig. 1. Histogram for $cos\theta$, where θ is the polar angle of the pion with respect to the di-pion system.

4) Drift Chambers

The sensitivity of the proposed experiment depends critically on the mass resolution one can achieve. Impressive mass resolution (δ(mass)$\simeq$ 30 MeV at mass $\simeq$ 9.5 GeV) was already obtained in the E605 experiment[8] with closed aperture and an extended target. The use of the Si detectors together with an open-aperture configuration will lead to excellent vertex determination and also improve the mass resolution. In addition, we propose replacing the existing station 1 MWPCs with high-rate drift chambers to obtain better position resolution at station 1. This will improve not only the mass resolution but also the ability to associate downstream tracks with tracks in the silicon vertex spectrometer. The proposed dimensions of these new drift chambers are listed in Table II. Monte-carlo simulation of the expected mass resolution (Section IV) yields $\sigma \sim 3$ MeV at m = 5.3 GeV.

5) Hodoscope Scintillators

For the proposed spectrometer setting, the profile of accepted 5.3-GeV-mass events at station 1 is about half the vertical size of the existing station 1 hodoscopes. We propose to rebuild the station 1 hodoscopes with the same number of scintillators but half the current vertical size. This will improve the trigger matrix definition at the lowest trigger level.

6) Target

We will employ a tungsten target with the dimension 3 mm$\times$ 0.5 mm $\times$ 10 mm (length $\times$ height $\times$ width). The short length of the target will facilitate the separation between primary and decay vertices. The small height of the target will help to reject those background tracks whose 3-momenta point back to the target and to provide a further cut on the 3-momenta of the dihadron which will be required to point to the target.

IV. MONTE-CARLO SIMULATIONS OF SPECTROMETER PERFORMANCE

1) Acceptance

The dynamics of b-quark production in hadron interactions was recently investigated by E. Berger.[9] His model is capable of reproducing the existing data from UA1[10] and π+nucleus[11] experiments. Figure 4 shows the x_F and p_t distributions predicted by Berger for b-quark production in p+p collisions. We assume similar distributions for B meson production in our monte-carlo simulation (x_F distribution $\propto e^{-x_F^2/2\sigma^2}$, $\sigma = 0.17$; p_t distribution $\propto e^{-(p_t^2/7GeV^2)}$). Figures 5(a) and 5(b) show the acceptance of the spectrometer as a function of SM12 current and target location, respectively. The choice SM12 = 2000 amps and Z = -80 inches is used throughout this proposal. Data taken during the February 1988 test on singles rates in the spectrometer vs. target location and magnet excitation will be used to optimize further the tradeoff among acceptance, resolution, and singles rates.

Figures 6(a) and 6(b) show the spectrometer acceptance as a function of the x_F and p_t of the B meson. The acceptance as a function of dihadron mass is shown in Figure 6(c). Note that the acceptance for mass $\sim$ 9.5 GeV is quite large. Therefore the search for $\eta_b \rightarrow p\bar{p}$ decay does not require different spectrometer settings. Figures 7(a) and 7(b) show the acceptance folded with Berger's production model for x_F and p_t; the p_z distribution is shown in Figure 8(a). At 800 GeV, the accepted B mesons have rather large momentum ($< P_z > \simeq 165GeV$). This implies that the average distance between the primary production vertex and secondary decay vertex is $\sim$ 1.0 cm, as shown in Figure 8(b).

To determine the dimensions of the Si strip detectors, we show in Figure 9 the distribution vs. θ_x and θ_y in the upper hemisphere for events accepted by the downstream spectrometer. The symmetry of the spectrometer implies nearly identical acceptance for the lower hemisphere.

2) Mass Resolution

To simulate the mass resolution of the spectrometer, multiple-scattering in the various materials and the finite position resolutions of the chambers are taken into account. Figure 10 shows the result of the monte-carlo simulation of mass resolution at the B meson mass. The large p_t kick of the SM12 magnet and the vertex determination by the Si vertex detectors are responsible for the excellent mass resolution of $\delta \mathrm{M}/M \simeq 0.6 \times 10^{-3}$.

3) Vertex Reconstruction

Figure 11(a) shows the Z-vertex resolution for accepted B meson events, and Figure 11(b) shows the corresponding distribution in proper lifetime. Figure 11(c) shows the distribution of the reconstructed impact parameter of the $h^+ - h^-$ events.

V. SIGNALS AND BACKGROUNDS

1) Expected Yields of $B, \Lambda_b \to h^+h^-$

The expected number of events is calculated as

$$N_{det} = N_{beam} \times N_{targ} \times \sigma \times \epsilon \times BR \times Acc \times Eff \tag{8}$$

Assuming 10^5 spills for a fixed-target run with 3×10^{10} protons/spill, the total number of beam particles (N_{beam}) is 3×10^{16}. A 3mm-long W target (3% interaction length) gives $N_{targ} = 3.5 \times 10^{24}$ nucleon/cm^2. The production cross section $\sigma(pp \to b\bar{b}X)$ is estimated by Berger[9] to be $9nb > \sigma > 2nb$. ϵ is the probability that the produced $b, \bar{b}$ quarks will hadronize into a particular B meson or b-baryon. Bjorken has estimated[6] that $\epsilon(b \to B_d) \simeq 30\%$, $\epsilon(b \to B_s) \simeq 15\%$ and $\epsilon(b \to \Lambda_b) \simeq 15\%$. BR is the expected branching ratio for a specific $B, \Lambda_b \to h^+h^-$ decay. As discussed earlier, the spectrometer acceptance Acc is calculated to be $\sim 2\%$ at 5.3-GeV mass. Eff represents the efficiency of the B events to survive the various background-rejection cuts (mainly mass and Z-vertex cuts). We estimate Eff to be $\sim$35%. Table III lists the number of surviving events (N_{det}) after all cuts for various decay channels. In Table III we assume $\sigma(pp \to b\bar{b}X)$ to be 4.5 nb and BR $= 5 \times 10^{-5}$ for all decay modes. With the assumed branching ratios, the total number of reconstructed $B, \Lambda_b \to h^+h^-$ events is expected to be of order one thousand.

2) Backgrounds

There are two major types of background. The first arises from production of a pair of relatively long-lived particles which decay downstream of the target. The second is due to direct hadron pairs produced in the target. The nature of these backgrounds and the estimated efficiency to reject them are discussed below.

(a) Background from decays of pairs of long-lived particles

First we consider the production of D-meson pairs $D\bar{D}$ followed by $D \to K\pi$, $D \to K\pi\pi$, $D \to K\pi\pi\pi$ decays. The lifetimes of D mesons are comparable to those of B mesons but with production cross sections three orders of magnitude larger. The probability for a

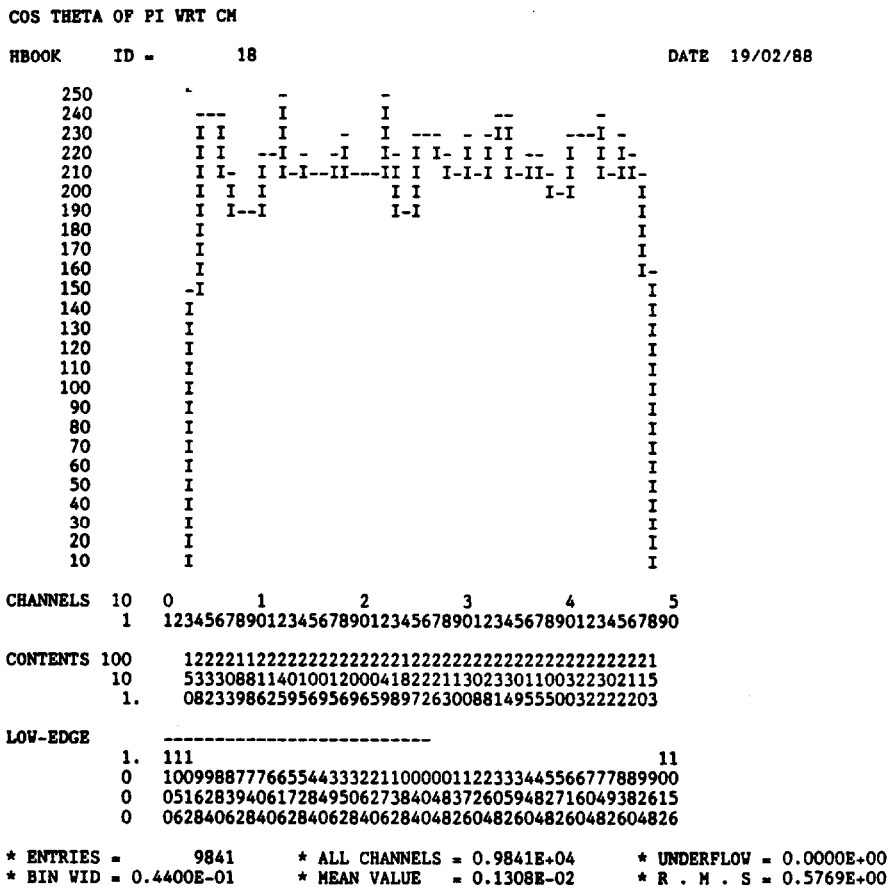

Fig. 2. Histogram for $cos\theta$, where θ is the polar angle of the pion with respect to the di-pion system.

Background:

1. Real QCD pairs at $m = 5$ GeV:

$\left.\frac{d^2\sigma}{dm\,dy}\right|_{y=0}$ $(cm^2\,GeV^{-1})$

	400 GeV *	800 GeV †	Observed pairs /GeV
$\pi^+\pi^-$	2×10^{-31}	4.5×10^{-31}	4.5×10^{9}
K^+K^-	4×10^{-32}	9×10^{-32}	9×10^{8}
$p\bar{p}$	5×10^{-32}	10^{-31}	10^{9}
$K^+\bar{p}$	1.5×10^{-32}	3×10^{-32}	3×10^{8}

* Kephart et al. PRL 39, 1440 (1977)

† scaled following Jöstlein et al. PR D20, 53 (1979)

2. Accidental pairs at $m = 5$ GeV:

Jöstlein et al:

$$\frac{\text{Accidentals}}{\text{Reals}} = \frac{\delta_{int}}{R} = \frac{10}{30}$$

But accidentals dominate if try to raise intensity or acceptance!

Figure 4.

Background Rejection:

Comes from mass resolution, decay vertex resolution

Mass resolution:

$\frac{\Delta m}{m}$ (rms)

	Monte Carlo	Expt
Υ:	0.1%	0.2%
B:	1 MeV	2 MeV?

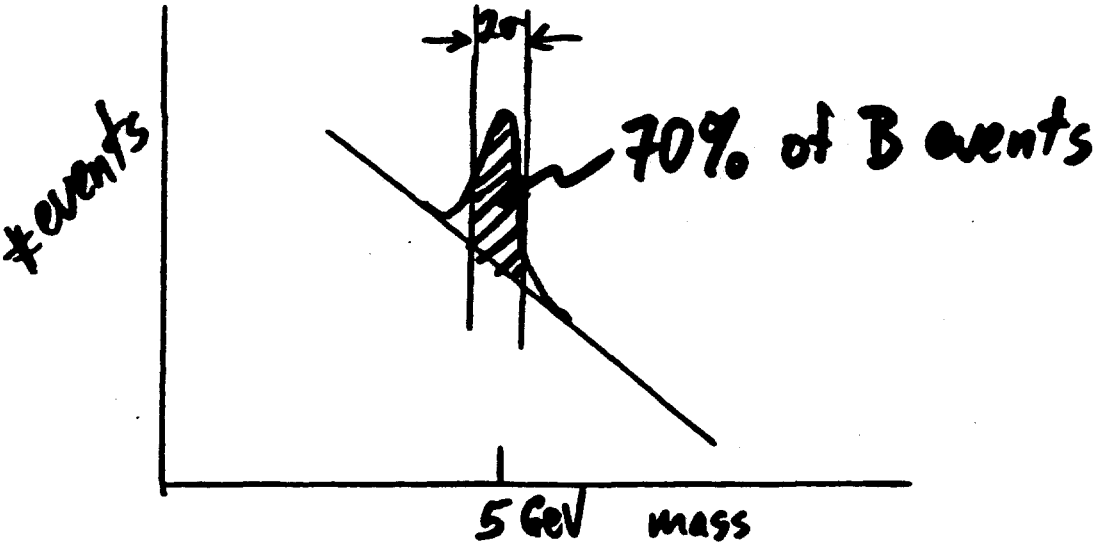

$$\frac{\text{Signal}}{\text{Background}} \simeq \frac{10^{-6}\,\text{GeV}}{2\Delta m} \times 70\%$$

$$\simeq \begin{cases} 2\times10^{-4} & \text{for } \Delta m = 2\ \text{MeV} \\ 4\times10^{-5} & \text{for } \Delta m = 10\ \text{MeV } (0.2\%) \end{cases}$$

Figure 5.

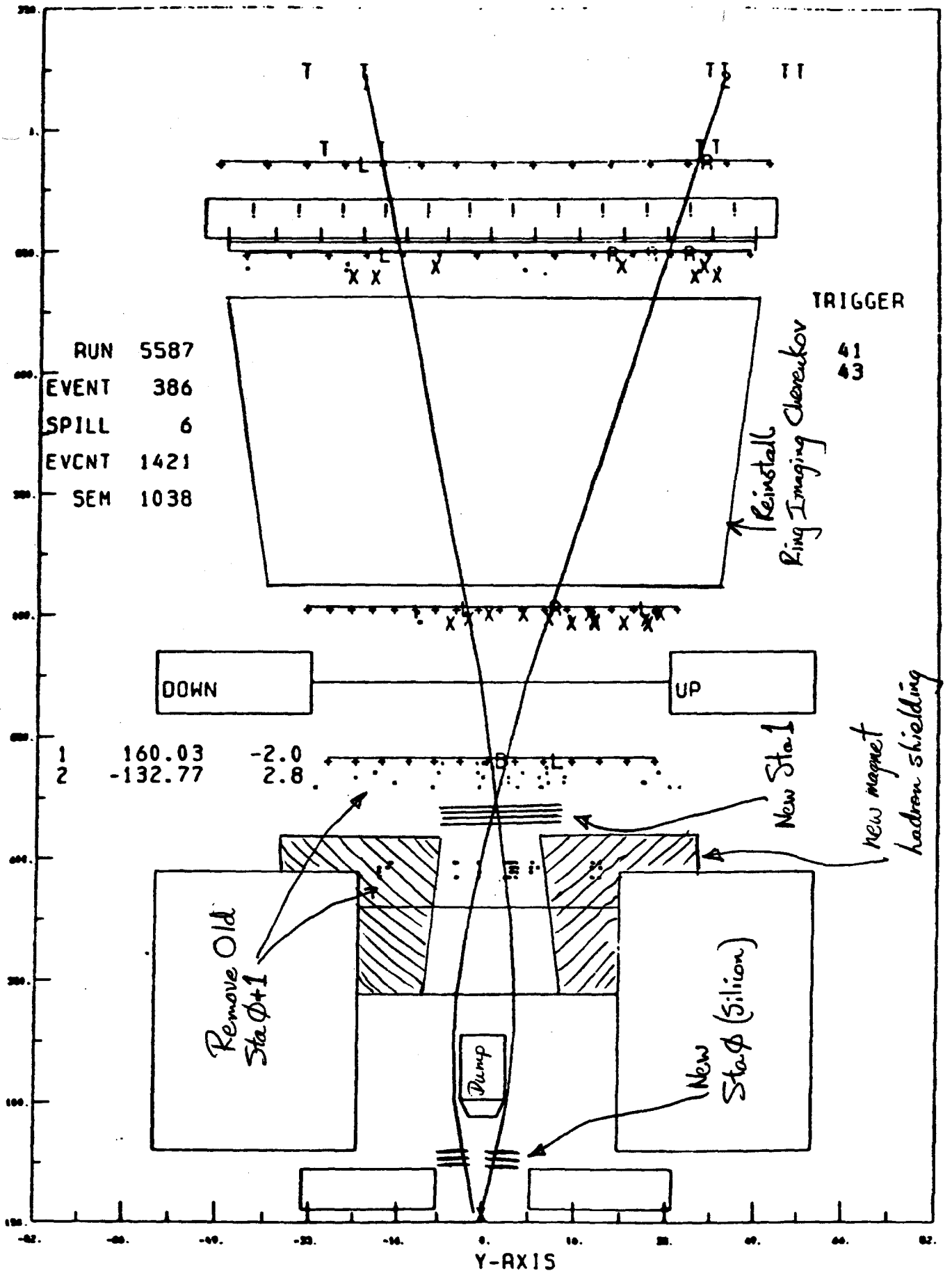
RUN 5587
EVENT 386
SPILL 6
EVCNT 1421
SEM 1038
TRIGGER
41
43
Reinstall Ring Imaging Cherenkov
DOWN
UP
1 160.03 -2.0
2 -132.77 2.8
New Sta1
new magnet hadron shielding
Remove Old Sta#1
New Sta# (Silicon)
Pump
Y-AXIS

Figure 26.

$\bar{B}B$ acceptance Calculation CNB 2/6/87

SMØ	-.85 GeV	Monte Carlo using Quigg's approx. $B\bar{B}$ production distributions
SM12	+4.3 GeV	
SM3	-1.1 GeV	

$B \rightarrow \pi^+\pi^-$

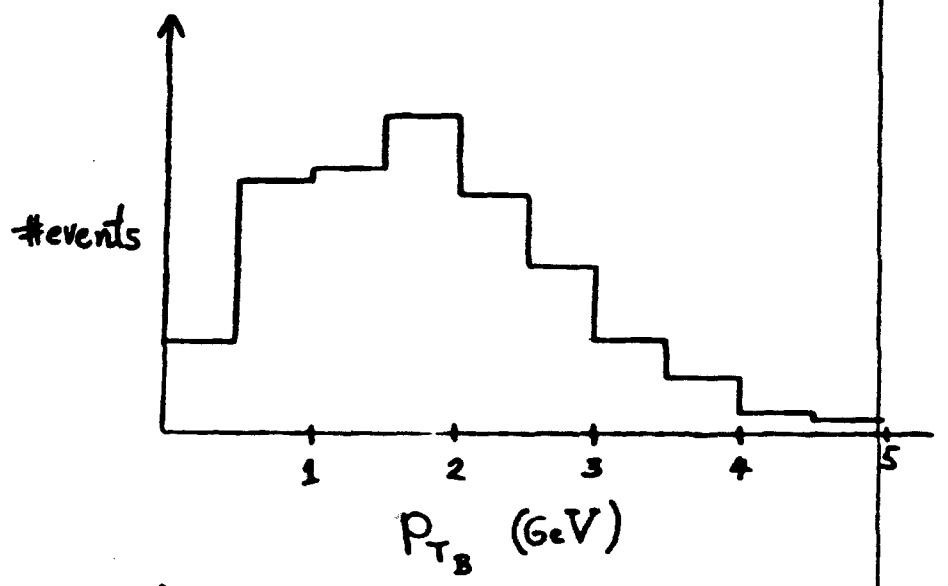

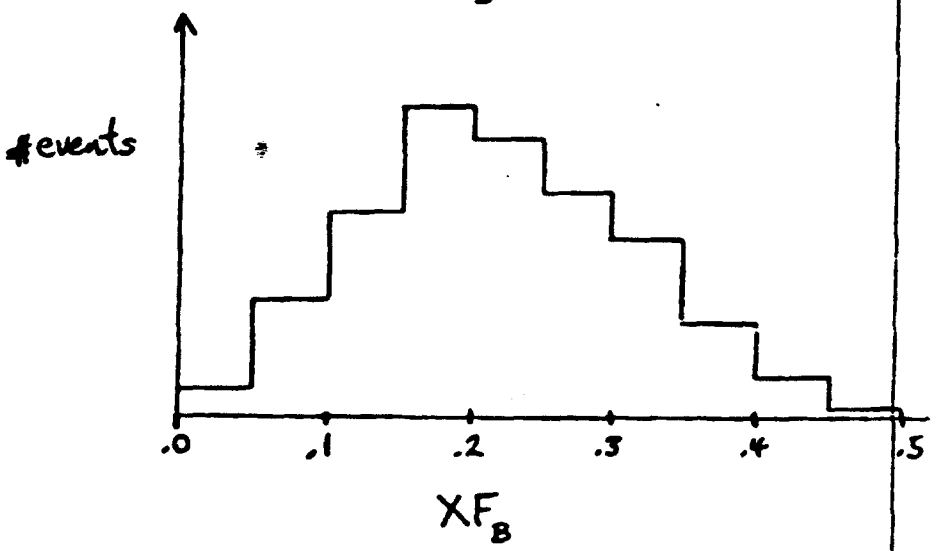

Target to Silicon 60"

δm	1.0 MeV	with Multiple Scat. and Detector Res.
$\delta \tau_{vertex}$	.042 psec.	

Figure 3.

Yield: $b \to h^+h^-$

At 10^{10} interactions/pulse (e.g. 3×10^{11} on 3mm W

$\times 10^5$ pulses / fixed-target run

$\times$ 3 nb $\left.\frac{d\sigma}{dy}\right|_{y=0}$

$\times$ .07 $\text{Acceptance}|_{y=0}$

$\times$ 5.7 $\sqrt[3]{A}$

$\times$ 2.5×10^{-8} nb^{-1} $\frac{1}{\sigma_T}$

$\times$ 2 $(b+\bar{b})$

$= 6\times10^7$ b or $\bar{b}$ into detector

Hadronization:

30%	B_u
30%	B_d
15%	B_s
15%	Λ_b

BR: 10^{-4}

→

2,000	B_d
1,000	B_s
1,000	Λ_b

per 2-body mode

Figure 1

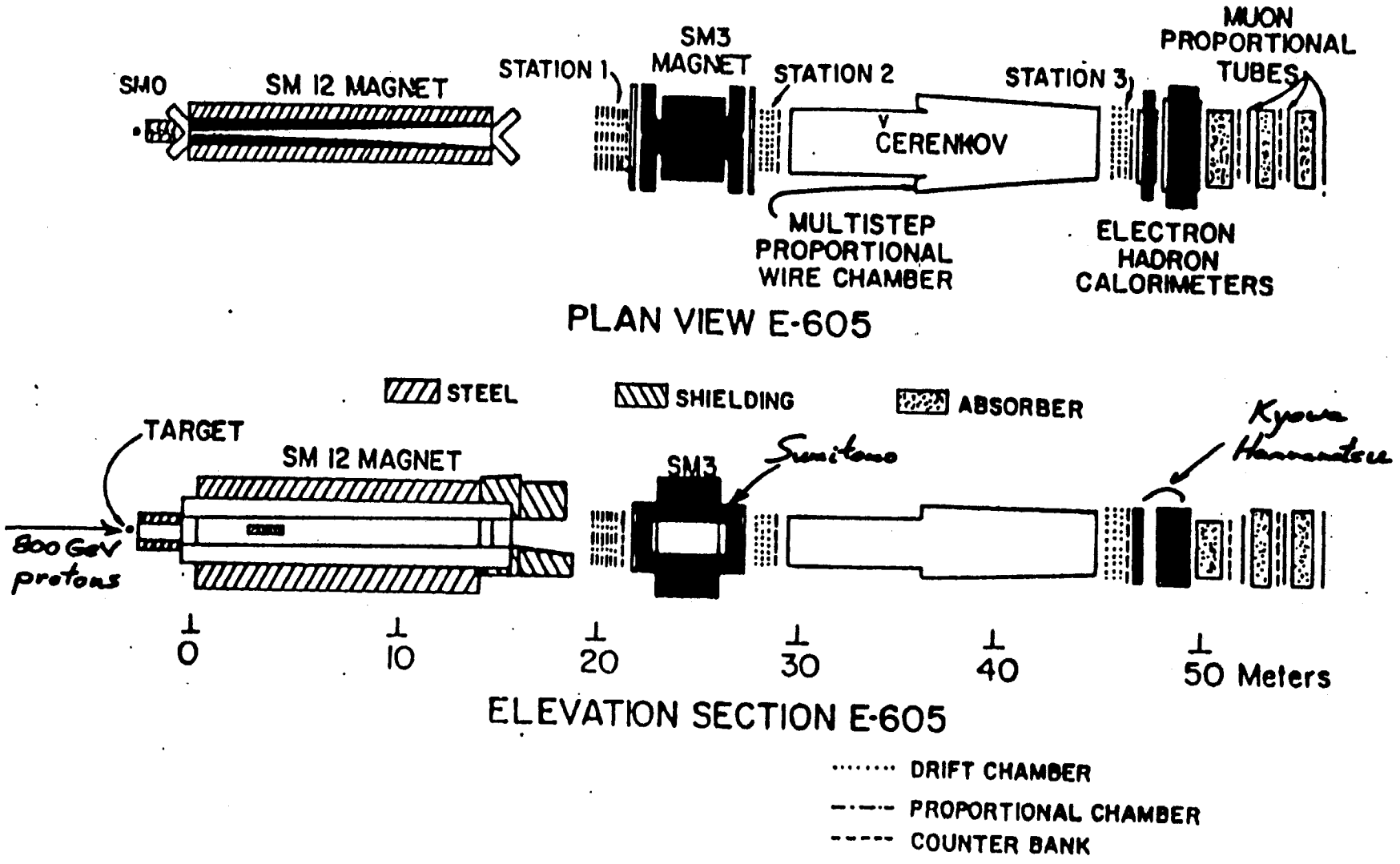
SM0
SM 12 MAGNET
STATION 1
SM3 MAGNET
STATION 2
STATION 3
MUON PROPORTIONAL TUBES
CERENKOV
MULTISTEP PROPORTIONAL WIRE CHAMBER
ELECTRON HADRON CALORIMETERS
PLAN VIEW E-605
STEEL
SHIELDING
ABSORBER
TARGET
SM 12 MAGNET
SM3
Sumitomo
Kyoto Hamamatsu
800 GeV protons
0
10
20
30
40
50 Meters
ELEVATION SECTION E-605
DRIFT CHAMBER
PROPORTIONAL CHAMBER
COUNTER BANK

Figure 2a.

1. Addition of silicon vertex spectrometer: 5 planes in each of the "up" and "down" arms, each plane consisting of 1500 50-micron strips (read out every strip at small vertical angles, decreasing to every few strips at large angles).

2. New shielding wall at downstream end of SM12 analyzing magnet.

3. New station 1 wire chambers: 6 drift-chamber planes having 1cm cells, to cover aperture of 32" vert. x 45" horiz.

4. Re-install photon detectors and associated electronics on Ring-Imaging Cherenkov counter.

5. High-speed vertex processor.

These are changes which we believe are feasible in the time available before the next fixed-target run.

VI. SUMMARY

We propose to reconfigure E605/772 to detect two-body hadronic decay modes of neutral B mesons and baryons. The calculations given above are based on an assumed cross-section of 3 nb/unit rapidity for b-bbar production at rapidity near zero and branching ratios per two-body hadronic decay mode of 10**-4. This experiment will provide important first measurements of these quantities, or upper limits should these assumptions prove optimistic.

REFERENCES

1. J.D. Bjorken, "Rare B-Decays: Experimental Prospects and Problems," International Symposium for the Fourth Family of QUarks and Leptons, UCLA, February 26-28, 1987; also, J.D. Bjorken, notes from High-Rate B-Physics Working Group, Fermilab, August 1987.

2. W. Schmidt-Parsifal (ARGUS Collaboration), "Weak Decays of B Mesons," International Symposium on Electron and Photon Interactions at High Energies, Hamburg, Germany, July 1987.

3. R.K. Ellis and C. Quigg, "A Pinacoteca of Cross Sections for Hadroproduction of Heavy Quarks," Fermilab preprint FN-445, January 1987; E.L. Berger, "Dynamics of Bottom Quark Production in Hadron Collisions," Argonne preprint ANL-HEP-PR-87-90, August 1987. Since b quarks are produced in pairs, we have here multiplied the 5 nb estimated cross-section by 2.

4. E605, private communication.

5. N. Croitoru et al., Nucl. Instr. & Meth. A234, 444 (1985).

6. R.D. Kephart et al., Phys. Rev. Lett. 39, 1440 (1977); H. Jostlein et al., Phys. Rev. D20, 53 (1979).

FIGURES

1. Yield calculation for a branching ratio of 10**-4 into a two-body decay mode.

2. a) Existing E605/772 spectrometer. b) Schematic showing proposed changes.

3. Acceptance of spectrometer in Feynman x and transverse momentum for b-quark production according to the models of Reference 3.

4. Calculation of the hadron-pair continuum background.

5. Calculation of the rejection factor for a gaussian peak on a smooth background of hadron pairs.

half-lifetime cut should thus give a background rejection of 5 sigma, or 3 x 10**-7 !! Realistically, if we achieve a rejection of 10**-3, while retaining 60% of the B-decay events, we will be left with a data sample as follows:

B-species	products	bkgnd	signal	significance
Bd	Pi+ Pi-	9 x 10**3	800	8 sigma
Bd	K+ K-	2 x 10**3	800	18 sigma
Bs	Pi+ K-	3 x 10**3	400	7 sigma
$\overline{\text{Lambda-b}}$	K+ pbar	6 x 10**2	400	16 sigma

This discussion brings out the importance of particle-species identification. Without species identification, each background event will enter nine times, and at nine different masses, as each particle-species assumption is tried out in turn: Pi+ Pi-, Pi+ K-, Pi+ pbar, etc. Thus the background will be nine times larger. The ring-imaging Cherenkov counter, installed in our apparatus in 1982, is capable of performing species identification over the necessary range of particle momentum.

IV. TRIGGER RATE

The remaining problem which needs to be addressed is trigger rate. We have seen above that the rate of real and accidental hadron pairs with mass exceeding 5 GeV is 10**10 per fixed-target run. Even if a trigger can be devised which selects only such events, the

resulting rate of 10**5 per pulse far exceeds the rate capability of our data buffering system (4096 events or 4 megabytes per pulse). To avoid large deadtime, we need to keep the average trigger rate below about 2000 per pulse; this is also desirable from the viewpoint of off-line analysis computing load. Past experience suggests that our existing low-level hadron-pair trigger, which is based on hodoscope roads in combination with calorimeter energy-deposition, can be expected to count at the rate of a few to several x 10**5 per pulse. The tight mass cut available from our trackfinding trigger processor is likely to reduce this rate by an order of magnitude, giving < 10**4 per pulse. To reduce the rate beyond this, it will be necessary to utilize vertex information in the trigger. We propose to construct a fast vertex processor, which in a period of about 5 microseconds can test all relevant hit combinations in the silicon planes, and identify those consistent with a particle originating outside of the target and having transverse momentum exceeding 1 GeV. Since in the time available, easily available memories, PALs, and ALUs can perform only 100 to 200 steps, a high degree of parallelism will be required in the design of this processor in order to reduce the 400 (typical) hit combinations per event to the 50 or so relevant ones. Since the vertex processor will be designed to have a decision time less than that of the track processor by a factor of two to five, it will also help to reduce the overall deadtime. More work is required in order to estimate the rejection achievable with such a processor.

V. SPECIFIC CHANGES TO THE SPECTROMETER

material of the magnet and beam dump. The observed rate allows us to rule this out as a substantial counting-rate background, however the enhanced radiation-damage cross-section of fast (MeV) neutrons in silicon might still pose a problem. To investigate this, we exposed a Harshaw DN156 PIN diode fast-neutron dosimeter at the same location. It registered 50 Rad per 10**12 interactions, corresponding to 50 kRad per fixed-target run, which is negligible compared to the charged-particle dose. Since the PIN diode is most sensitive to exactly the neutron-energy range which is most effective in damaging silicon, we are confident that neutron damage will not be a problem.

III. BACKGROUNDS AND BACKGROUND REJECTION

A substantial background for the observation of two-body hadronic B decays is correlated production of hadron pairs. The cross-section has been measured for 200-, 300-, and 400-GeV incident protons [6]. Using the fit of Jostlein et al. [6], we can extrapolate to 800 GeV, giving the results shown in Figure 4. Since the background is a mass continuum, the number of background events is proportional to the width of the mass bin in which one looks. Pion pairs are seen to have the highest background, at 4.5 x 10**9 pairs per GeV, and pbar-K+ the smallest, at 3 x 10**8, the other species combinations being intermediate between the two. Jostlein et al. also characterized the accidental hadron-pair rate (Figure 4). We see that 10 interactions/bucket is approximately the optimal interaction rate: taking into account the typical spill-structure duty factor of 2, accidentals and reals are comparable at that rate, whereas accidentals

would dominate by an order of magnitude at 100 interactions/bucket.

Rejection of the hadron-pair continuum background depends on mass resolution and decay-vertex resolution. Figure 5 illustrates the effect of the mass cut. Based on the Monte Carlo prediction of 1 MeV (rms) mass resolution, a +- 1-sigma cut retains 70% of the signal events while retaining background events as given in the following table for a few representative species combinations:

B-species	products	bkgnd	signal	ratio
Bd	Pi+ Pi-	9 x 10**6	1400	2 x 10**-4
Bd	K+ K-	2 x 10**6	1400	7 x 10**-4
Bs	Pi+ K-	3 x 10**6	700	2 x 10**-4
$\overline{\text{Lambda-b}}$	K+ pbar	6 x 10**5	700	10**-3

It is clear that a further rejection of at least 10**-3 is required from the decay vertex cut in order to study B decays. We choose to operate with a short (3mm) target in order to optimize the vertex reconstruction. Thus the target length contributes less than 10% (rms) of the mean B decay length. Furthermore, Monte Carlo simulation indicates that the high precision of the silicon and wire-chamber measurements, combined with the long lever arm and large transverse-momentum kick of the spectrometer, yields vertex z extrapolation to better than 10% of the mean decay length. (Multiple-scattering in the silicon is the dominant contribution to the vertex resolution according to the Monte Carlo.) Naively, a

zero, which is quite comparable to our present Upsilon acceptance. Preliminary acceptances vs. transverse momentum and Feynman x are given in Figure 3. The outstanding questions are: 1) can we operate the vertex detector and the downstream spectrometer at interaction rates in the neighborhood of 10/bucket, and 2) is the signal to background ratio adequate in order to identify B decays unambiguously?

We can estimate the rates in the vicinity of the target as follows. A standard approximate parametrization for the bulk of the single-hadron inclusive invariant cross-section is

$$A \exp(-6 Pt) ,$$

independent of rapidity. This leads to the result (integrating over momentum and azimuth)

$$N = n \ln(\theta_2 / \theta_1) , \qquad (1)$$

where N = number of charged particles per interaction produced between θ_1 and θ_2 and n = charged multiplicity per unit rapidity (= 3 at 800 GeV on the rapidity plateau, i.e. y near 0). The acceptance of the downstream spectrometer is restricted to vertical angles such that the produced charged particle is magnetically deflected around the beam dump without striking the magnet yokes. This means that the vertex detector only needs to cover the vertical angular range 15 mrad $< |\theta - y| <$ 55 mrad. From equation (1), and approximating $\theta - y = \theta$, the total rate into this angular range is 4 charged particles per interaction. In x the vertex detector needs to cover the +-27 mrad horizontal aperture. Thus each detector covers about 90 degrees

in phi and sees 1 charged particle per interaction. If no other background dominates (an assumption to be examined in detail below), then at 10 interactions per bucket each detector sees an average rate of 10 charged tracks per bucket. Taking into account the typical spill-structure duty factor of 2, a typical event would contain 20 tracks in each detector. This is an acceptable rate from the viewpoint of pattern recognition if each plane consists of about 1000 elements (2% random hit probability).

From the viewpoint of radiation damage, silicon strip detectors are known to die after 10**14 charged particles per cm**2 [5] (4 MegaRad). If the first vertex detector plane is placed 1m downstream of the target, its area is 20 cm**2, so it should last for 2 x 10**15 interactions. This is twice as long as a "standard" fixed-target run of 10**5 pulses, if we operate at 10 interactions/bucket. It seems quite feasible to replace the detector planes every running period, should this prove necessary.

In order to test these estimates, we have placed a Silicon Strip Detector (borrowed from E653) downstream of the first analyzing magnet (SM0). We read out one strip, covering an area of 100 microns in x by 5cm in y. The detector is located at z = 100" and centered vertically at theta-y = 85 mrad. It counts at 10**-4 per interaction, in good agreement with the prediction of 6 x 10**-5 based on the above model. In addition to charged particles from the target, the detector might be bathed in a "sea" of low-energy neutral particles created by the interaction of high-energy primary and secondary particles in the

I. INTRODUCTION

Bjorken [1] has summarized the theoretical issues and the experimental situation regarding B mesons. Recent results from ARGUS [2] indicate that there is unexpectedly strong mixing between the neutral B mesons and their antiparticles. Combined with earlier results, they also allow the parameters of the Kobayashi-Maskawa matrix to be substantially pinned down [2]. It seems clear from this not only that mixing is large (in the vicinity of 20%), but that CP violation may well be observable in neutral B-meson decay. Bjorken estimates that an experiment which can reconstruct 10,000 B decays and measure their lifetimes has a chance of observing CP violation through a modulation of the exponential decay distribution. This is a goal far beyond the reach of present-day electron-positron collider experiments, and it seems attainable only in a carefully-designed fixed-target experiment of very ambitious scale.

In this proposal we consider the suitability of the existing E605/772 apparatus for a near-term look at the two-body hadronic decay modes of neutral B mesons and baryons. We conclude that it appears feasible to reconstruct between 1,000 and 2,000 Bs per two-body hadronic decay mode in a typical 6-month Tevatron fixed-target run. Such an experiment has the potential to measure the masses, lifetimes, and cross-sections times branching ratios to two hadrons of various mesonic and baryonic b states, including discovery of the B-sub-s meson and the Lambda-sub-b baryon. (In particular, a very interesting test of present models of weak decays is measurement of the lifetime

ratio of B-sub-s to B-sub-d.) In addition, it will explore the possibility (of great potential importance for the observation of CP violation) of substantial production-rate asymmetries.

For a rough indication of the required sensitivity, we use a B cross-section in 800 GeV proton-nucleon collisions estimated at 10 nanobarns [3], and we assume two-body hadronic branching ratios of 0.01% [1]. In comparison, the Upsilon cross-section times branching ratio into muon pairs is about 5 picobarns [4], and the present run of E772 is recording some 30,000 Upsilon-decay events. We could thus expect to record of order 10**4 B-decay events in each two-body hadronic mode, provided we could maintain the same interaction rate of 100 per RF bucket. Considering that in order to detect B decays we need to open up the aperture and operate a vertex detector near the target, a more reasonable goal is to run at 10 interactions per bucket and record approximately 1,000 events per two-body decay mode. The details of the yield calculation are given in Figure 1. E605/772 is the only existing experiment to approach this level of sensitivity.

II. EXPERIMENT

The proposed experimental arrangement is shown in Figure 2. The only new elements are the vertex detector and the precision tracking detector, which replace the former Station 0 and Station 1 chambers (respectively). Together, these new detectors improve our vertex z resolution from 2cm to the 1mm necessary in order to identify B decays unambiguously. Monte Carlo simulation indicates an acceptance (with optimal choice of magnetic field settings) of 6% for rapidity near

VI. RESULTS FROM TEST RUN

In January and February 1988, after the completion of experiment 772, we performed several tests to evaluate the spectrometer configuration of P789. The major goals of these tests were:

a) To check the singles rates in various detectors in the proposed open-aperture configuration.

b) To measure the rate of charged-particle production from the interaction of an 800 GeV proton beam with a 3mm tungsten target. The neutron flux was also measured. These measurements are crucial for evaluating the radiation damage of and count rates in the Si strip detectors.

c) To measure the trigger rate.

For the tests, we removed from E772 the SM0 magnet and the hadron absorber wall. The SM12 current was set at 2000 amps and the SM3 current at -4250 amps. The exit of SM12 was collimated to 20" high $\times$ 28" wide. 1mm and 3mm W targets and beam intensities varying between a few $\times$ 10^{10} and a few $\times$ 10^{11}/spill were used. We present results normalized to the proposed beam intensity of 3×10^{11}/spill.

1) Singles rates on hodoscopes and chambers

Table V lists the singles rates at the various hodoscope stations. The maximum rate is ~6 MHz, well within the rate capability of these counters. The currents drawn by the wire chambers at stations 1, 2 and 3 were 50, 100 and 300 μamps, respectively. The hit multiplicities on the stations for reconstructed dihadron events were 12, 10, and 15. These chamber currents and multiplicities are similar to or less than those observed during E605 data taking.

2) Rates on the Si strip detectors

We installed a Si strip detector (5 cm $\times$ 5 cm, 50 μm pitch) 60 inches downstream

of the target. In addition, a finger scintillator (3" × 1/8" × 1/8") was mounted on a motor-driven frame 49 inches downstream of the target. The minimum ionization band was clearly visible on the photo-tube output of the scintillator. The vertical position of the finger scintillator was varied between 6mr $\leq |\theta_y| \leq$ 90 mr. Figure 14 shows the scintillator count rates as a function of the vertical position of the counter. Also shown are target-out rates. The beam axis can be well determined from Figure 14. The preamp output of the Si detector also showed a clear minimum ionization band. Three adjacent strips of the Si detector were read out. The Si detector was placed at two different heights corresponding to θ_y = 50 mr and θ_y = 96.5 mr. The rates measured by the finger scintillator are in agreement with the rate measured by the Si detector within a factor of two.

From the count rates measured by the finger scintillator (Figure 14), we can now make a realistic prediction of the rates on the Si strip detectors to be used in P789. We consider a Si detector located 63 cm downstream of the target covering -26 $\leq \theta_x \leq$ 26 mr, 18 mr $\leq \theta_y \leq$ 65 mr. This detector has 512 horizontal strips of 70 μm pitch with a total area of 2" × 1.4". In Table VI we list the predicted count rate/strip on various strips as a function of θ_y, as well as the flux per cm^2 integrated over one running period. (The integrated fluxes for a plane located 126cm downstream of the target are given for comparison.) The results in Table VI are also plotted in Figure 15. Table VI implies that the average count rate/strip is 1.4 MHz and the average number of hits per RF bucket on the Si detector is ~14. Assuming the radiation damage limit for Si detectors is 10^{14} minimum-ionizing particles/cm^2, we conclude that the upstream Si detector should last for a few months of beam time. We anticipate that the upstream planes can be replaced part-way through the run, should this prove necessary, at a cost of $7K per silicon wafer.

The neutron flux was measured in the target cave behind a few inches of concrete shielding. This was done in order to estimate the possible radiation damage to the silicon detector and its preamplifiers. The neutron rates were considerably lower than the direct charged particle rates from the target. With a modest amount of shielding, the neutron rates 1/2m east and west of the beam axis (where the preamplifiers will be located) can be reduced to less than 50 krads for 10^5 pulses. We have been assured by D. Christian that this level should prove not to be a problem for the new generation of preamplifiers.

The neutron rates on axis will cause less damage to the silicon wafers than the charged particle rates.

3) Trigger Rate

As indicated in a previous section, it is expected that 2×10^3 target di-hadrons per spill will be accepted by the spectrometer. Unless a highly efficient trigger can be devised which selects only such events, the resulting volume of data would most likely exceed the maximum storage of our data buffering system (4096 events or 4 megabytes per pulse). While we intend to increase this storage limit at least fourfold, it is essential that a clean di-hadron trigger be constructed. Past experience suggests that our existing low-level hadron-pair trigger, which is based upon hodoscope roads in combination with calorimeter energy deposition, could be the starting point for this trigger. The rejection power of the trigger processor, calculating the mass of the apparent hadron pair, should then bring the data rate within the capacity of the buffer.

Several tapes of di-hadron test data were recorded using a variety of hodoscope and calorimeter based triggers under various beam and target conditions. These serve to measure the relevant trigger rates and to check the di-hadron production cross sections. The results of these studies are shown in Table VII. The various trigger conditions applied are defined as follows: The 3/4 L·R hodoscope coincidence requires 3 out of 4 hodoscope planes on the both the left and right side of the apparatus to record hits. E_{tot} requires a total energy deposition threshold in the calorimeter of at least 70 GeV. h^+h^- is a 6-fold matrix hodoscope hit pattern consistent with two oppositely charged particles originating from the target.

By using all three of these trigger conditions in coincidence a raw trigger rate of 1.2×10^4 per spill was observed at 1.4×10^{11} protons per spill incident on a 3mm W target. This is expected to scale up to about 4×10^4 at 3×10^{11} incident protons per spill. Table VII indicates that about half of the event rate is due to particles coming from the beam dump. These beam dump triggers will be more efficiently rejected by the trigger matrix when the new, finer-grained Y1 hodoscope is employed. Furthermore, a requirement on the presence of two energy clusters in the calorimeter can be applied to remove the background of high

energy single hadrons. Nevertheless, this trigger rate is already well within the bandwith of our trigger processor, which requires only 10 to 20 μsec per event. In past running the trigger processor has provided a trigger rate reduction of 5 to 10 times by requiring a pair of opposite-sign tracks originating near the target. This would place the number of events per spill safely inside the anticipated capacity of the upgraded data buffer. If necessary, the processor is capable of making a tight mass cut on these target-track pairs to reduce the data rate still further. While we are planning on adding a silicon vertex track processor to our triggering system, it is not anticipated that this information will be needed in the trigger, but will merely serve to reduce the amount of tapewriting and hence also the off-line computing load.

VII. COST ESTIMATES

A number of changes to the E605/772 spectrometer are required for P789. These include the installation of a silicon vertex detector and a new station 1 drift chamber, construction of a partially-open aperture wall in the SM12 magnet, rehabilitation of the RICH detector, upgrades to the data acquisition system including a vertex processor, and rebuilding of two hodoscope planes. The total estimated cost is $590K. This is based primarily on the P789 impact statement written by D. Christian dated November 29, 1987 and assuming that the existing 6000 channels of MWPC electronics will be used for the silicon vertex detector readout. The breakdown of the costs is as follows:

1) Silicon Detectors

Silicon (8 planes + spares)	$150K	
Mounts	35K	
Preamps (6K channels)	55K	
A/C & RF shielding	30K	
Re-shielding target cave	30K	
Total		$300K

2) New Station 1 Drift Chamber

Mechanical	$40K	
Readout electronics	10K	
Total		$50K

3) Partially Open Magnet Aperture

Machining and rigging	$50K	
Total		$50K

4) RICH Detector

Readout electronics (2000 chan.)	$120K	
Misc. rehabilitation	20K	
Total		$140K

5) DAQ upgrade

Megamemory replacement	\$30K	
Si vertex processor	10K	
Total		\$40K

6) Hodoscope rebuild

Rebuild 2 planes - mechanical	\$10K	
Total		\$10K

Total Estimated Cost \$590K

VIII. SUMMARY

We propose to reconfigure the E605/772 spectrometer to study the two-body, two-prong decay modes of neutral B mesons and baryons. The superb mass resolution and high-rate capability of this instrument are uniquely suited to this objective. Based upon plausible assumptions for cross sections and branching ratios, a sample of order 10^3 b-decays can be obtained. These data will provide important first measurements of the masses, lifetimes and branching ratios for a variety of non-charm decays into π, K, and protons. While some upgrades to the spectrometer are required, the anticipated cost (\$590K) and level of effort involved are reasonable in light of the potential physics insight that can be obtained.

References

1. H. Albrecht *et al.*, *Phys. Lett.* **192B** (1987) 245.

2. C. Albajar *et al.*, *Phys. Lett.* **186B** (1987) 247.

3. W. Schmidt-Parzefall, Invited talk at the 1987 International Symposium on Lepton and Photon Interactions at High Energies, Hamburg, W. Germany, July 27–31, 1987.

4. Particle Data Group, *Phys. Lett.* **170B** (1986) 74.

5. F. J. Gilman, Invited talk at the Workshop on High Sensitivity Beauty Physics at Fermilab, Batavia, Illinois, Nov. 11–14, 1987.

6. J. D. Bjorken, Invited talk at the International Symposium for the Fourth Family of Quarks and Leptons, UCLA, Los Angeles, California, February 26–28, 1987.

7. I. I. Bigi and B. Stech, Contribution to the Workshop on High Sensitivity Beauty Physics at Fermilab, Batavia, Illinois, Nov. 11–14, 1987. SLAC-PUB-4495.

8. E605 Collaboration, to be published.

9. E. L. Berger, Invited paper at the XXII Rencontre de Moriond, Les Arcs, France, March 15–21, 1987.

10. C. Albajar *et al. Phys. Lett.* **186B** (1987) 237.

11. M. G. Catanesi *et al. Phys. Lett.* **187B** (1987) 431.

12. R. D. Kephart *et al. Phys. Lett.* **39** (1977) 1440.

13. H. Jöstlein *et al.*, *Phys. Rev.* **D20** (1979) 53.

14. A. L. S. Angelis *et al*, *Nucl. Phys.* **B209** (1982) 284.

Table I. Si strip detector configuration.

Plane	Z (cm)	Size (X cm × Y cm) (H × V)	No. of strips	Spacing (μm)
Y1	60	4.0 × 3.4	512	66
U1	60	4.0 × 3.4	244	200
Y1′	68	4.0 × 3.4	512	66
V1	68	4.0 × 3.4	244	200
Y2	124	7.0 × 6.8	512	132
U2	124	7.0 × 6.8	244	400
Y2′	132	7.0 × 6.8	512	132
V2	132	7.0 × 6.8	244	400

Total number of strips = 3024 × 2 = 6048.

The U,V strips are on the reverse side of the Y silicon wafers.

Table II. New station 1 drift chambers.

Chamber	Size (cm × cm) (H × V)	No. of channels	Cell size (cm)
Y1	110 × 72	72	1
Y1′	110 × 72	72	1
U1	110 × 72	96	1
U1′	110 × 72	96	1
V1	110 × 72	96	1
V1′	110 × 72	96	1

Table III. Estimated number of events (per 10^{15} interactions).

Decay Mode	ε	BR	No. of events
$B_d, \bar{B}_d \to \pi^+\pi^-$	0.6	5×10^{-5}	100
$B_d, \bar{B}_d \to K^\pm\pi^\mp$	0.6	5×10^{-5}	100
$B_d, \bar{B}_d \to K^+K^-$	0.6	5×10^{-5}	100
$B_d, \bar{B}_d \to p\bar{p}$	0.6	5×10^{-5}	100
$B_s, \bar{B}_s \to \pi^+\pi^-$	0.3	5×10^{-5}	50
$B_s, \bar{B}_s \to K^\pm\pi^\mp$	0.3	5×10^{-5}	50
$B_s, \bar{B}_s \to K^+K^-$	0.3	5×10^{-5}	50
$B_s, \bar{B}_s \to p\bar{p}$	0.3	5×10^{-5}	50
$\Lambda_b, \bar{\Lambda}_b \to p^\pm\pi^\mp$	0.3	5×10^{-5}	50
$\Lambda_b, \bar{\Lambda}_b \to p^\pm K^\mp$	0.3	5×10^{-5}	50

Table IV. Number of signal and background events.

Decay Mode	No. of Events	Background	Significance
$B_d, \bar{B}_d \to \pi^+\pi^-$	100	40	8σ
$B_d, \bar{B}_d \to K^+K^-$	100	4	10σ
$B_d, \bar{B}_d \to p\bar{p}$	100	4	10σ
$B_d \to K^+\pi^-$	50	20	6σ
$\bar{B}_d \to K^-\pi^+$	50	10	6σ
$B_s, \bar{B}_s \to \pi^+\pi^-$	50	40	5σ
$B_s, \bar{B}_s \to K^+K^-$	50	4	7σ
$B_s, \bar{B}_s \to p\bar{p}$	50	4	7σ
$\Lambda_b \to p\pi^-$	25	30	3σ
$\Lambda_b \to pK^-$	25	5	5σ
$\bar{\Lambda}_b \to \bar{p}\pi^+$	25	5	5σ
$\bar{\Lambda}_b \to \bar{p}K^+$	25	2	5σ

Table V. Maximum count rates in hodoscopes (3×10^{11} protons on 3mm W).

Plane	Rate (MHz)
X1R	3.0
Y1R	2.4
Y2R	1.6
X3R	4.4
Y3R	6.5
X4R	0.25
Y4R	0.10

The X1R,Y1R rates are shown for the reduced size planes.

Table VI. Si detector count rate/strip (3×10^{11} proton/spill on 3mm W).

θ_y(mr)	Rate (MHz) per strip	Hits/RF bucket	Integrated flux/cm^2 Z = 63cm	(per 10^{15} interactions) 126cm
18.1	2.99	0.059	2.5×10^{14}	0.62×10^{14}
21.2	2.49	0.050	2.1×10^{14}	0.52×10^{14}
26.2	1.92	0.038	1.6×10^{14}	0.40×10^{14}
31.2	1.74	0.035	1.4×10^{14}	0.36×10^{14}
36.2	1.38	0.028	1.1×10^{14}	0.28×10^{14}
46.4	0.95	0.019	0.78×10^{14}	0.20×10^{14}
56.4	0.68	0.014	0.55×10^{14}	0.14×10^{14}

Table VII. Results of Trigger Rate Study with 3mm W Target.

Trigger	Target	Protons/spill	Triggers/spill
$(3/4L \cdot R) \cdot E_{tot}$	In	3.4×10^{10}	1.9×10^{4}
$(3/4L \cdot R) \cdot E_{tot}$	Out	3.6×10^{10}	1.2×10^{4}
$(3/4L \cdot R) \cdot E_{tot}$	In	9.8×10^{10}	7.5×10^{4}
$(3/4L \cdot R) \cdot E_{tot}$	Out	1.4×10^{11}	7.0×10^{4}
$(3/4L \cdot R) \cdot E_{tot} \cdot (h^+h^-)$	In	2.6×10^{10}	1.2×10^{3}
$(3/4L \cdot R) \cdot E_{tot} \cdot (h^+h^-)$	Out	2.1×10^{10}	5.2×10^{2}
$(3/4L \cdot R) \cdot E_{tot} \cdot (h^+h^-)$	In	1.4×10^{11}	1.2×10^{4}
$(3/4L \cdot R) \cdot E_{tot} \cdot (h^+h^-)$	Out	1.3×10^{11}	6.7×10^{3}

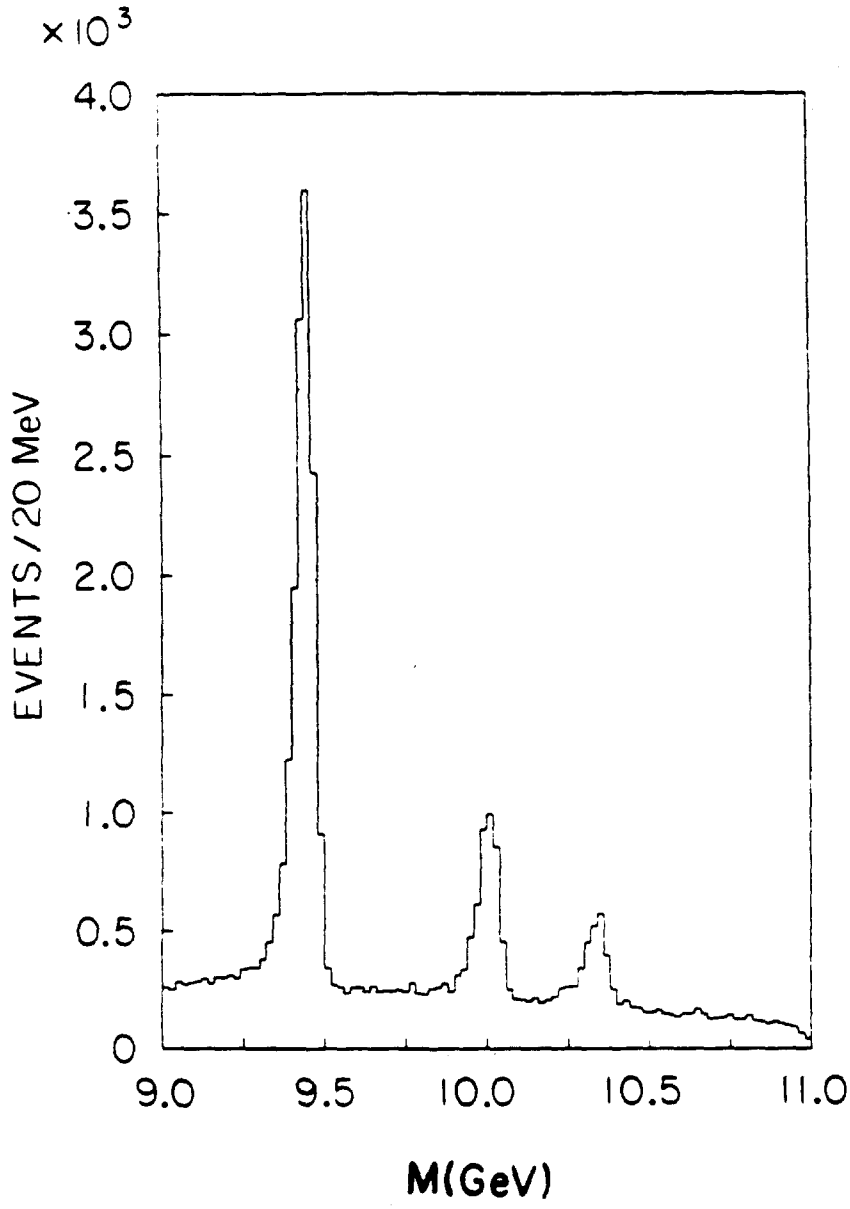

Figure 2.

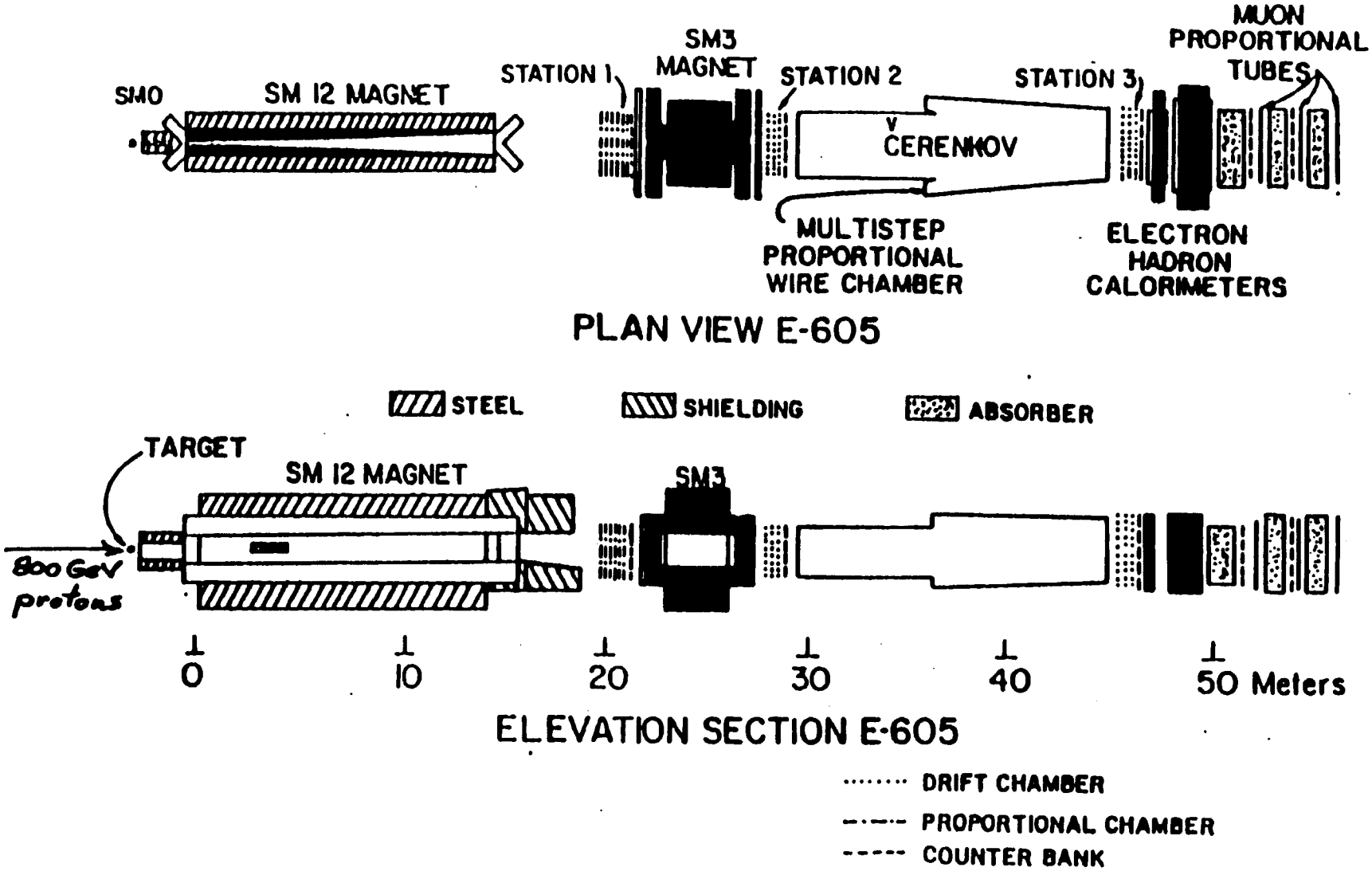
SM0
SM 12 MAGNET
STATION 1
SM3
MAGNET
STATION 2
STATION 3
MUON
PROPORTIONAL
TUBES
CERENKOV
MULTISTEP
PROPORTIONAL
WIRE CHAMBER
ELECTRON
HADRON
CALORIMETERS
PLAN VIEW E-605
STEEL
SHIELDING
ABSORBER
TARGET
SM 12 MAGNET
SM3
800 GeV
protons
0
10
20
30
40
50 Meters
ELEVATION SECTION E-605
DRIFT CHAMBER
PROPORTIONAL CHAMBER
COUNTER BANK

Figure 1.

Figure 3.

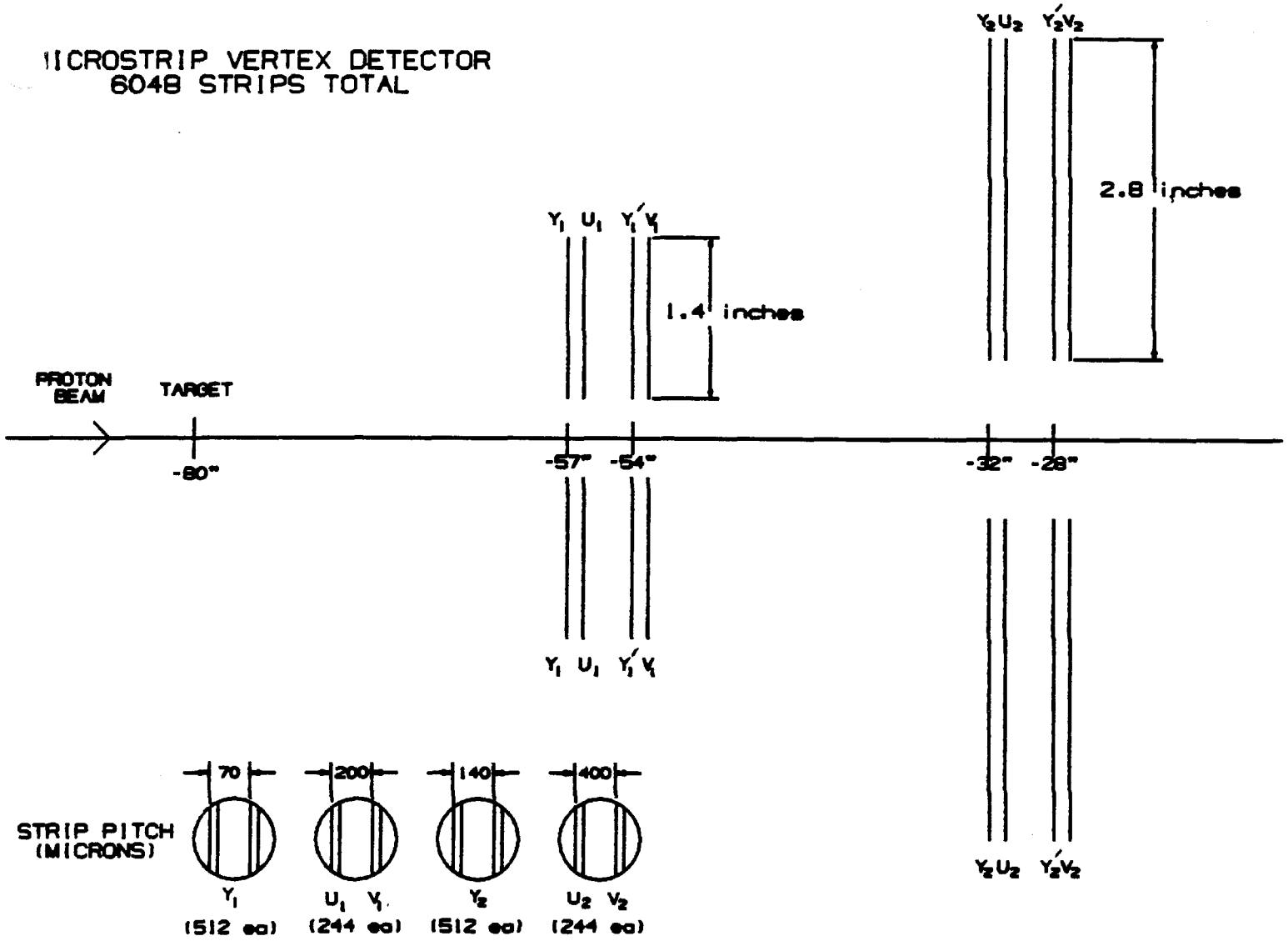
MICROSTRIP VERTEX DETECTOR
6048 STRIPS TOTAL
Y2 U2 Y'2 V2
2.8 inches
Y1 U1 Y'1 V1
1.4 inches
PROTON BEAM
TARGET
-80"
-57"
-54"
-32"
-28"
Y1 U1 Y'1 V1
Y2 U2 Y'2 V2
STRIP PITCH (MICRONS)
70
200
140
400
Y1
(512 ea)
U1 V1
(244 ea)
Y2
(512 ea)
U2 V2
(244 ea)

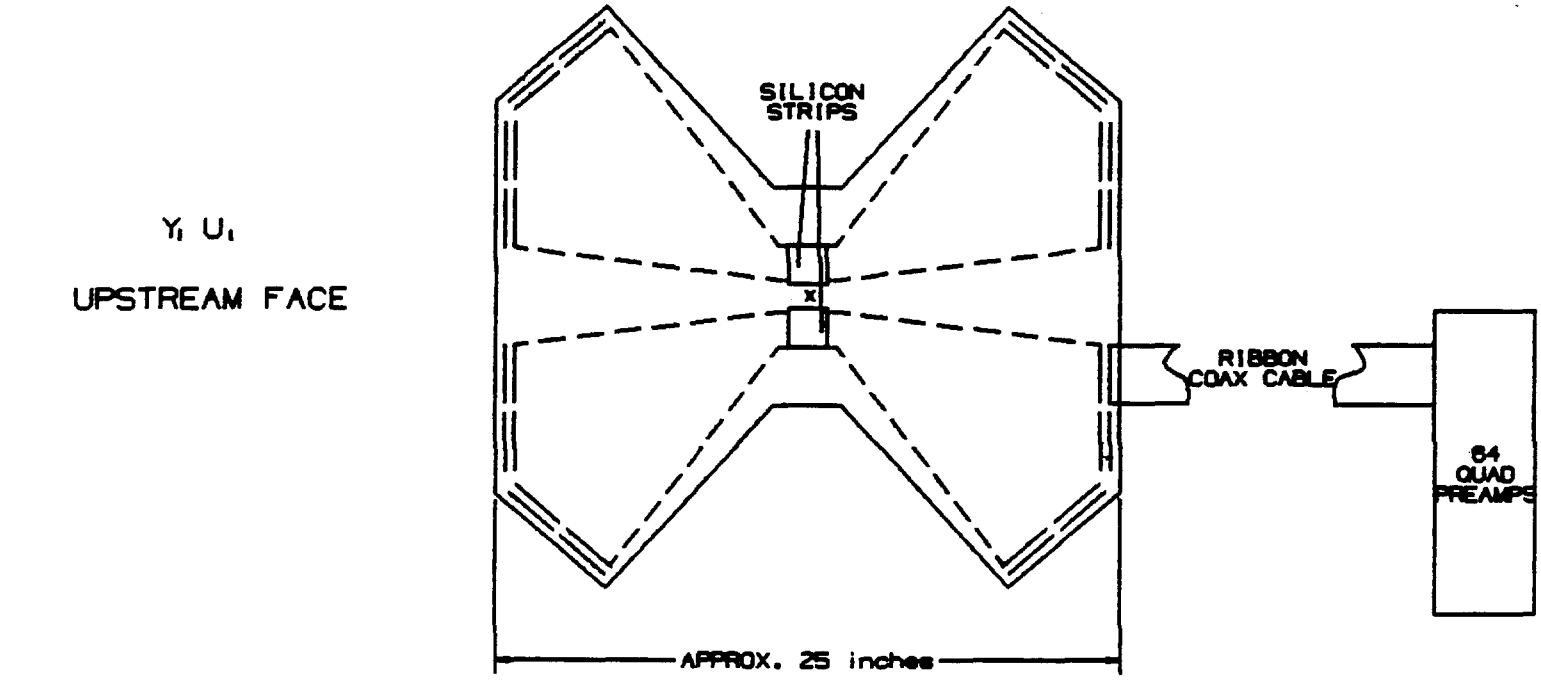
Y1 U1
UPSTREAM FACE
SILICON STRIPS
RIBBON COAX CABLE
64 QUAD PREAMPS
APPROX. 25 inches

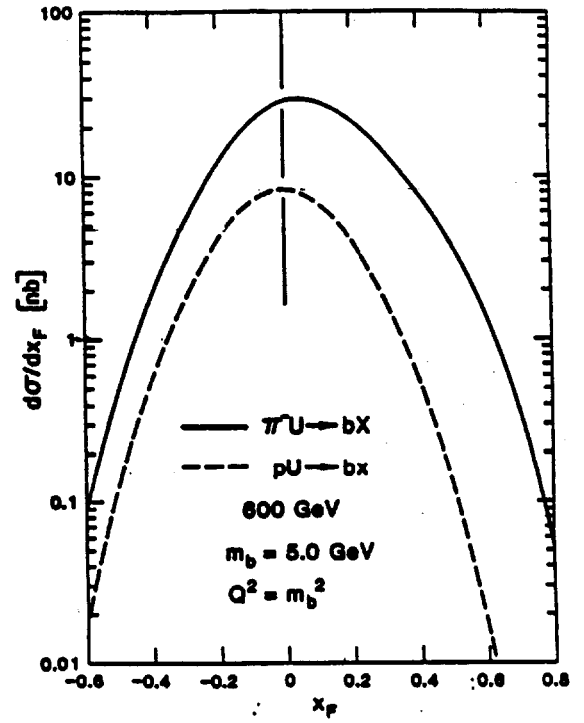
100
10
1
0.1
0.01
$d\sigma/dx_F$ [nb]
$\pi^-U \rightarrow bX$
$pU \rightarrow bx$
600 GeV
$m_b = 5.0$ GeV
$Q^2 = m_b^2$
-0.6 -0.4 -0.2 0 0.2 0.4 0.6 0.8
x_F

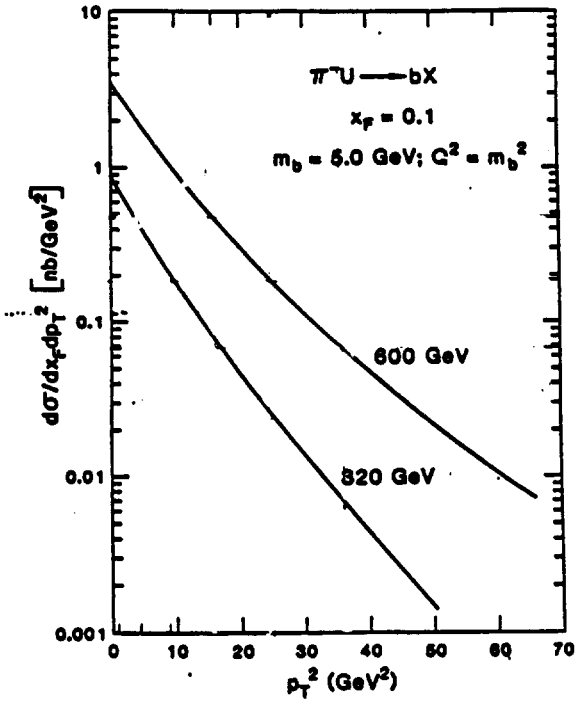
10
1
0.1
0.01
0.001
$d\sigma/dx_F dp_T^2$ [nb/GeV^2]
$\pi^-U \rightarrow bX$
$x_F = 0.1$
$m_b = 5.0$ GeV; $Q^2 = m_b^2$
600 GeV
320 GeV
0 10 20 30 40 50 60 70
p_T^2 (GeV^2)

Figure 4.

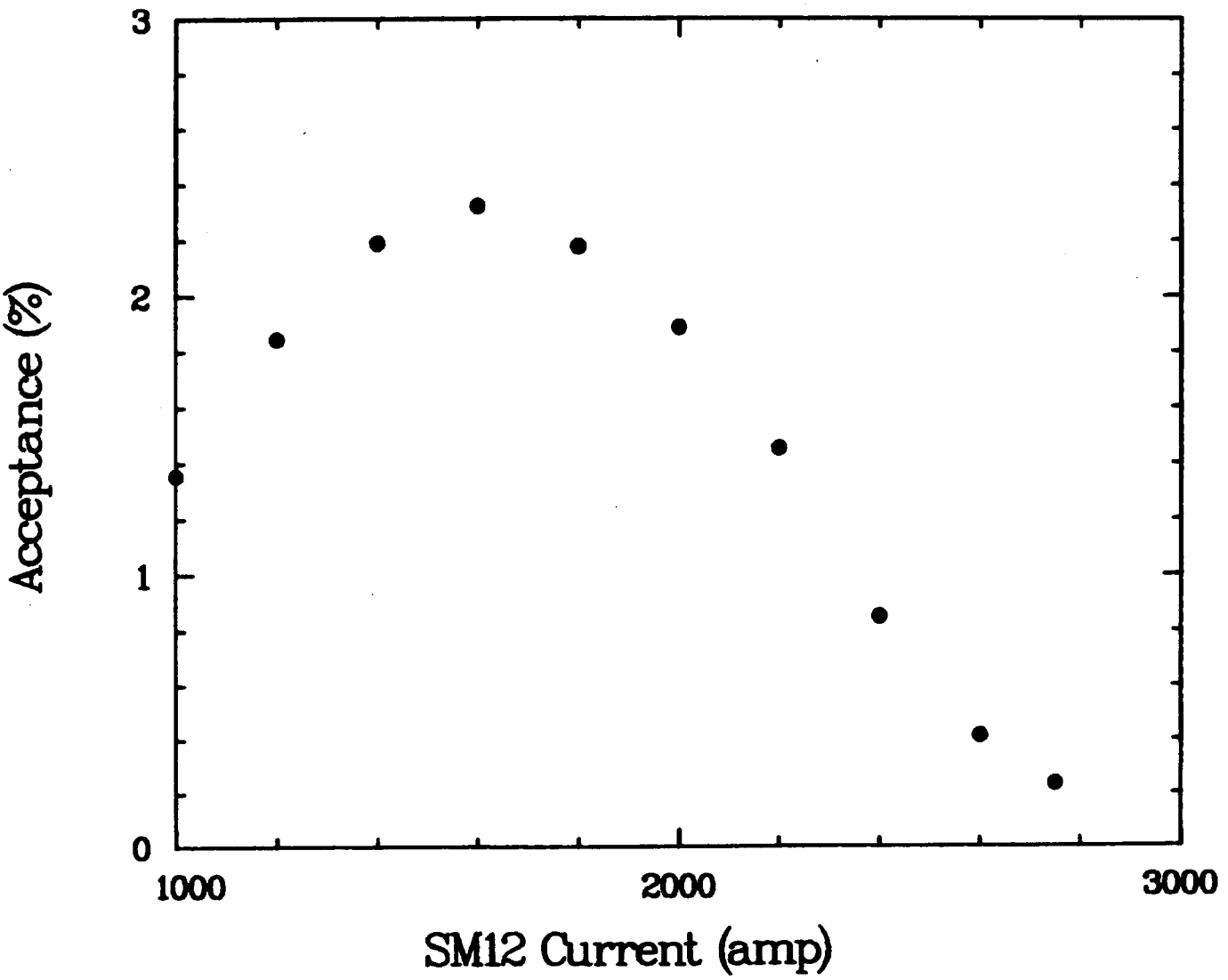

Figure 5(a).

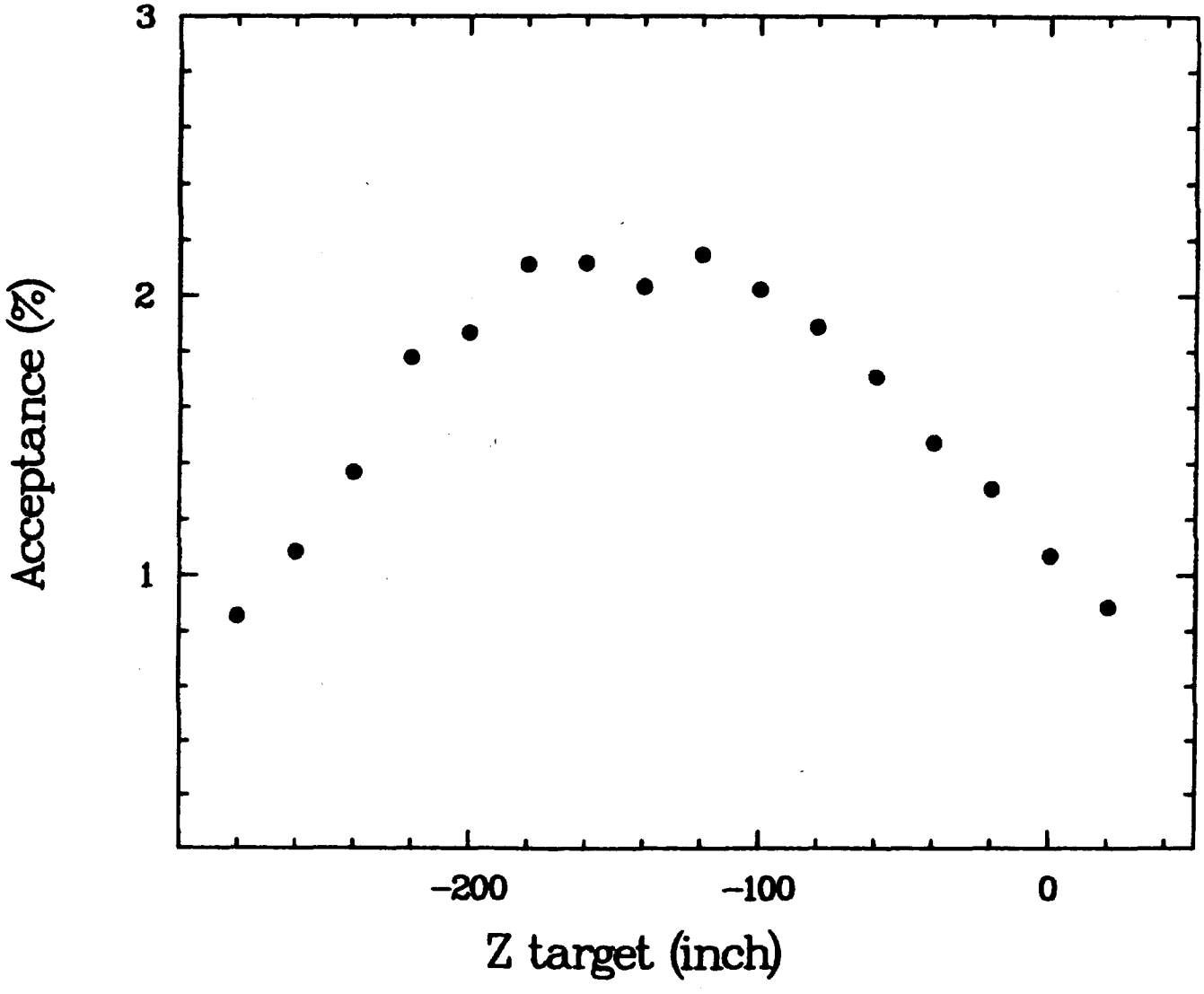

Figure 5(b).

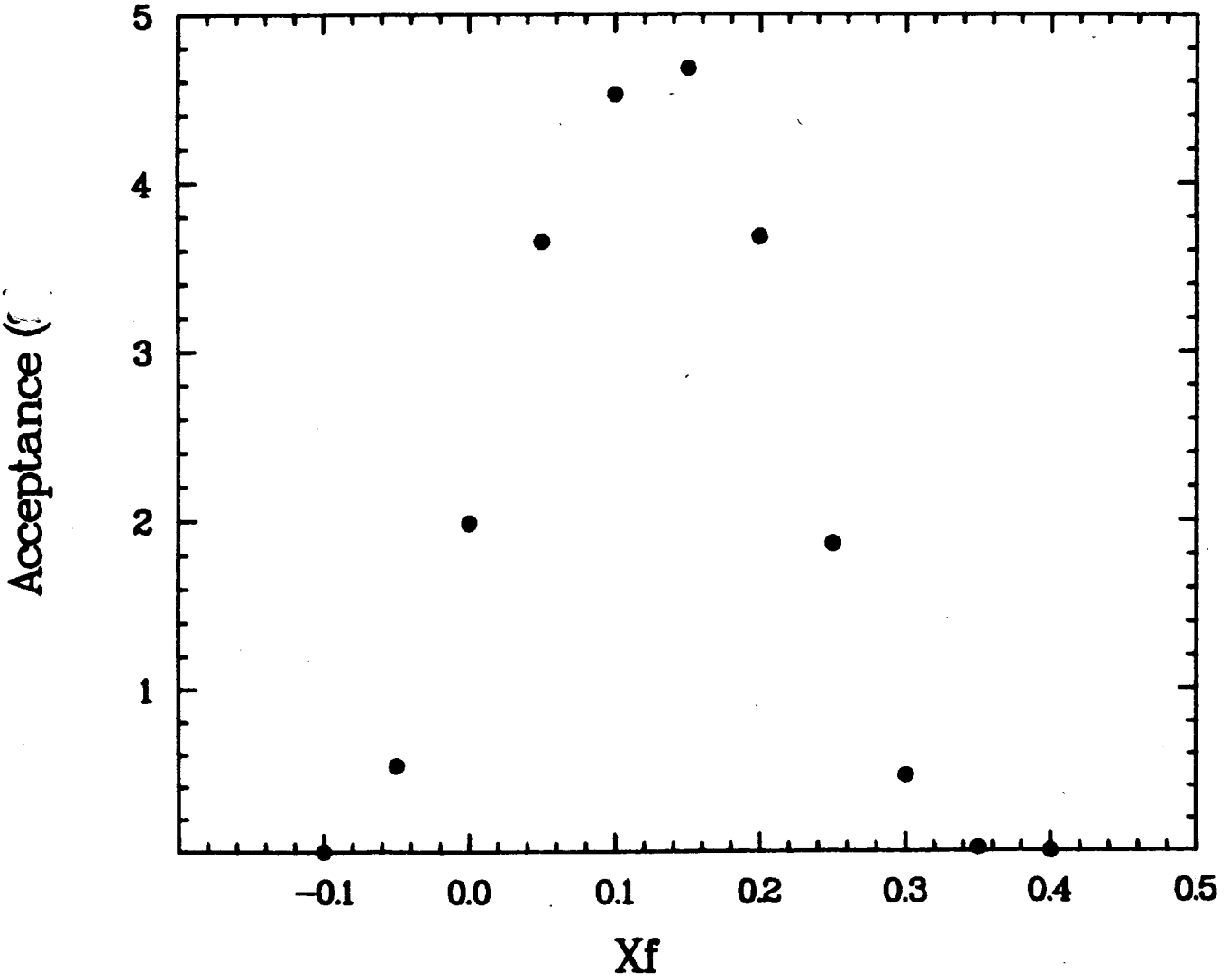

Figure 6(a).

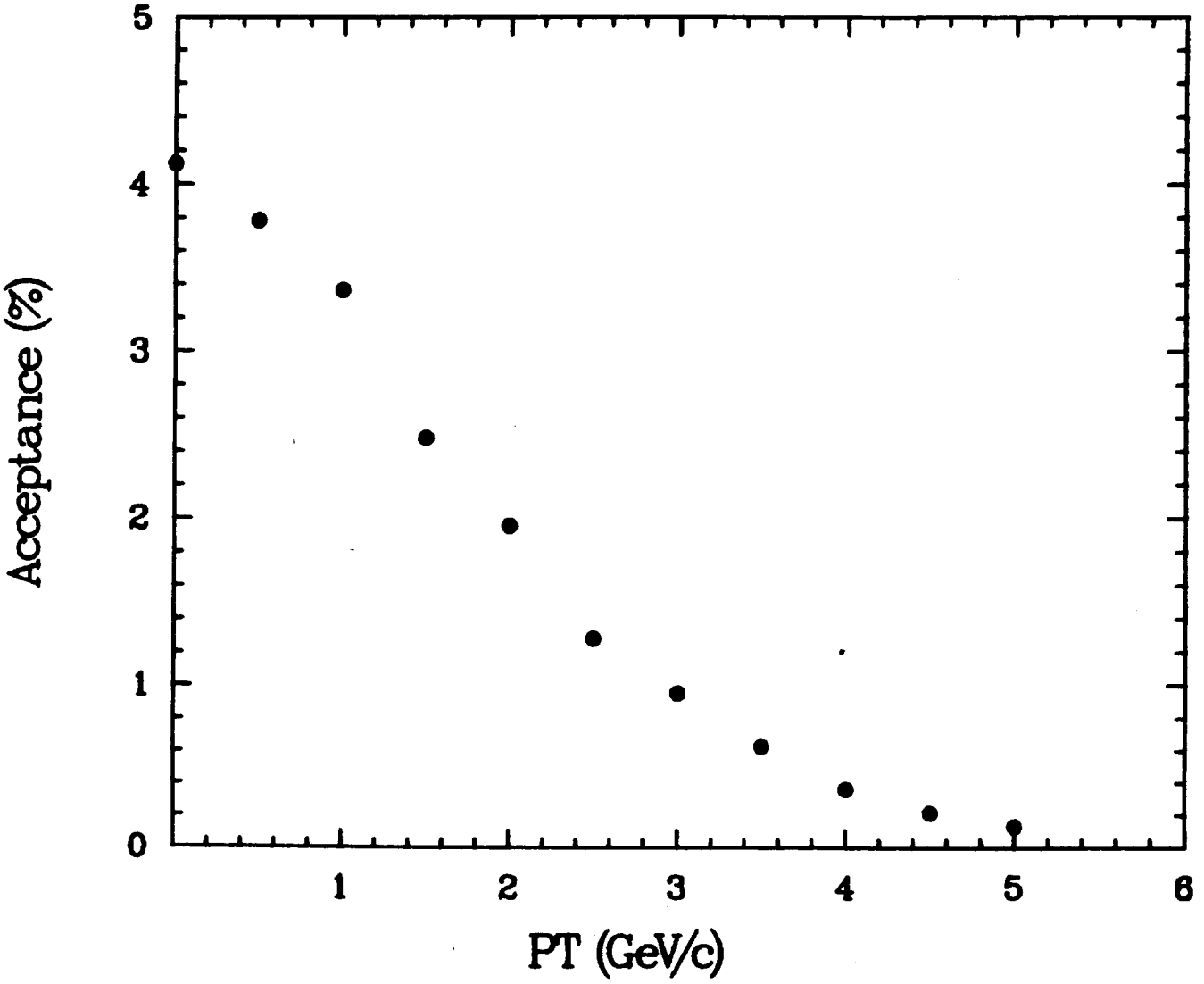

Figure 6(b).

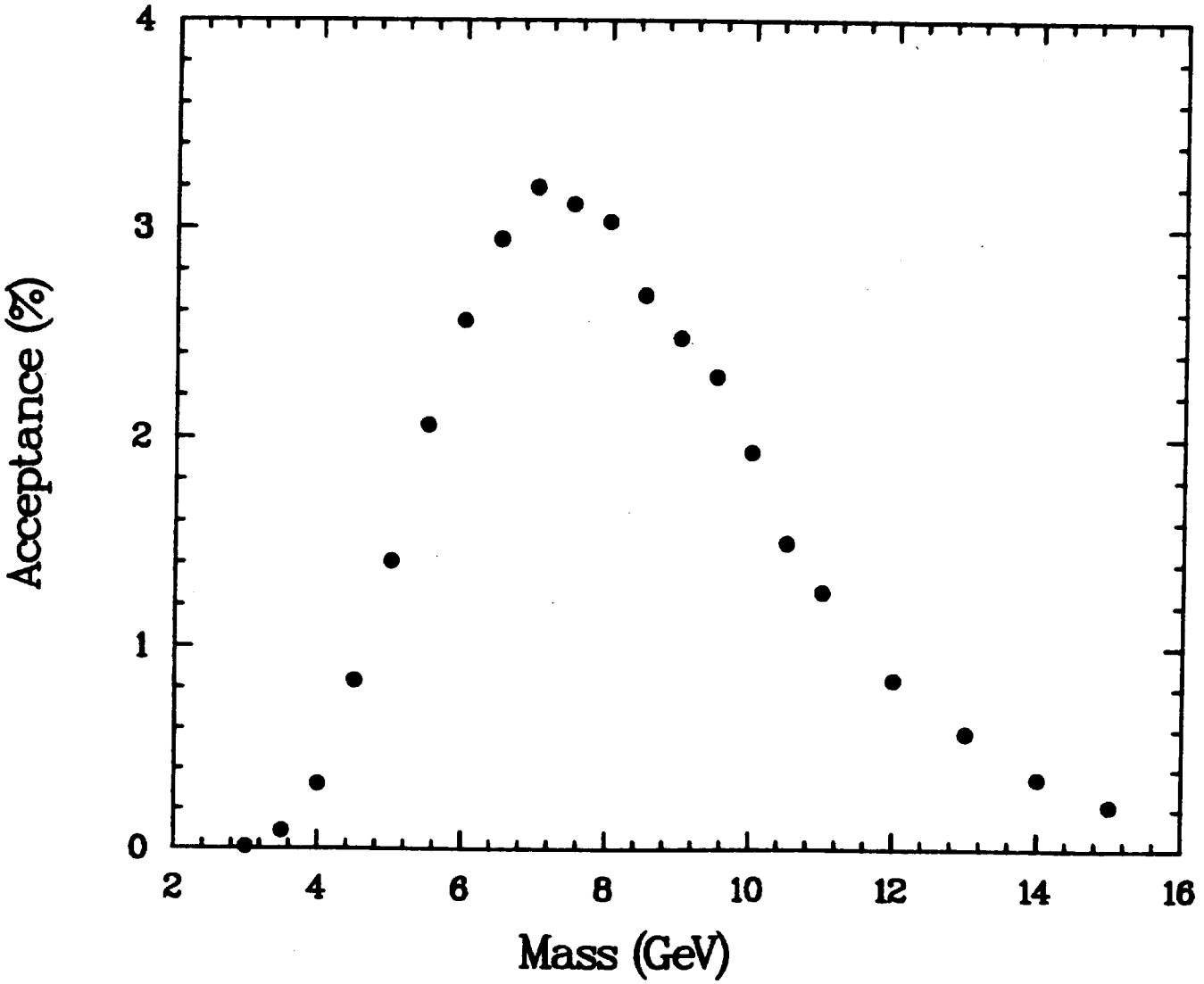

Figure 6(c).

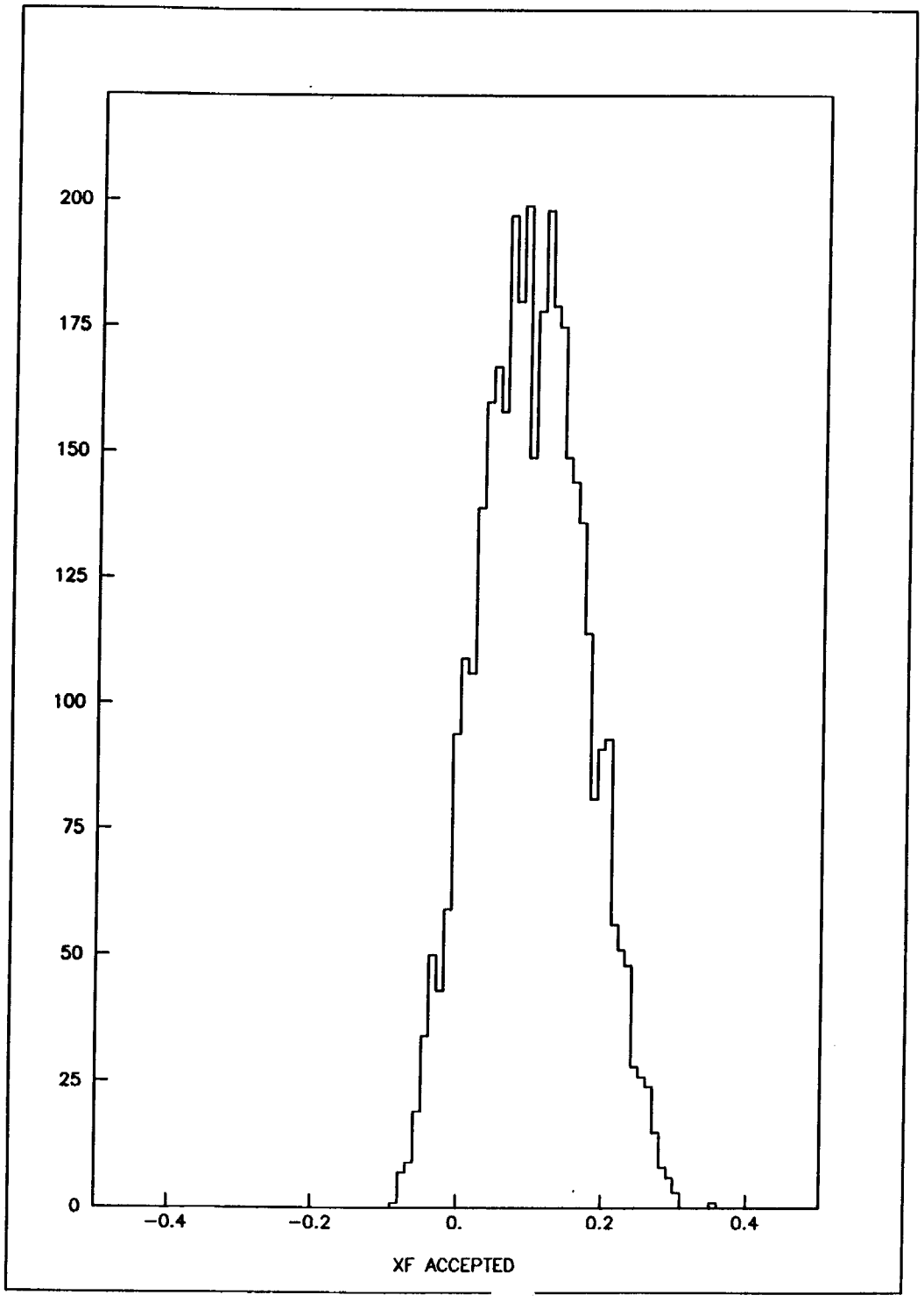

Figure 7(a).

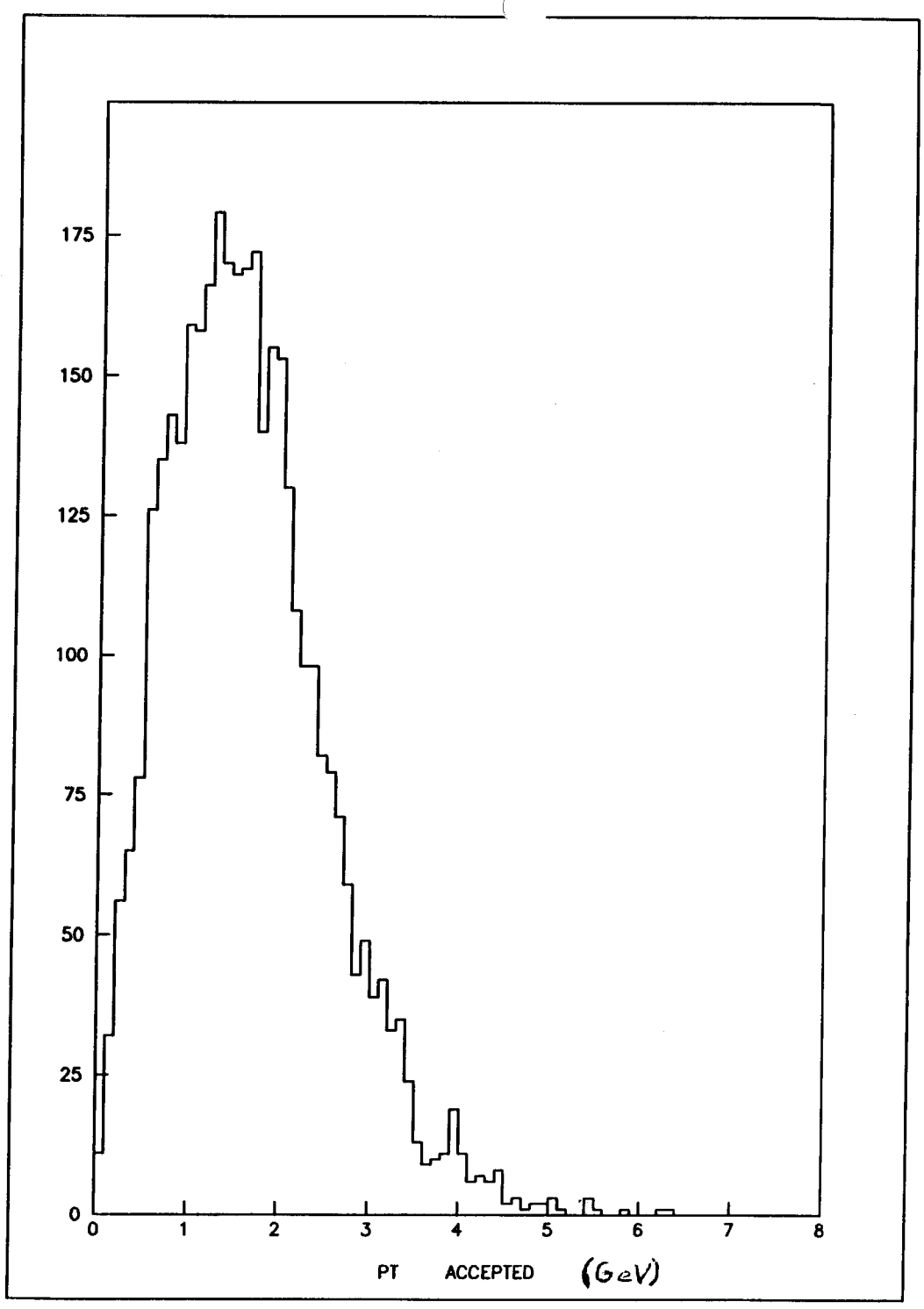

Figure 7(b).

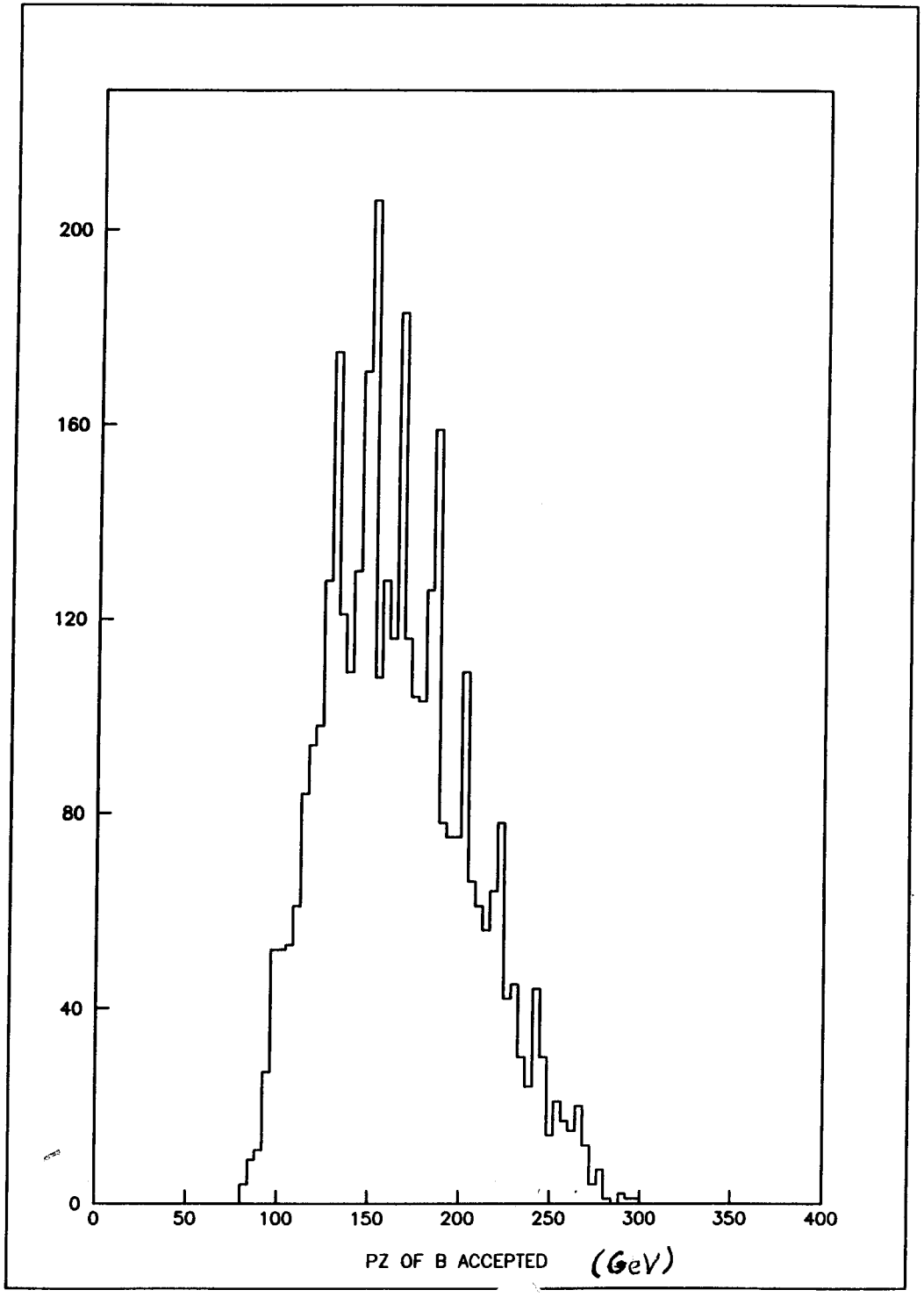
200
160
120
80
40
0
0
50
100
150
200
250
300
350
400
PZ OF B ACCEPTED (GeV)

Figure 8(a).

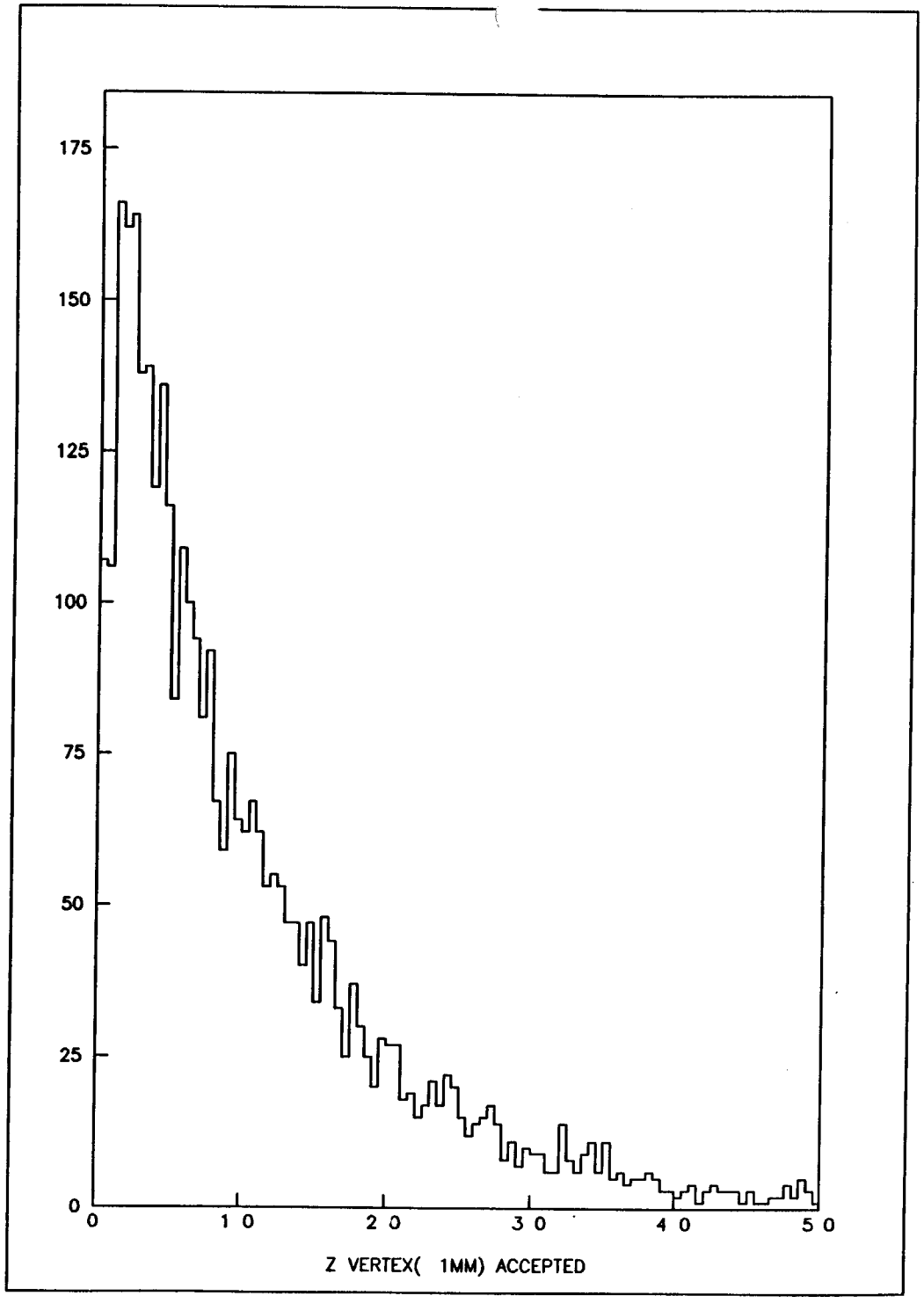

Figure 8(b).

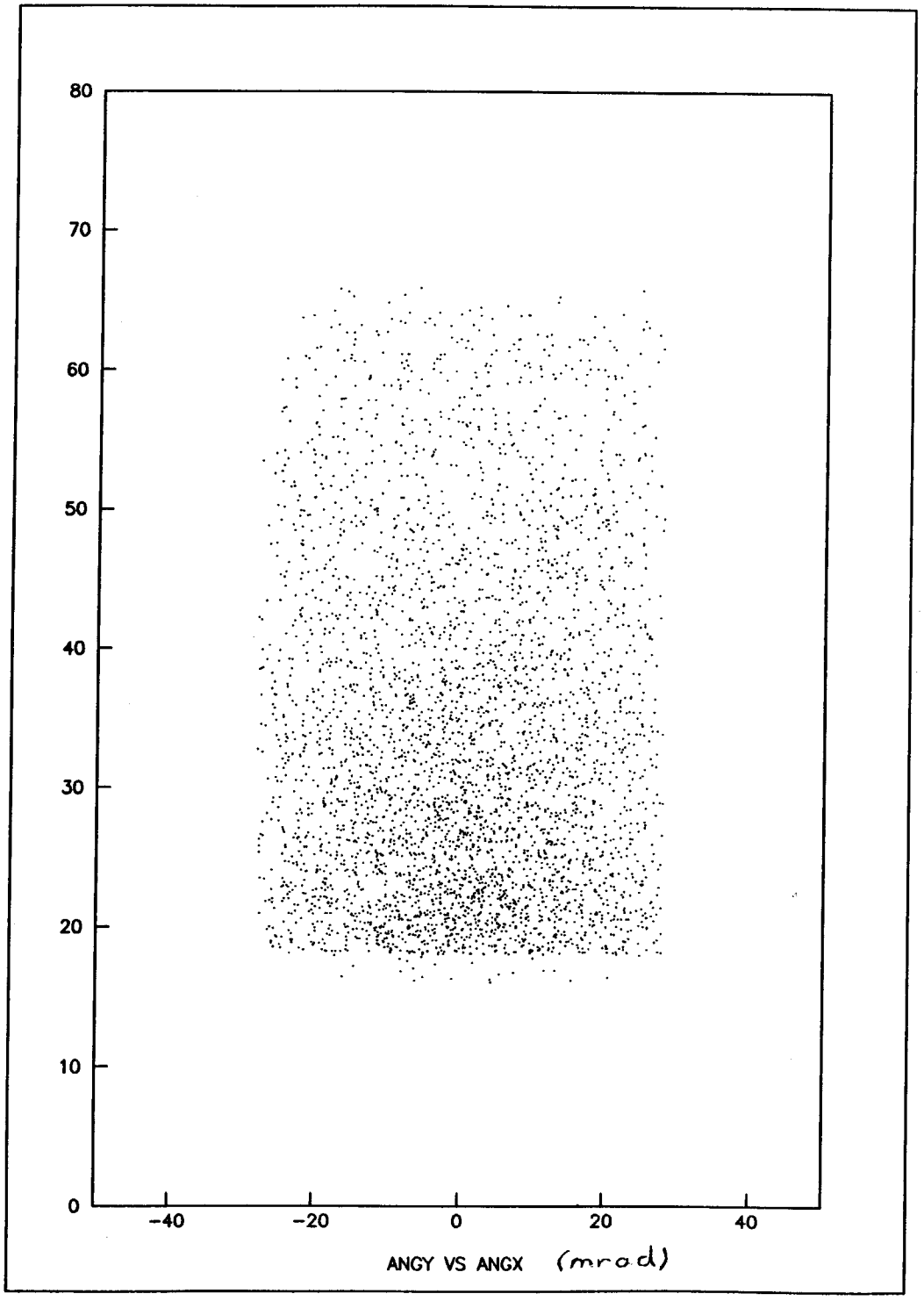

Figure 9.

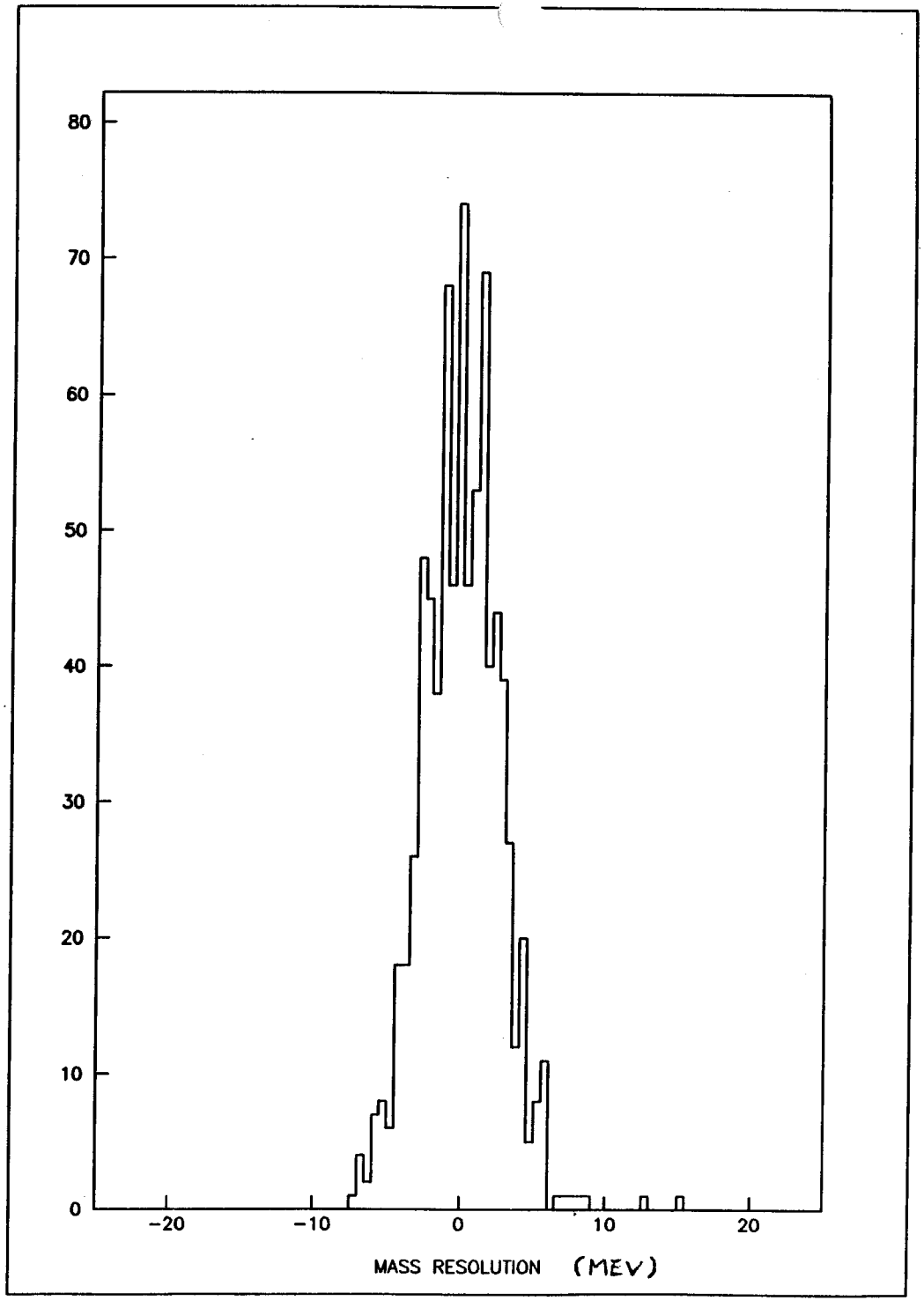

Figure 10.

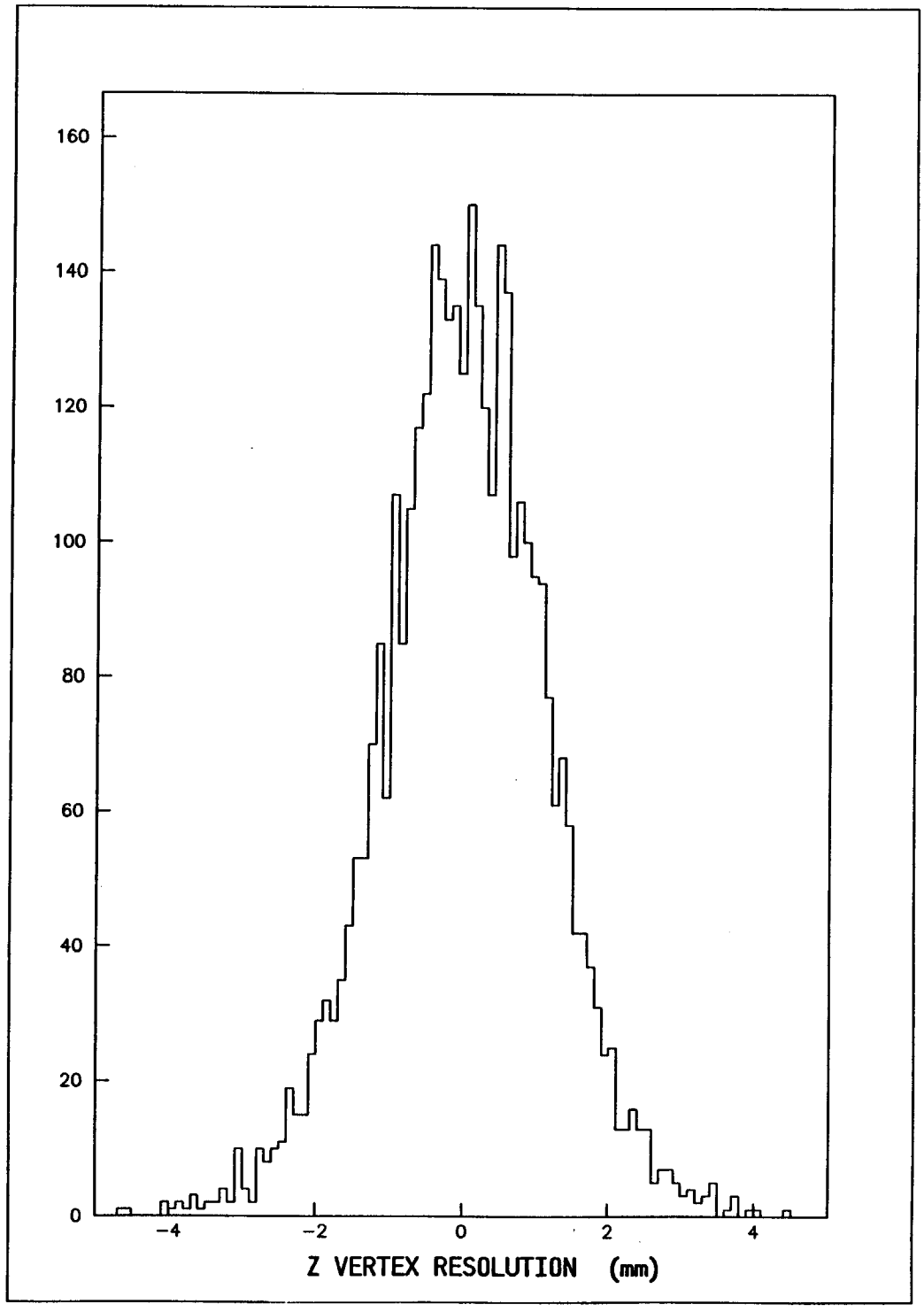

Figure 11(a).

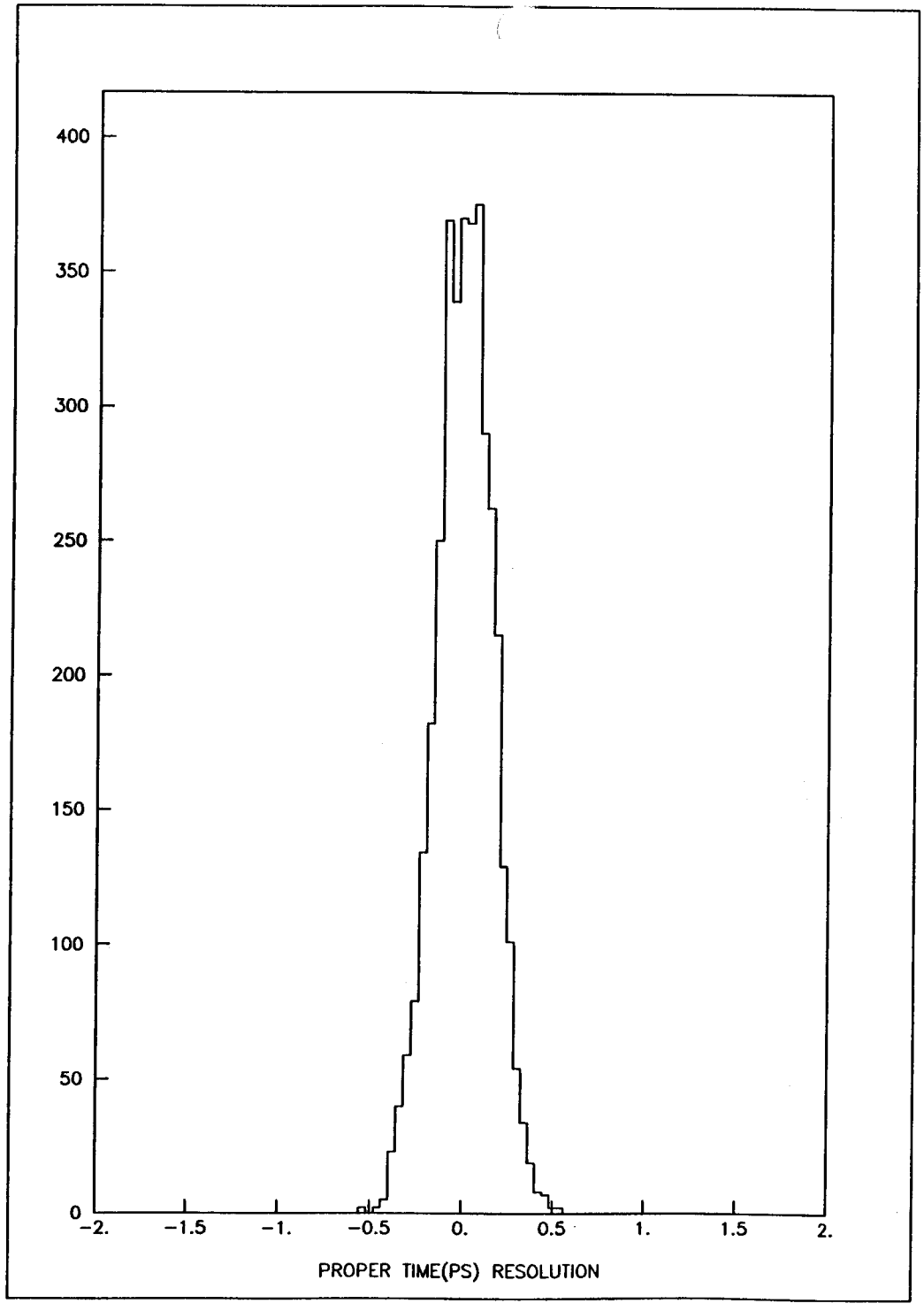
400
350
300
250
200
150
100
50
0
-2.
-1.5
-1.
-0.5
0.
0.5
1.
1.5
2.
PROPER TIME(PS) RESOLUTION

Figure 11(b).

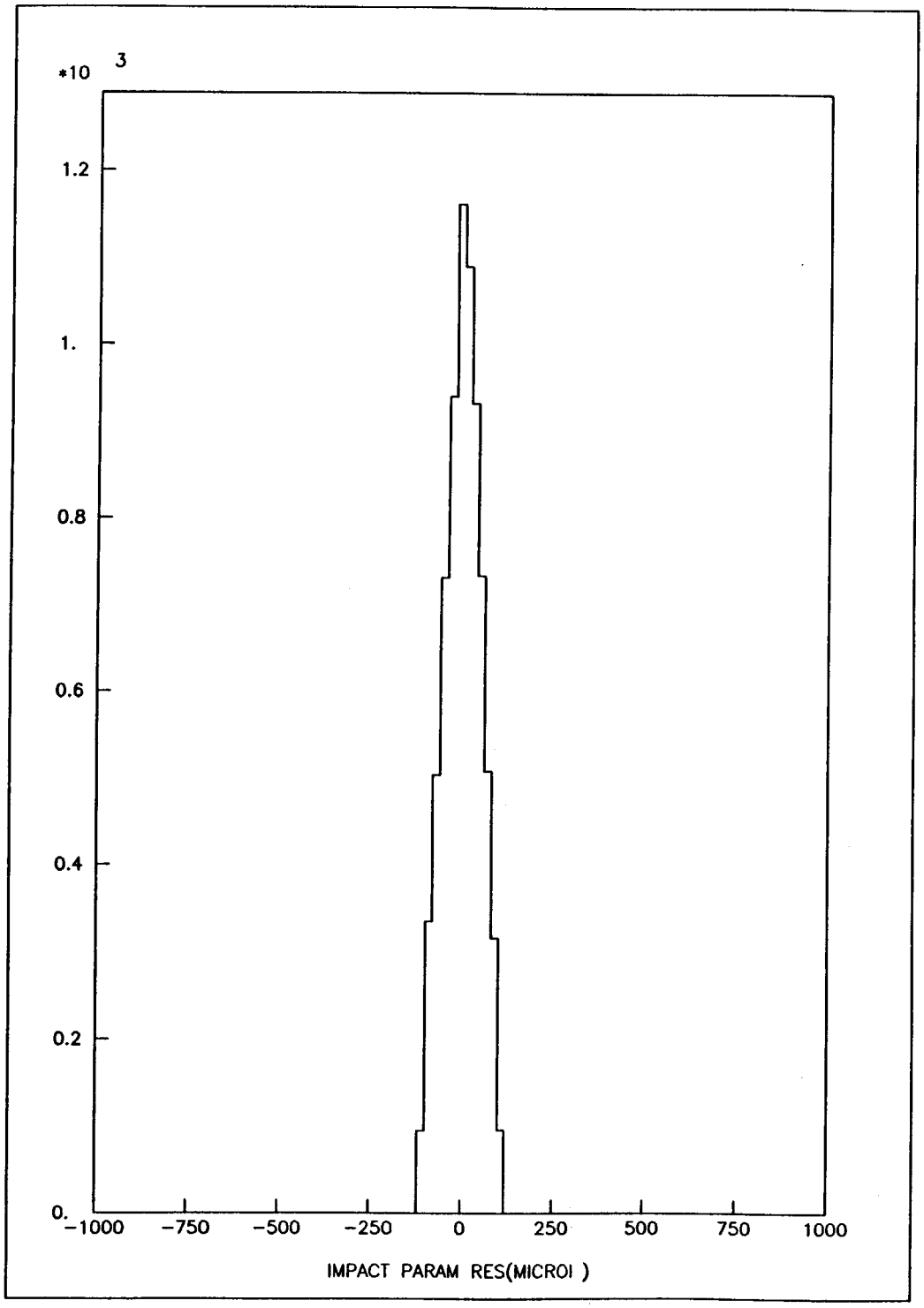
*10 3
1.2
1.
0.8
0.6
0.4
0.2
0.
-1000
-750
-500
-250
0
250
500
750
1000
IMPACT PARAM RES(MICROI)

Figure 11(c).

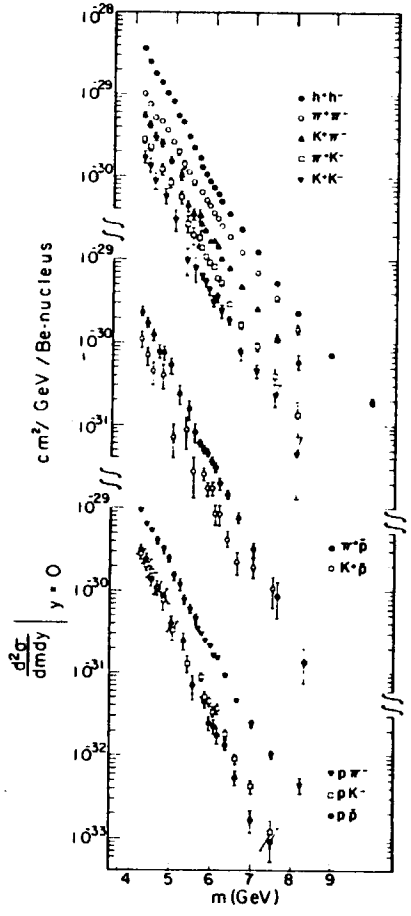

FIG. 2. The dihadron production cross sections $[d^2\sigma/dm\,dy]_{y=0}$ for hadrons and identified pairs of opposite charge vs mass m. The data are averaged over our rapidity acceptance which is peaked at $y \approx 0$ and includes the interval $-0.2 \leq y \leq 0.3$.

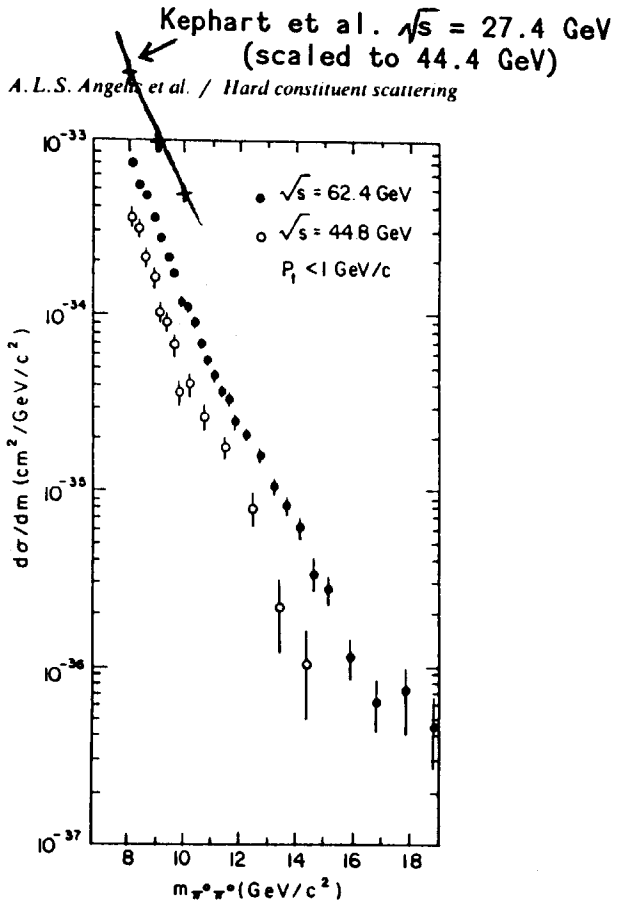

Fig. 5. $d\sigma/dm$ (as defined in eq. (1)) versus m for events with $P_T < 1.0$ GeV/c.

Figure 12.

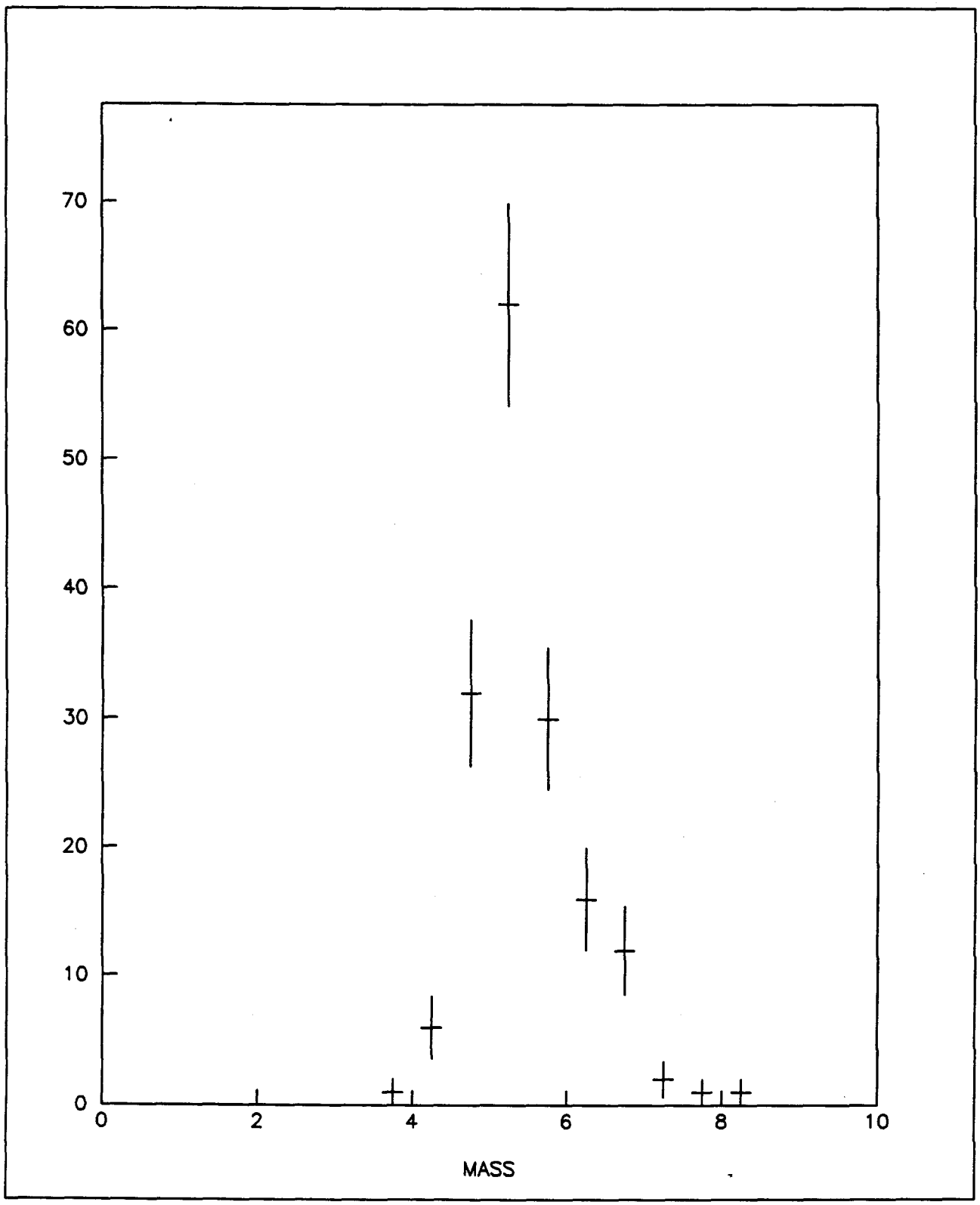

Figure 13.

FERMILAB PROPOSAL P-789

STUDY OF NON-CHARM DI-HADRON DECAY OF NEUTRAL B MESONS AND Λ_b

Spokesmen: D. M. Kaplan and J. C. Peng

Participants: D. M. Alde, H. W. Baer, T. A. Carey, J. S. Kapustinsky, A. Klein, M. J. Leitch, J. W. Lillberg, P. L. McGaughey, C. S. Mishra, J. M. Moss, J. C. Peng,
Los Alamos National Laboratory

C. N. Brown, W. E. Cooper, Y. B. Hsiung,
Fermilab

D. M. Kaplan, R. S. Preston,
Northern Illinois University

M. L. Barlett,
University of Texas

ABSTRACT

We propose using an upgraded version of the E605/E772 spectrometer to measure a large sample ($\sim 10^3$ events) of two-body, two-prong decays of neutral b-quark hadrons. An integrated luminosity of 1.1×10^{41} cm^{-2} combined with $\sim 2\%$ acceptance at the B mass gives an effective luminosity of 2×10^{39} cm^{-2}. The excellent mass resolution ($\sim$3 MeV at m = 5.3 GeV) and high-rate capabilities of this spectrometer are uniquely suited to this objective. Masses and lifetimes of the B_d^0, B_s^0, and Λ_b^0 will be determined, as well as branching ratios for two-body non-charm decay into π, K, and protons. Major upgrades to the spectrometer are: a) addition of a vertex array employing silicon strip detectors, b) refurbishing of the E605 ring-imaging Cherenkov detector, and c) construction of a new station of high-precision, high-rate drift chambers (6 planes).

I. PHYSICS MOTIVATIONS

This proposal is motivated by two important recent discoveries in b-quark physics. The first is the observation[1,2] of unexpectedly large mixing in the neutral meson system, B^0 and $\bar{B}^0$. This result suggests the possibility that CP-violation could be observed in a high-statistics study of B^0 meson decays. The second discovery[3] is that the amplitude for b $\rightarrow$ u conversion is surprisingly large. The absence of non-charm decay of B mesons led to the determination $0 < |V_{ub}| \leq 0.008$ by the Particle Data Group[4] in 1986. This situation was changed by the recent discovery by the ARGUS[3] group of the decays $B^+ \rightarrow \bar{p}p\pi^+$ and $B^0 \rightarrow \bar{p}p\pi^+\pi^-$. Combined with previous data, the reported branching ratio of $(3.7 \pm 1.3 \pm 1.4) \times 10^{-4}$ for $B^+ \rightarrow \bar{p}p\pi^+$ and $(6.0 \pm 2.0 \pm 2.2) \times 10^{-4}$ for $B^0 \rightarrow \bar{p}p\pi^+\pi^-$ implies[5] $0.07 < |V_{ub}|/|V_{cb}| < 0.19$. The large magnitude of V_{ub} suggests that the branching ratios for $B^0_{d,s} \rightarrow h^+h^-$ non-charm decays could be of order 10^{-4} to 10^{-5}. Such di-hadron decays have not yet been observed experimentally. It is clear that the observation of non-charm h^+h^- decays will have important impact on the determination of V_{ub}.

Even though the existing data on B meson production and decay originate almost exclusively from e^+e^- collider experiments, the luminosity at existing colliders severely limits the production rate. An alternative[6] is the detection of b decays in fixed-target experiments at FNAL, where the production rate of b-quark hadrons is orders of magnitude greater than that at current e^+e^- colliders. The crucial questions to be answered of course are: (a) How many b's can be produced? and (b) To what extent can non-b-physics events be rejected from the data set. We propose that the existing E605/E772 spectrometer, characterized by its superb mass resolution and high-rate capability, is uniquely suitable for detecting the hadron pairs $(\pi^+\pi^-, K^+K^-, p\bar{p}, \pi^\pm K^\mp, p\pi^-, \bar{p}\pi^+, pK^-, \bar{p}K^+)$ emitted in the decays of neutral B mesons (B_d, B_s) and b-baryons $(\Lambda_b, \bar{\Lambda}_b)$. Based on the total number of b decays estimated for a single fixed-target running period — of order one thousand — we will be able to measure the masses of the B^0_s and Λ^0_b for the first time and accurately determine their lifetimes.

Beyond these goals it is interesting to note that measurements of the time dependence of $\Gamma(B \rightarrow h^+h^-)$ could lead to the observation of $B^0 - \bar{B}^0$ mixing and CP-violation provided

that a large production asymmetry exists between B^0 and $\bar{B}^0$. It is straightforward to derive[7]

$$\Gamma(B_{d,s}^{neutral} \to K^-\pi^+) \quad \propto \quad e^{-\Gamma_{d,s}t}\left(\frac{1}{2}(1+e^{-\Delta\Gamma_{d,s}t}) - \frac{\bar{N}-N}{\bar{N}+N}cos\Delta m_{d,s}t\right) \qquad (1)$$

where $N, \bar{N}$ are the numbers of B^0, $\bar{B}^0$ produced.

Equation (1) shows that even without flavor tagging of the B mesons, it is possible to observe an oscillatory component in the time evolution of $B^0 \to K^{\mp}\pi^{\pm}$ decay. Such an observation could lead to the determination of Δm and $(\bar{N}-N)/(\bar{N}+N)$. Unfortunately, it is difficult to predict the best kinematic region for a large production asymmetry.

The asymmetry in $B^0 \to K^{\mp}\pi^{\pm}$ decays is also sensitive to CP-violation. Bigi and Stech[7] obtain the following relation

$$\frac{Yield(K^-\pi^+)_B}{Yield(K^+\pi^-)_B} = \frac{1+Af(t)}{1-Af(t)}\frac{|Ampl(\bar{B}\to K^-\pi^+)|^2}{|Ampl(B\to K^+\pi^-)|^2} \qquad (2)$$

where $A = (\bar{N}-N)/(\bar{N}+N)$, and $f(t) = 2e^{-1/2\Delta\Gamma t}/(1+e^{-\Delta\Gamma t})cos\Delta mt$. CP-violation is established if the second factor in Eq. (2) is different from unity. For $B_d^0 \to K^{\mp}\pi^{\pm}$ decays, CP asymmetry as large as 10% could occur.[7]

II. PROPOSED MEASUREMENTS

The goals of this experiment are the following:

(1) To determine the values (or upper limits) of the branching ratios of the following decays:

(a) $B_d \to \pi^+\pi^-$

(b) $B_d \to K^+K^-$

(c) $B_d \to p\bar{p}$

(d) $B_d \to \pi^\pm K^\mp$

(e) $B_s \to \pi^+\pi^-$

(f) $B_s \to K^+K^-$

(g) $B_s \to p\bar{p}$

(h) $B_s \to \pi^\pm K^\mp$

(i) $\Lambda_b \to p\pi^-$

(j) $\Lambda_b \to pK^-$

(k) $\bar{\Lambda}_b \to \bar{p}\pi^+$

(l) $\bar{\Lambda}_b \to \bar{p}K^+$

None of these decays has been observed.

(2) To search for B_s and Λ_b.

Neither the B_s nor the Λ_b has been seen. This experiment could lead to the first observation of these particles.

(3) To measure the mass and lifetime of B_d, B_s and Λ_b.

The Si strip vertex detectors, necessary for rejecting the backgrounds originating from the target, will determine the time evolution of various decays. We also expect excellent mass resolution ($\sigma \simeq 3$ MeV at mass $\cong 5$ GeV) with the E605/E772 spectrometer.

(4) To study the dynamics of b-quark production in hadron-hadron collisions.

We expect to measure the cross section and the x_F and p_t distributions of B_d production in p+W collisions at 800 GeV.

2 Introduction

We propose to build a small, $\sim 4\pi$ special purpose magnetic detector for the Tevatron. See Fig. 1. The detector design has been optimized to identify prompt electrons and secondary vertices coming from bottom quark decays. It has very good mass resolution for charged decay modes which is necessary in discriminating bottom from combinatorial backgrounds. It has no hadron calorimetry. Only modest particle identification comes from dE/dX measurements. The main emphasis of this detector is to:

(a) Detect the large bottom cross section at the Tevatron which in general is isotropically produced and quite soft. See Fig. 2.

(b) Provide complete electron coverage down to $p_t \sim 1\ GeV/c$ over ± 4 units of pseudo-rapidity. The lepton spectrum is soft and peaks at $p_t \sim 1\ GeV/c$. See Fig. 3.

(c) Provide complete efficient triggering on electrons over the full solid angle of the detector.

(d) Demonstrate the principle of tagging a large sample of bottom mesons in a hadron collider environment using a vertex detector.

(e) Demonstrate the ability to count charged prongs from a secondary vertex. This permits the reconstruction of charged exclusive decay modes with very little background. Investigate the ability to identify tertiary vertices (i.e. the vertex from bottom cascade to charm).

(f) Provide excellent rejection of pairs from gamma conversions.

2.1 Mixing/CP Violation

In the standard six-quark electroweak theory, the particle states to which the weak intermediate vector bosons couple are mixtures of the physical particle states. The charged weak current is given by

$$J^{\mu} = (u, c, t)\gamma^{\mu}(1+\gamma^5)U \begin{pmatrix} d \\ s \\ b \end{pmatrix}$$

where u, c, t are charge $2/3$ quark fields and d,s,b are the -$1/3$ fields. The 3×3 unitary matrix U is characterized by 3 Cabibbo-like mixing angles and a phase factor. This parametrization is due to Kobayashi and Maskawa and is given by

$$U = \begin{pmatrix} V_{ud} & V_{us} & V_{ub} \\ V_{cd} & V_{cs} & V_{cb} \\ V_{td} & V_{ts} & V_{tb} \end{pmatrix} = \begin{pmatrix} c_1 & s_1 c_3 & s_1 s_3 \\ -s_1 c_2 & c_1 c_2 c_3 - s_2 s_3 e^{i\delta} & c_1 c_2 c_3 + s_2 c_3 e^{i} \\ -s_1 s_2 & c_1 s_2 c_3 + c_2 s_3 e^{i\delta} & c_1 s_2 c_3 - c_2 c_3 e^{i\delta} \end{pmatrix}$$

where $s_i = \sin\theta_i$ and $c_i = \cos\theta_i$ for $i = 1, 2, 3$. The V_{ij}'s denote the coupling of the quarks $q_i q_j$'s to the W^{+-} intermediate vector bosons. The unitarity of the matrix prevents flavor changing neutral currents. The precise measurment of $s_1 = 0.2270 \begin{smallmatrix} -0.011 \\ +0.0104 \end{smallmatrix}$ comes from comparing $O^+ \to O^+$, nuclear β decay of O^{14} and AL^{26m} with μ decay. However, until recently, values of the K-M angles s_2 and s_3 could be as large as 0.5. New knowledge of the angles s_2 and s_3 comes from measurements of the long B meson lifetime and the improved limit on $R = \Gamma(b \to u)/\Gamma(b \to c)$. The value of $\tau_b = (1.11 \pm 0.16) \times 10^{-12}$s is longer than charmed hadron lifetimes despite the enhancement expected in the rate of b decay from $(m_b/m_c)^5$. This implies a very small mixing angle to the second quark generation. The limits on R are presently best determined from the shapes of lepton spectra from CLEO and CUSB groups. They find R less than about 5% which says the b quark is almost completely decoupled from the first generation of quarks. Together these measurements determine s_2 to be very small and s_3 to be consistent with zero. The contour plot in the $s_2 - s_3$ plane is shown in Fig. 4 for various top quark masses and B parameter values. (The latter parametrizes the matrix element of the $\Delta S = 2$ operator. $B = 1$ for vacuum insertion. Most estimates of B are included in the range 0.2 to 1.5). In addition, further constraints arise from a study of the CP-violating mixing parameter ϵ_m. The box diagram of Fig. 5 gives the main short distance contribution to ϵ_m and is thought to be reliable. This leads to a contour in the $s_2 - s_3$ plane for given B, m_t, and τ_b and is seen in Fig. 4. Ginsparg et al argue the small $s_2 s_3$ determined from the τ_b require the top mass to be large. However uncertainties in the B parameter calculations weaken this statement. This point is illustrated in Fig. 6. Experimental information from UA1 regarding the top quark seems unclear and therefore does not provide a mass window around the top quark.

The box diagram in Fig. 5 leads to $B^o \bar{B}^o$ mixing from either B_d or B_s. The amount of mixing depends on the ratio of the $B\bar{B}$ mixing amplitude ΔM and the

total b decay width Γ_b. The decay widths $\Gamma(B_s^o)$ and $\Gamma(B_d^o)$ are similar but the mass differences differ by a factor of $(\sin\theta_c \sim 0.23)^2$. The mass mixing in the B_d system is expected to be at most a few percent while in the B_s system substantial mixing is possible. For a given top quark mass and τ_b fixed, *the range of s_2 allowed is quite narrow.* As a measure of mixing we define

$$r(B_s) = \Gamma(B_s^o \to l^+\nu x)/\Gamma(B_s^o \to l^-\nu x)$$

The value of $r(B_s)$ could be as large as one. From the Mark-II a limit on this ratio at PEP gives $r_{continuum} < 0.12$. This excludes full mixing in B_s and by including the amount of B_s expected in the continuum at PEP energies, typically 0.15, the theoretical value becomes $r(B_s) < 0.08$, lower than the Mark-II limit. Mixing leads to like sign dileptons and a convenient measure is

$$R_{ll}(bb) = N^{++} + N^{--}/N^{+-}$$

Estimates of $R_{ll}(bb)$ range from $10^{-3} - 0.02$ for B_d to $0.12 - 0.75$ for B_s. The stated range represents the uncertainties from the B parameter, where a larger B gives a larger $R_{ll}(bb)$. The prospects for observing mixing look good.

2.2 Measurement of $b \to u$

In the standard six quark model the bottom quark can decay to either a charm or up quark and a W^-. The best determination of the K-M matrix element $|V_{bu}|$ has come from the study of the leptonic decay of the virtual W^-. The CLEO group has studied the momentum spectrum of leptons from $B \to Xl\nu$. The CUSB group studied just the electrons. The mass of the charm quark is $m_c = 1.8\ GeV/c^2$ and that of the up quark is $m_u = 0.33\ GeV/c^2$. Therefore the shape of the electron momentum spectrum from $B \to ce\nu$ is softer than the $B \to ue\nu$. The end-points are 2.35 and 2.55 GeV respectively. Experimently the decay spectrum is completely consistent with only $B \to ce\nu$. The published 90%-confidence-level upper limit on $\Gamma(b \to ul\nu)/\Gamma(b \to cl\nu)$ of 4% by CLEO and 5.5% by CUSB. When combined with the b lifetime expression

$$\tau_b^{-1} \sim G_F^2 m_b^5/192\pi^3 \left[2.95|V_{cb}|^2 + 6.33|V_{ub}|^2\right]$$

this gives $|V_{ub}| < 0.0051$ and $|V_{cb}| = 0.044 \pm .005$. This says the b quark decouples from the first two generations with the coupling to the first being extremely small

though still consistent with other measurements and constraints on the K-M mixing angles.

Recently, the model of Altarelli et al. being used to describe the end-point behaviour has encountered some problems. It has been suggested that the limits are too stringent. The more reasonable limits are probably around 8%.

It has been pointed out that calculations of partial rates to the exclusive mode $B \rightarrow \rho^o e^- \nu_\mu$ permit the determination of $|V_{ub}|$. This mode is about 1% of the total $b \rightarrow u$ rate and is thought to be reliably calculated. It is this mode and $B \rightarrow \rho\pi$ which we seek to measure in this experiment being proposed.

3 CP/Mixing Experimental Estimates

3.1 Mixing with Like Sign Dileptons

In the semileptonic decay of the b quark, $b \rightarrow e$ and $\bar{b} \rightarrow \bar{e}$, the sign of the lepton determines whether the parent is particle or antiparticle. The signal for mixing will be the presence of like sign pairs. The mixing parameter is defined as

$$r \equiv \frac{N^{++} + N^{--}}{N^{+-} + N^{-+} + N^{++} + N^{--}}$$

Consider the experimental situation. We take the bottom cross section to be 25 μb at 2 Tev. The acceptance times p_t cut is $\sim$ .9 per B meson. So the useable cross section $\sigma_{b\bar{b}}$ is $25 \times .81 \sim 20\mu b$. For the electron trigger we fold in the branching ratio, 12%, the probability the p_t of electron is > 2 GeV/c , and the impact parameter requirement of $\frac{\delta}{\sigma} > 3$ cuts $\sim$ 50%. Therefore, the cross section for useable dielectrons is about 8 nb. The track acceptance reduces this to about 5 nb assuming a possible worst case of 10% loss on each track.

The running period of two weeks at a luminosity of $5 \times 10^{31} cm^{-2} sec^{-1}$ gives $80 pb^{-1}$ total integrated luminosity. This gives 4×10^5 di-electrons. The 2σ limit is then simply $\frac{2}{\sqrt{N}}$ or $\sim$ 0.003. The standard model prediction for the range of r is $0.01 - 0.2$.

3.2 CP Violation with Dileptons

If CP is violated a slight preponderance of one species is expected. The asymmetry

parameter is

$$a = \frac{N^{++} - N^{--}}{N^{++} + N^{--}}$$

Using the number of di-electrons calculated in the mixing section, and assuming a standard model value of r between $0.01 - .2$, we obtain a like sign sample of $6400 - 128,000$ events. At the 2σ level, this gives a best limit of $.025 - .006$. The standard model is at the $10^{-3} - 10^{-4}$ level, but "new physics" scenarios do allow a $\sim 10^{-2}$. If we assume a high luminosity run of $5 \times 10^{31} cm^{-2} sec^{-1}$ for 10^7 sec, then limits are between $.01 - .002$, and this does begin to exclude the larger nonstandard model predictions.

3.3 CP Violation with Exclusive Modes

The basic idea is to look for a difference between $\Gamma(B^o \to f)$ and $\Gamma(\bar{B}^o \to \bar{f})$. The exclusive decay asymmetry turns out to be .

$$|A| = \frac{\Gamma(B^o \to f) - \Gamma(\bar{B}^o \to \bar{f})}{\Gamma(B^o \to f) + \Gamma(\bar{B}^o \to \bar{f})}$$

The experiment must discriminate between B^o and $\bar{B}^o$. This means tagging the bottom system on the other side with a lepton.

3.3.1 $B \to \psi K_s^o$

This mode is popular because the signature is clean, and the B meson is completely reconstructable. The expected value of the asymmetry $A \sim 4 - 12\%$. Other factors to fold in are the branching ratios of $B \to \psi K_s^o \sim 5 \times 10^{-4}$, $\psi \to \mu\mu = 0.074$ and $K_s \to \pi^+\pi^- = .68$. A conservative estimate of the trigger efficiency reduces this rate by a factor of 0.02. Including a 50% efficiency for K_s and 70% for ψ, the useful cross section is $2 \times 10^{-36} cm^2$, and gives about 160 events in $80 pb^{-1}$ of integrated luminosity. At the 2σ level, the minimal A measurable is $\sim 15\%$.

The transverse momentum spectrum of the μ pairs from the ψ and the π's from the K_s^o averages about a few GeV/c. This is hard enough that a small sample of these events would be reconstructed. A longer run, of $10^7 sec$ would give ~ 960 events and lower the minimal A measurable to 6%.

3.3.2 $B_s \rightarrow D^o\phi$

This is an interesting mode that has a large asymmetry, $\sim 60\%$, which does not suffer from competing modes from B_s with the opposite sign asymmetry. Consider $B_s \rightarrow D^o\phi$ where $D \rightarrow K\pi$, 2% and $\phi \rightarrow KK \sim 50\%$ of the time. The B_s is produced $\sim 15\%$ of the time and $B_s \rightarrow D\phi$ has a branching ratio of about 2×10^{-4}. Including the electron tag of 0.02 and a reasonable K identification probability of 50%, a useful cross section of about $10^{-38} cm^2$ gives about 1 event. It is clear a higher luminosity run would be required to see this decay mode. The momentum versus rapidity is shown in Figure 7 for kaons coming from $D \rightarrow K$ and $\phi \rightarrow KK$.

4 The $B \rightarrow \rho\pi$ and $B \rightarrow \rho^o e\nu$ Estimates

4.1 $B \rightarrow \rho e\nu$

The $B \rightarrow \rho e\nu$ decay mode has the advantage that it is large relative to the overall $b \rightarrow u$ rate and that it is a mode this detector will trigger on. The obvious disadvantage is that it does not reconstruct to the B meson mass and the ρ is a wide resonance. The background and signal was studied in detail by Monte Carlo. The events were generated using Isajet in the p_t range 5-10 GeV/c. The branching ratio of the exclusive mode $B \rightarrow \rho e\nu$ X is about 10^{-4}.

In the analysis chain, the event is first tagged with an electron of $p_t > 2$ GeV/c and an impact parameter significance of $\delta/\sigma > 3$. The two charged prongs were assumed to be identified cleanly. Both prongs were kept within ± 3 units of rapidity to enable a momentum measurement and each must have a momentum > 1 GeV/c so as to reduce multiple scattering effects. The major background comes from $B \rightarrow De\nu$ and $\bar{D} \rightarrow K\pi\pi$ and the $K \rightarrow K_L$ for example. The sum of the 2 prong decay modes have a branching ratio of about 5.5%. Some additional cuts were:

- reject an event if $K_s \rightarrow \pi\pi$ is present.
- reject an event if detectable 3rd vertex is present.

Additional cuts required the mass of the two charged prongs to be consistent with a ρ mass and if one prong was assumed to be a K, inconsistent with a D mass. The above cuts result in a signal to noise of about 1:20. A simple kinematic cut requiring the angle of one of the charged prongs relative to the B meson direction enhances

the signal by 10:1. It is concluded that the noise to signal ratio is about 2-3:1. From a data set taken in two weeks, 3000 events will be produced and 50 should survive the analysis cuts. A longer run of 3 months would make the signal quite evident.

The above estimates demonstrate that interesting physics with bottom requires many millions of events and collecting such a large sample is difficult to imagine at any other accelerator than the Tevatron. It is important to note that a more powerful detector would have trouble improving upon the above backgrounds the detection of π^o's coming from the B meson is very difficult at the Tevatron.

4.2 $B \rightarrow \rho\pi$

In $B \rightarrow \rho\pi$, the decay of interest is the 3 charged prong mode that reconstructs to the bottom mass. Unfortunately the branching ratio is the product of roughly 10^{-2} for the KM matrix elements and $\sim 10^{-3}$ for the rate relative to $b \rightarrow u$. This must now be combined with the trigger efficiency based on the single electron trigger. The effective branching ratio is then less or equal to 3×10^{-7}. For the 3 month run at a luminosity of 5×10^{31}, this is about 60 events produced and recorded. This rate should be measurable.

The background for this decay mode has been studied briefly using a small sample of Monte Carlo events. Bottom was generated with a p_t between 1 and 20 GeV/c and a rapidity between $\pm$ 6 units. First, a momentum cut of 0.5 GeV/c is applied to all charged tracks to reduce background effects from large multiple scatters. The $\pm$ 3 rapidity cuts have been applied to all charged decay products. In addition a track is assumed to be reconstructable only if its momentum is greater than 100 Mev/c. Now the remaining events with 3 charged prongs are analysed to see if they produce a rho mass, which is defined to be 770$\pm$ 300 Mev/c. If a ρ mass is found, the remaining prong is added to make a B meson mass. All tracks are assumed pions. The momentum resolution is $\delta p/p \sim \sqrt{(.001p)^2 + (.008)^2}$. Effects due to dip angle are included in the mass calculation. A candidate B meson must fall within 400 Mev/c of the average B meson mass. These cuts leave about 77% of the $B \rightarrow \rho\pi$ events.

The background comes from sources of 3 charged prongs at the vertex. The fraction of bottom decay modes which produce 3 charged prongs was estimated to be 4%. From a sample of 468 events produced, 149 pass the cuts up to the rho mass requirement on 2 of the prongs. One event out in the tail falls into the B mass region.

Taking into account the 4% for the branching ratios, this implies 0.04 events in the B meson mass region. Since the ratio of production is 10^5, the noise to signal ratio is about 10:1. After including the kaon identification from dE/dX measurements, and some kinematic constraints, a signal to noise of 1:1 seems attainable. The reconstruction probabilities not mentioned above are assumed to effect noise and signal equally. In addition the branching ratios for 3 prongs are just estimates and a more detailed analysis would not change the general conclusion.

Therefore it is concluded that this decay mode could be identified with a detector of this design.

5 General Description of the Detector

5.1 Introduction

The experimental design is driven by the need for a highly efficient detector which triggers on bottom events and provides sufficient information to reconstruct them in the complex environment of the Tevatron collider. The principle behind the design of this detector is to maximize the ability to reconstruct primary and secondary vertices as well as tag soft electrons from bottom decay over the full rapidity range in which bottom is produced. In addition, the size of the detector is kept small so as to minimize the cost and to allow easy installation into an existing intersection region.

This goal is achieved by a solenoidal spectrometer located between two dipole spectrometers. The chosen magnet geometry momentum analyses the charged tracks optimally, minimizes the size of the overall detector by matching the geometry of the detector volume to the laboratory angles of the tracks it is to encompass and provides uniform tracking over the full rapidity range.

A critical design feature involves the design of the silicon vertex detectors. Here it is believed that the combining of a central and forward piece, so necessary for utilizing the full luminosity, does not reduce the effectiveness of either system. In other words, the impact parameter resolution over the forward rapidity range is not reduced by the presence of the central silicon barrels. Clearly a major design feature is that the entire silicon vertex detector is inside the Tevatron vacuum vessel. This is absolutly necessary for tracing the low momentum charged decay products of the bottom mesons.

The principle for charged particle tracking is the same for both large and small

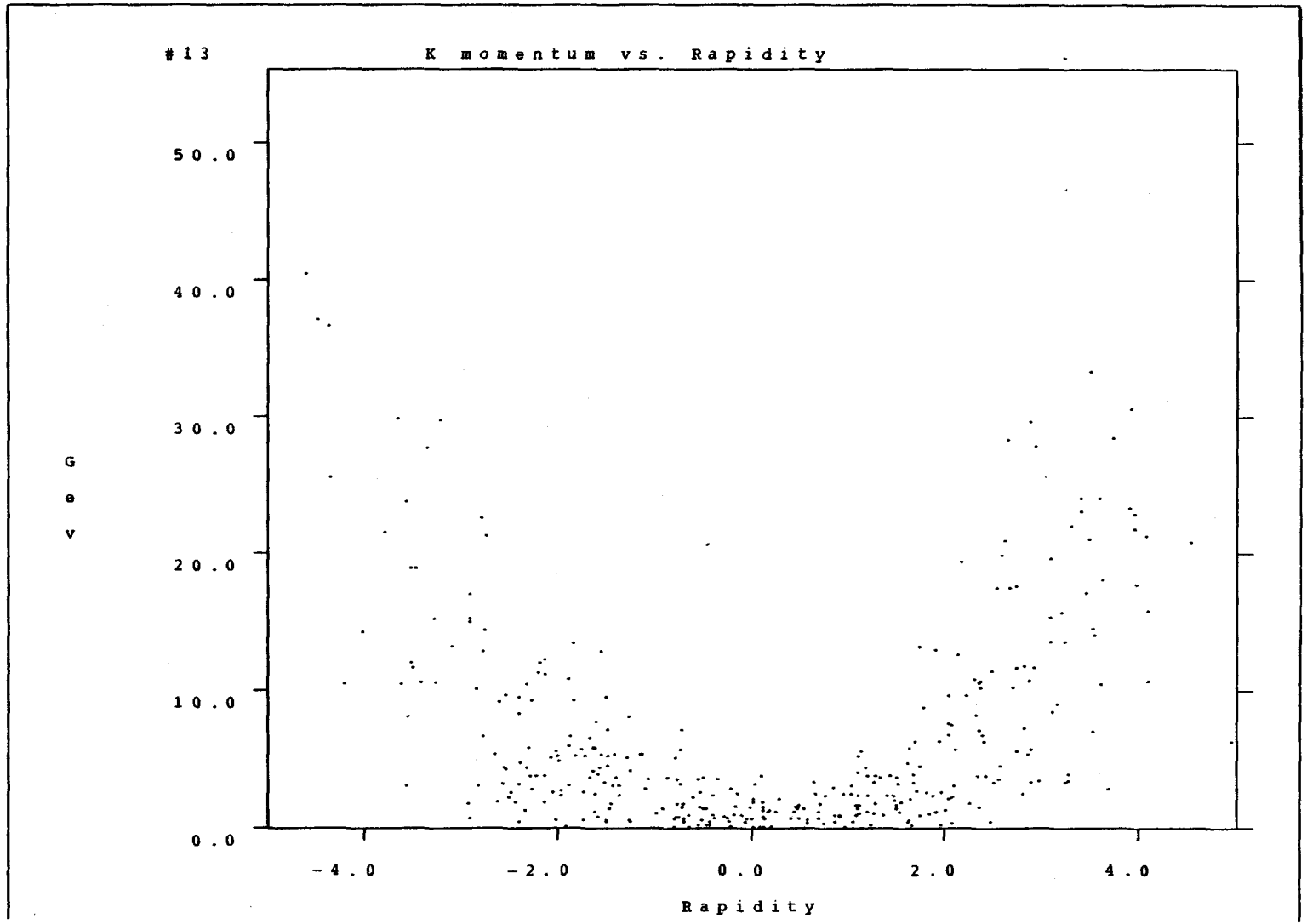
#13
K momentum vs. Rapidity
50.0
40.0
30.0
20.0
10.0
0.0
Gev
-4.0
-2.0
0.0
2.0
4.0
Rapidity

Figure 7

APPPENDIX A

Backgrounds to P789 from D Decays

The backgrounds from the decays of a pair of D-mesons to fake a $B \rightarrow \pi^+\pi^-$ decay have been studied in an earlier report.[1] However, only two-body and three-body decays of $D^+ - D^-$ pairs have been considered. We have recently extended the Monte-Carlo codes to include four-body decays as well as decays from $D^\circ - \bar{D}^\circ$, $D^\pm - D^\circ$ pairs. The results of these calculations are presented in this note.

Table I lists the branching ratios for various decay channels of D-mesons we included in the Monte-Carlo code. The three-body and four-body decays have branching ratios several times greater than two-body decays. Furthermore, these branching ratios are weighted by a large combinational factor which accounts for the fact that any of the pions in the decay channels can participate in a "fake-B" pair. Table II lists the "effective branching ratios" for a pair of D mesons to produce a pair of pions in various combinations of decay channels. Table II shows that decay channels involving four bodies have significantly larger "effective branching ratios" than the other channels.

Some details of the Monte-Carlo codes used in the simulation of D-meson decay background were given in Ref. 1. The code used in the present calculations includes the following modification: (1) D mesons can decay to four-body final states with a momentum distribution of the pion given by phase space. (2) The different lifetimes of charged and neutral D mesons are taken into account. (3) The acceptance of the pion-pair in the spectrometer is calculated in a more realistic fashion than in Ref. 1. The results of the calculations are summarized in Table III which lists the probability for a pion-pair emitted in various D-pair decay channels to resemble a real B-meson decay. The criteria for an accepted pion-pair are (1) 5.3 GeV < mass < 5.305 GeV, (2) Z (vertex) > 5 mm, (3) distance of closest approach between the two tracks is less than 100 μm, (4) both pions are accepted by the P789 spectrometer. The efficiency of these various requirements in rejecting the D-meson decay background is shown in Table IV. It is concluded that the mass cut and the spectrometer acceptance cut provide the most powerful rejection of the D-meson decay backgrounds. The extremely small spectrometer acceptance for the pion pair can be understood from Fig. 1 which shows the angular distribution of the pion in the rest frame of the di-pion system. In order to simulate a relatively heavy B-meson (5.3 GeV), the pion pairs in general consist of one pion with large longitudinal momentum and another pion with low longitudinal momentum. In order words, the polar angles of the pions with respect to the di-pion frame is strongly peaked at forward and backward directions. The acceptance of the P789 spectrometer, on the other hand, is centered around 90°. Therefore, the acceptance for the D-meson decay background is extremely small for the P789 experiment.

To find out the relative importance of the D-meson decay background in P789 with respect to the expected B-meson signals, we need to know the cross sections for D-meson pair production. The cross sections have been measured[2] at 400 GeV to be: $\sigma(D^+D^-) = 2.5 \pm 0.6\mu b$, $\sigma(D^+\bar{D}^\circ) = \sigma(D^-D^\circ) = 3.1 \pm 0.55\mu b$ and $\sigma(D^\circ\bar{D}^\circ) = 5.9 \pm 1.3\mu b$. These results imply that charged-D meson cross section is 11.2 μb. The measurements[3] at 800 GeV give $16.5 \pm 3.5\mu b$ as the charged D meson cross sections. We therefore scale the cross

section at 400 GeV by a factor of 16.5/11.2 to obtain the cross sections at 800 GeV for various D-meson pairs. Table V lists all the quantities we take into account to calculate the expected number of counts for the $B \rightarrow \pi^+\pi^-$ decays, the expected background from D-pair decay is between 0.05 and 0.10. We therefore conclude that the D-meson decay fackgrounds to not pose any problem for the experiment 789.

References

1. D. M. Kaplan, J. C. Peng, G. S. Abrams and I. E. Stockdale, Proceedings of the Workshop on Beauty Physics, Fermilab, 1987.
2. M. Aguilar-Benitez *et al.*, Phys. Letts. **189**, 476 (1987).
3. S. Rencroft, 6th International Conference on Physics in Collision, Chicago, 1986.

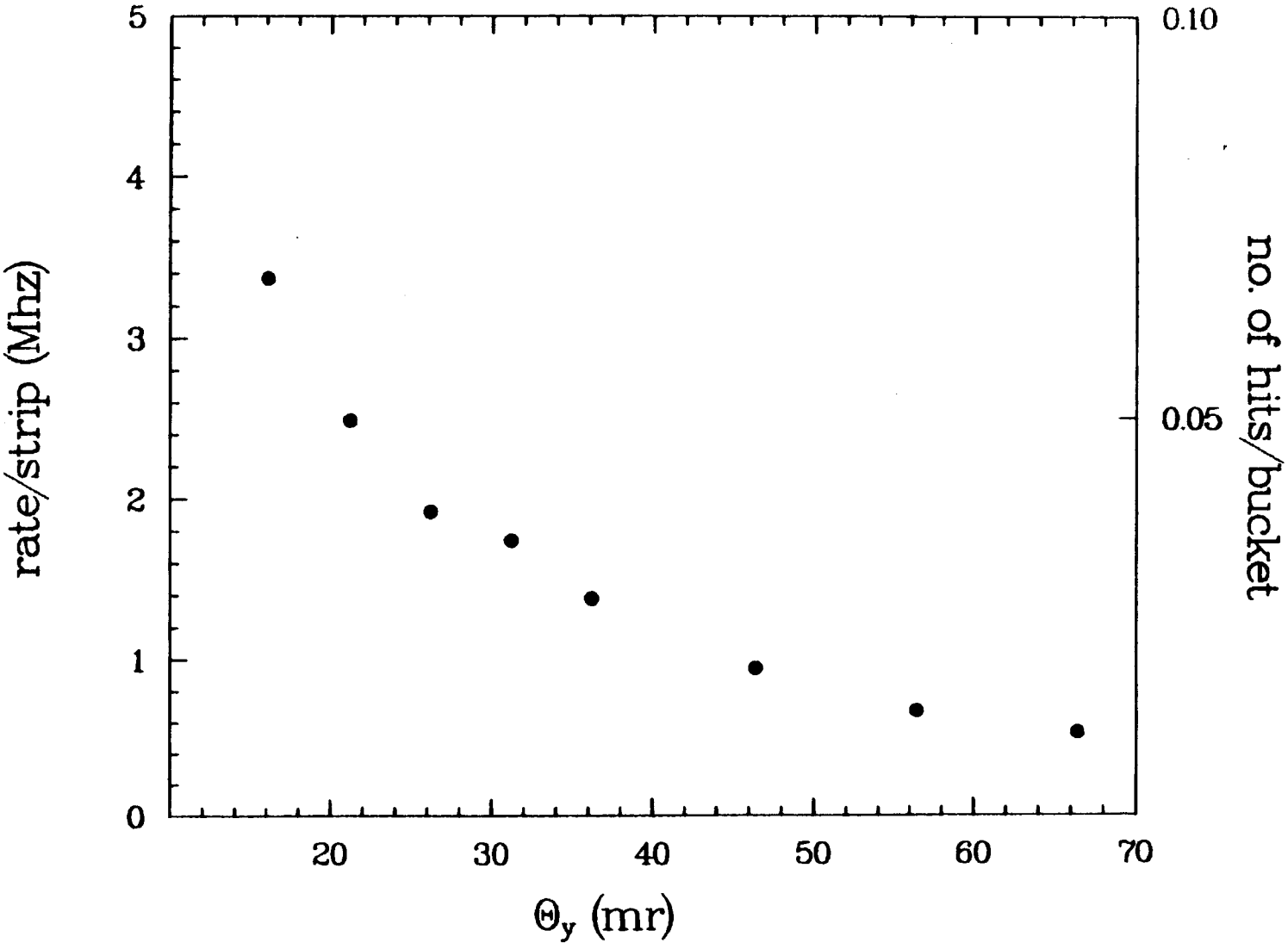
rate/strip (Mhz)
no. of hits/bucket
0
1
2
3
4
5
0.05
0.10
20
30
40
50
60
70
Θy (mr)

Figure 15.

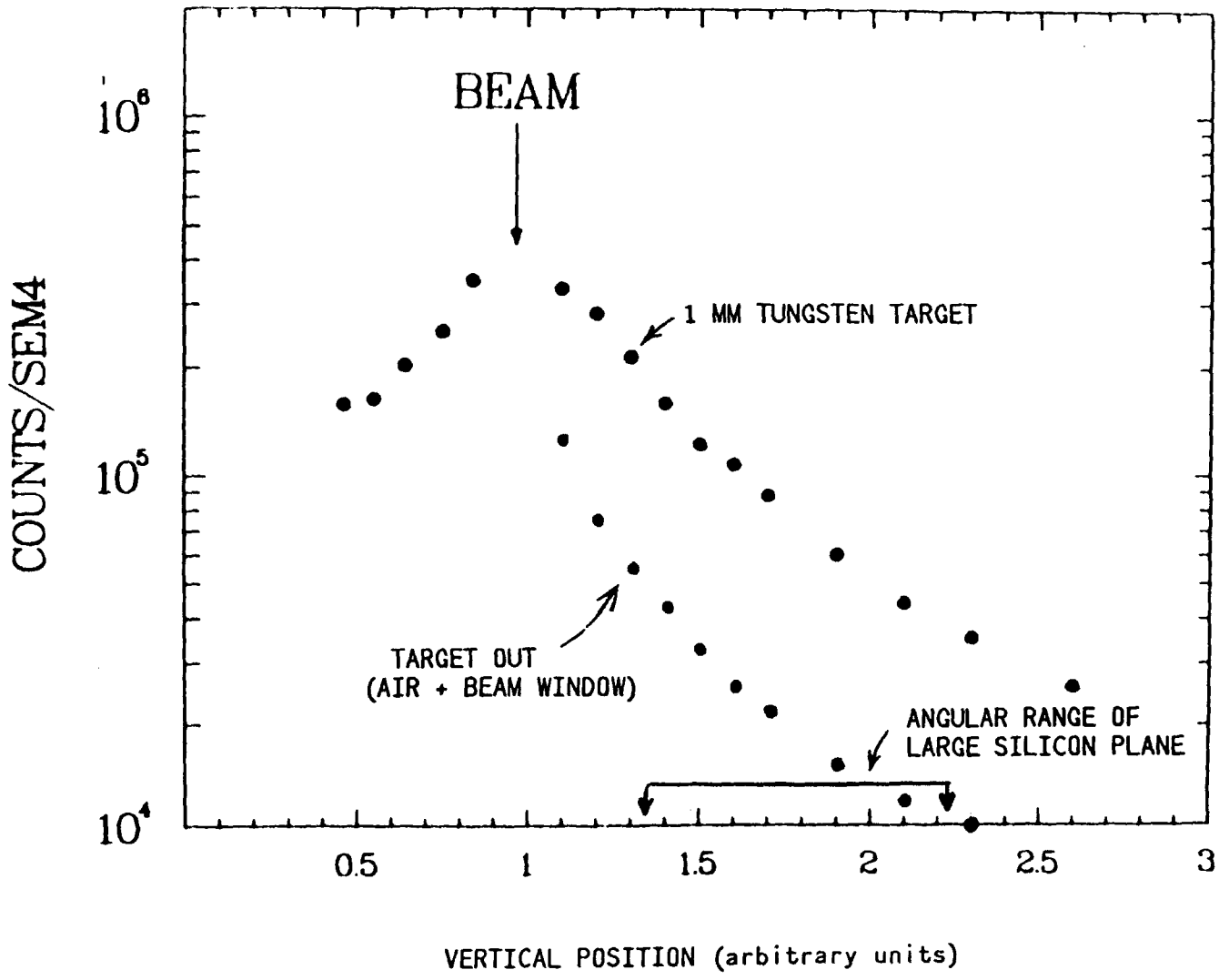
BEAM
1 MM TUNGSTEN TARGET
TARGET OUT
(AIR + BEAM WINDOW)
ANGULAR RANGE OF
LARGE SILICON PLANE
COUNTS/SEM4
10^6
10^5
10^4
0.5
1
1.5
2
2.5
3
VERTICAL POSITION (arbitrary units)

Figure 14.

APPENDIX B

Backgrounds to $B^\circ \to \pi^+\pi^-$ from $K^\circ\bar{K}^\circ \to \pi^+\pi^- X$ Decays

We consider here a source of background which contributes to the measurement of $B^\circ \to \pi^+\pi^-$ decays. Specifically, we consider the production of $K^\circ\bar{K}^\circ$ pair followed by the $K_s \to 2\pi$ decays. The K^+K^- pair cross section $d^2\sigma/dmdy$ at y=0 and 800 GeV beam energy can be parametrized as $ce^{-m/0.53GeV}$, where c = 6.0 x 10^{-27}/Gev/nucleon. (This represents the CFS cross section scaled down by a factor of 10 to agree with the CCOR and preliminary E605 data as discussed in the main text.)

In the Monte-Carlo simulation, we assume that the $K^\circ\bar{K}^\circ$ pair is produced with a Gaussian distribution in X_F ($\bar{X}_F$= 0.0, σ= 0.165) and a distribution in P_T as $e^{-P_T^2/7}$(< P_T >= 2.4 GeV). The $K^\circ\bar{K}^\circ$ pair then decays isotropically into $K^\circ, \bar{K}^\circ$, which subsequently decay into $\pi^+\pi^-$ isotropically.

The result of the Monte-Carlo simulation is shown in Table I. The various cuts are the following; Mass: 4.9 GeV< $M(\pi\pi)$ <5.5 GeV, Zcut: $0.5cm < Z < 2cm$, R(closest) cut:$R < 0.1mm$. Fig. 1 shows the $K^\circ\bar{K}^\circ$ mass distribution for the accepted events. A striking feature is the large acceptance of the P789 spectrometer for such background. Fig. 2 shows the angular distribution of the pion with respect to the di-pion frame. Contrary to the situation in the D-meson pair decays, the angular distribution is now nearly isotropic. An additional way to reject the background is to require that the summed momentum of the two pions point back to the target. By requiring $|\Delta y| \leq 2.5mm$, one gains an additional rejection factor of 4. Table II shows the expected yields for the $B \to \pi^+\pi^-$signal and the $K^\circ\bar{K}^\circ \to \pi^+\pi^- X$ background. The signal to background ratio is 25 to 1. We conclude that the $K^\circ\bar{K}^\circ$ background is more important than that from the D-meson pair decays, but still much smaller than the expected signal.

Table I. Efficiency of various cuts for rejecting pion pairs from $K^\circ\bar{K}^\circ$ decay.

Events thrown	4.9 < M < 5.5 GeV	Mass cut and Z > 5mm	Mass cut and Z > 5mm and $\gamma_{close} < 0.1mm$	Mass cut and accepted by spectrometer
1×10^6	9945	1107	22	442

Table II. Expected Number of Events Accepted by Experiment P789.

	$B \to \pi^+\pi^-$	$\pi^+\pi^-$ from $K^\circ\bar{K}^\circ$ decays
Interaction/pulse	10^{10}	10^{10}
Pulse/run	10^5	10^5
σ production	9 nb	260 nb
$A^{0.29}$	4.5	4.5
$1/\sigma_T$	$2.5 \times 10^{-8} nb^{-1}$	$2.5 \times 10^{-8} nb^{-1}$
Effective B.R.	$0.3 \times 5 \times 10^{-5}$	0.235
Acceptance	$2\% \times 35\%$	0.51×10^{-9}
Total Events	100	4

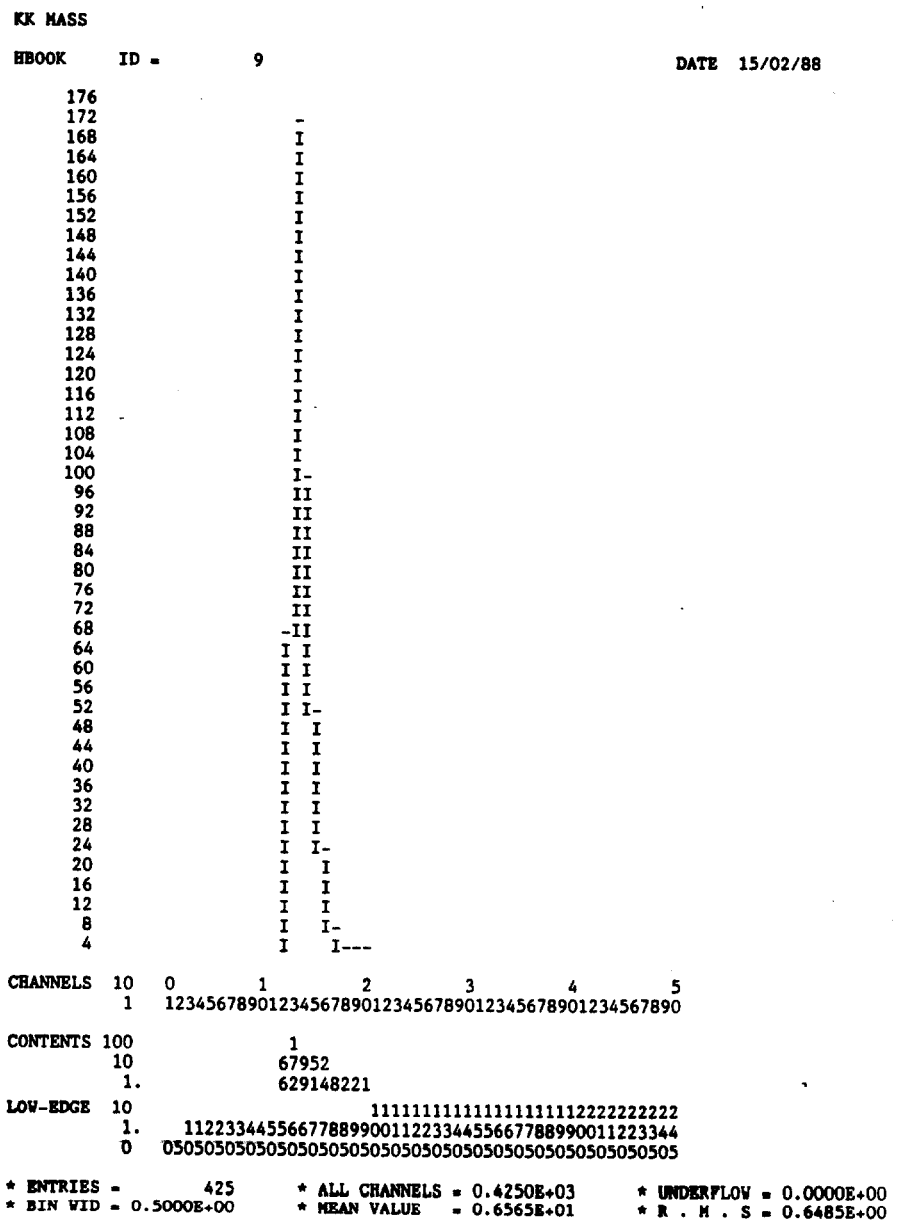

Fig. 1. Histogram for $K^\circ\bar{K}\circ$ pair mass in GeV

A New Method of Measuring $\sin^2\theta_W$ in Deep-Inelastic Scattering

R.H. Bernstein, F. Borcherding
Fermi National Accelerator Laboratory †
Batavia, Illinois 60510

Improved measurements of $\sin^2\theta_W$ are of central importance to physics. The value of $\sin^2\theta_W$ has now been determined in a variety of ways: the W and Z masses, atomic parity violation, electroweak interference effects, and deep-inelastic lepton-nucleon scattering have provided a consistent set of values of $\sin^2\theta_W$ but the errors are no better than a few percent. As we progress in testing the Standard Model we must measure $\sin^2\theta_W$ in as many processes as possible: each channel measures a different function of $\sin^2\theta_W$ and examines different physics, making improved measurements a natural way to search for new phenomena. A determination of $\sin^2\theta_W$ from the W and Z masses "defines" $\sin^2\theta_W$;[1] probing radiative corrections, for example, requires a measurement in a different reaction. Amaldi *et al.*[1] provide a compelling argument for improved experiments:

> Our motivations for this study are to test the standard model at the level of radiative corrections, to extract as accurate a value of $\sin^2\theta_W$ as possible for comparison with grand unified theories, supersymmetry, etc., and to search for indications of (or set limits on) such new physics as additional Z bosons, heavy fermions, or nonstandard Higgs representations.

At present, the most precise value of $\sin^2\theta_W$ comes from deep-inelastic $\nu_\mu N$ scattering experiments and comparisons are limited by the errors on other processes. However, within the next several years the W and Z masses will be determined at the colliders to $\approx 0.1\%$, HERA will begin operation, and the atomic parity violation measurements will continue to improve. In a short time, the $\nu_\mu N$ measurements will have the largest errors and limit the search for new physics.

---

†Operated by Universities Research Association Inc. under contract with the United States Department of Energy.

[1]This is the Sirlin renormalization scheme, which defines $\sin^2\theta_W = 1 - M_W{}^2/M_Z{}^2$. See [1].

We give a brief example of the physics reach of an improved measurement. The radiative correction parameter Δr is defined through:

$$M_W = \frac{A_0}{\sin\theta_W(1-\Delta r)^{1/2}} \quad (1)$$

$$M_Z = \frac{M_W}{\cos\theta_W} \quad (2)$$

where $A_0 = (\pi\alpha/\sqrt{2}G_F)^{1/2} = 37.281\ GeV$. The value of Δr is predicted[1] to be 0.0713 ± 0.0013 for $m_t = 45GeV$ and $m_H = 100GeV$. The value of Δr, and the error, are functions of m_t, m_H, and other assumptions and hence a precise value of Δr can be used to constrain new physics and search for inconsistencies. A measurement of M_W/M_Z alone can "absorb" Δr into a definition of $\sin^2\theta_W$; hence a comparison to another process is necessary. (Even the *existence* of the radiative corrections is not overwhelmingly established; the significance of the measurements depends critically upon the error analysis of the experiments and of their common theoretical uncertainties: Amaldi *et al.* estimates 3σ but that has been challenged[2].) The current error on the measured Δr is dominated by the error in M_W. Using the Particle Data Book value for M_W and simple error propagation we find an error of ± 0.037 on Δr; the error from $\sin^2\theta_W$ is only 0.012, and when added in quadrature this error is negligible. Consider, however, the situation in a few years when the W and Z masses are known an order-of-magnitude better: at that time the error from $\sin^2\theta_W$ will dominate. Without an improved measurement, the error from $\sin^2\theta_W$ will be of the same size as the theoretical error and provide few constraints. It will also be true that the precise size and reliability of the error will significant in the ability to test the theory. In Section B we will discuss the existing measurements of $\sin^2\theta_W$ in $\nu_\mu N$ scattering and see that there is considerable uncertainty in the treatment of several systematic errors; whether one adds statistical and systematic errors linearly or in quadrature will strongly change the amount and nature of the physics that can be extracted. The precise size of the errors on $\sin^2\theta_W$, now not a critical input to the Standard Model, will be in just a few years. Furthermore, one cannot argue that other experiments will supplant the DIS measurements: each process, such as $\nu_\mu N$ or $\nu_\mu e$ scattering, has a different dependence on the parameters and so only an ensemble of high-precision experiments can sort out the contributions from different physics.

This Letter-of-Intent discusses a new method of determining $\sin^2\theta_W$ in deep-inelastic scattering in a tagged-neutrino beam with an error of $\approx \pm 0.004$; with future fixed-target upgrades at FNAL, the method could reduce the error to as little as $\pm$ (0.002 – 0.003). We state the relevant properties of the tagged line in Section A. In Section B, we briefly cover old results, concentrating on the systematic errors in previous DIS determinations of $\sin^2\theta_W$. Section C sketches the neutrino detector and states the necessary statistical power. Section D explains the principles of this measurement and discusses the systematic errors. The final

Section compares this experiment to current data and future plans.

A. The Tagged-Neutrino Line

The tagged line uses a beam of K_L and the semileptonic decays $K_L \to \pi\mu\nu_\mu$ and $K_L \to \pi e\nu_e$ to produce a beam of ν_μ, ν_e and their antiparticles. A tagging spectrometer reconstructs the charges, momenta and species of the hadron and lepton from the K_L decay. We then know whether the neutrino is a ν_e or ν_μ and can distinguish neutrino from antineutrino. We can also use the momenta as measured in the tagging spectrometer to calculate the momentum vector of the neutrino. This provides an energy determination with $\sigma/E \approx 7\%$ and a prediction of the impact point in the neutrino detector of about 10 cm. This paper concentrates on the *use* of the tagging scheme in a determination of $\sin^2\theta_W$; details of a particular neutrino-tagging scheme have been presented in Fermilab Proposal P-788.[3] Fig. 1 is a schematic of the tagging spectrometer. We show a π and μ passing through the spectrometer. It contains drift chambers for tracking the hadron and lepton, and a large aperture (2.5 m) dipole with a p_T kick of 0.5 GeV/c for momentum analysis. Particle identification is accomplished in two stages: a TRD separates electrons from π's and μ's and a Fe filter folowed by scintillator is used to identify muons. The errors in the determination of neutrino species were carefully studied in P-788. That proposal emphasized searches for neutrino oscillations, where correct identification is critical. That analysis calculated the level of confusion between ν_e and ν_μ to be < 5 events (scaled upwards to the data sample of this Letter-of-Intent). The number of particle/antiparticle misidentifications, although not calculated in the Proposal, will be discussed in Section D. The resultant error in $\sin^2\theta_W$ will be more than an order-of-magnitude smaller than the statistical error.

P-788 used the CCFR detector[4] as a model; here we will continue to use a high-density Fe detector, but believe a CDHS style of detector[5] is a more appropriate model for reasons we will describe. We have not attempted to perform a simulation of the neutrino detector with expected resolutions; rather, for this Letter-of-Intent, we have used measured resolutions and our knowledge of previous analyses in the CCFR and CDHS detectors to estimate backgrounds and systematic errors.

B. Old Methods of Measuring $\sin^2\theta_W$ in DIS [6]

Previous DIS measurements of $\sin^2\theta_W$ have used the Llewllyn-Smith relations R_ν and $R_{\bar{\nu}}$:

$$R_\nu = \frac{\int \frac{d\sigma_{NC}^{\nu N}}{dy} dy}{\int \frac{d\sigma_{CC}^{\nu N}}{dy} dy} = \rho^2 \left[\frac{1}{2} - \sin^2\theta_W + \frac{5}{9}\sin^4\theta_W(1+r)\right] \qquad (3)$$

and

$$R_{\bar{\nu}} = \frac{\int \frac{d\sigma_{NC}^{\bar{\nu}N}}{dy} dy}{\int \frac{d\sigma_{CC}^{\bar{\nu}N}}{dy} dy} = \rho^2 \left[\frac{1}{2} - \sin^2\theta_W + \frac{5}{9}\sin^4\theta_W(1+\frac{1}{r})\right] \quad (4)$$

where

$$r = \frac{\int \frac{d\sigma_{CC}^{\bar{\nu}N}}{dy} dy}{\int \frac{d\sigma_{CC}^{\nu N}}{dy} dy} \quad (5)$$

These expressions apply for an isoscalar target with no strange quarks. The magnitude and x and Q^2 dependence of the strange sea contributes a significant theoretical error and must be included in an accurate determination.

A plot of R_ν *vs.* $R_{\bar{\nu}}$ as a function of $\sin^2\theta_W$ appears in Fig. 2. We see that for values of $\sin^2\theta_W \approx 0.23$, $R_{\bar{\nu}}$ is insensitive to the Weinberg angle and all the information about $\sin^2\theta_W$ is contained in R_ν. Further, the charged-current denominator provides no information about $\sin^2\theta_W$. It serves only as a normalization: without it, we would have to determine the absolute cross-section for $\nu_\mu N$ neutral-current scattering. The use of the charged-current normalization carries a price: the differences in charged- and neutral-current scattering cross-sections are responsible for a large theoretical error of order 2.5% and for an experimental systematic error of equal magnitude. The total theoretical error on $\sin^2\theta_W = 0.233$ is ± 0.0054 (from Amaldi *et al.*)

What are these differences, and, more generally, what are the systematic errors in determining $\sin^2\theta_W$ through R_ν?[2] They arise from three sources. The first, and most difficult to calculate, arise from the production of charm from s and d quarks. This "flavor-changing" channel is not available for neutral-current interactions. The cross-section for the excitation of charm is not well-known but has been modeled through "slow-rescaling," which makes the replacement:

$$x \to \xi = x(1 + \frac{m_c^2}{Q^2}) \quad (6)$$

where x is the momentum fraction carried by the struck quark and m_c is now a phenomenological parameter. A value of $m_c = 1.5\ GeV/c^2$ is a natural choice but is not well-constrained by experiment or dictated by theory. The data on slow-rescaling come from opposite-sign dimuon production, where the produced charmed quark decays semileptonically into a μ. Even if the slow-rescaling *ansatz* were known to be correct, the extraction of m_c from opposite-sign dimuon data contains potential errors: one concern is that the branching fraction $c \to \mu$ has some energy variation, most pronounced at low energy (as pointed out by Amaldi *et al.*) and another is that the slow-rescaling function varies steeply with Q^2, making resolution effects important. The best estimate from dimuon production in CCFR[7] is $m_c = 1.2^{+0.4}_{-0.6}\ GeV/c^2$. The experimental groups have used varying estimates of m_c: CCFR used $m_c = 1.5 \pm 0.4\ GeV/c^2$ and CDHS quotes a value for $1.5 \pm 0.3\ GeV/c^2$ but also chooses to provide a value of $\sin^2\theta_W$ as a function of m_c. Amaldi *et al.*, which we use as a benchmark, used $1.5 \pm 0.3\ GeV/c^2$ in their estimate of the error, leading to an error of ± 0.004 on $\sin^2\theta_W$. The errors from slow-rescaling are uncertain: the experimental evidence is not precise and the theory is not settled.

Furthermore, the size and shape of the strange sea also play a role, along with uncertainty in the Kobayashi-Maskawa-Cabibbo angles[2] and a variety of QCD effects. The sum of all such errors is an additional ± 0.0037 (again from Amaldi *et al.*), almost 2% once more. Hence while the value of m_c in the slow-rescaling parameterization is the single largest error, other errors which arise in the neutral-current to charged-current ratio add up to an approximately equal error. It will be difficult, if not impossible, for the standard methods to significantly reduce the error on $\sin^2\theta_W$.

The third source of error is misidentification of charged-current as neutral-current events. If the μ in a charged-current event escapes detection (by either ranging out inside the hadronic shower or exiting the detector before it can be identified) the event will be classified as a neutral-current interaction, and any error in the classification is a direct correction to R_ν. In the two high-Z detectors, CDHS and CCFR, no tracking has been used to identify muons because the absolute reconstruction efficiency is hard to determine to the necessary 1% precision. Instead, the *length* of the event as determined by scintillation counters has been used. Hadronic showers die out after a few meters of steel, but the muon will continue, firing scintillation counters far downstream of the shower's end. The distribution of event length in CCFR is shown in Fig. 3.

We see that a subtraction of order 20% must be performed for muons which fall under the shower peak. These muons arise from two (approximately equal) sources: first, muons

[2]The quoted errors usually assume three fermion families; for more than three, Amaldi *et al.* quote $\Delta \sin^2\theta_W = ^{+0.008}_{-0.001}$, a significant source of error.

which range out within the hadronic shower, and second, wide-angle muons which exit the spectrometer before they can be analyzed. The charged-current subtraction is then sensitive to the x distributions, since x and the muon angle are related:

$$\theta_\mu^2 = \frac{2m_N x(E_\nu - E_\mu)}{E_\mu E_\nu} \tag{7}$$

CCFR used the E_ν *vs.* r correlation in their dichromatic run to *cut* on y,[3] reducing the error by a factor of two (but also cutting the event sample by $\approx$ 50%). However, the final error was still ± 0.006 on a 5% subtraction after the cut. CDHS cut on an energy-dependent event length and quotes a slightly smaller error of ± 0.004 with an average 20% subtraction.[4] In any case, the error is again of order 2.5% of $\sin^2\theta_W$ for either experiment.

C. Apparatus and Statistical Errors

In the next Section, we will see that the antineutrino neutral-current cross-section is the statistically-limiting channel and in order to achieve a 1–2% determination of $\sin^2\theta_W$ we will need $> 20K$ events. For our estimates we have used a 900 GeV primary proton beam with 3.0 x 10^{18} *pot* at the Tevatron. A fixed-target energy of 1.2 TeV instead of 900 GeV would provide an additional doubling of statistics, equally divided between an improved acceptance and the increased neutrino cross-section. It would also make charged-current muons more energetic and less likely to be missed by a detector. Hence a fixed-target upgrade would only improve the measurement. Table 1 shows the expected event sample in each category.

	ν_μ	$\bar{\nu}_\mu$
CC	$218K$	$92K$
NC	$68K$	$29K$

Table 1. Statistical Power in Various Interaction Channels.

Previous detectors, such as CCFR (690 tons of Fe) or CDHS (1250 tons) would only provide a $\approx$ 3% measurement. In order to further reduce the statistical errors, we are proposing a detector with three times the mass of CDHS, or 3500 tons. Obviously a detector with three times the mass of the CDHS detector is a large undertaking. However, the device need not be as complicated. The tracking is far less important for cross-section,

[3] An effective cut of $y < 0.7$.

[4] The CDHS data is based on two runs.[8] The first has an 18% charged-current subtraction and is based on a run with 200 GeV secondary beam energy; the second, with a 22% subtraction, is based on a 160 GeV run.

oscillation, and $\sin^2\theta_W$ measurements (the overall goals of the tagged-neutrino program)[5] than it was for the structure function and dimuon measurements of previous high-energy neutrino programs. The simplest idea would be to make a long detector with perhaps half the tracking planes but the same number of scintillator planes per interaction length of previous Fe-target detectors. The target will be 60 meters long (an 11 ft diameter is good for both acceptance and shower containment) and so acceptance for muons in a downstream toroid will be poor. A magnetized target, like CDHS, would be best, as opposed to the simpler CCFR apparatus. With the outline of a detector in mind, we can now study this measurement.

D. A Measurement of $\sin^2\theta_W$ in the Tagged-Line

The tagged neutrino scheme does not need the charged-current flux normalization. We propose to measure

$$R'(y) = \frac{\frac{d\sigma^{\bar{\nu}N}_{NC}}{dy}}{\frac{d\sigma^{\nu N}_{NC}}{dy}} = \frac{[g_R{}^2 + g_L{}^2(1-y)^2] + [g_L{}^2 + g_R{}^2(1-y)^2]\left(\frac{\bar{Q}}{Q}\right)}{[g_L{}^2 + g_R{}^2(1-y)^2] + [g_R{}^2 + g_L{}^2(1-y)^2]\left(\frac{\bar{Q}}{Q}\right)} \tag{8}$$

where

$$g_L{}^2 = \epsilon_L(u)^2 + \epsilon_L(d)^2 = \frac{1}{2} - \sin^2\theta_W + \frac{5}{9}\sin^4\theta_W \tag{9}$$

$$g_R{}^2 = \epsilon_R(u)^2 + \epsilon_R(d)^2 = \frac{5}{9}\sin^4\theta_W \tag{10}$$

$$\epsilon_L = T_i^3 - \sin^2\theta_W Q_i \tag{11}$$

$$\epsilon_R = -\sin^2\theta_W Q_i \tag{12}$$

where we have substituted the values of T_i^3 (3^{rd} component of weak isospin) and the quark charge Q_i for the individual species. $\bar{Q}$ and Q are the quark and antiquark structure functions evaluated at a specific y; for any species Q, $Q = \iint xQ(x,q^2)\,dx\,dq^2$.

This new ratio R' only depends on neutral-current scattering. There are no approximations for strange-sea content or isoscalarity, unlike Eqs. (1) and (2). The direct measurement of this ratio is possible because of the tagging scheme with the neutral K_L beam. In the dichromatic beams where charged π's and K's produce the neutrinos, the beam must be

[5]The tagging scheme can also open new regions for neutrino oscillation searches (discussed in P-788). We expect a factor of 100 improvement in the $\nu_e \rightarrow \nu_\tau$ oscillation limits at small $\sin^2\theta_{e\tau}$, probing to $m_{\nu_\tau} \approx 10eV/c^2$ and an order-of-magnitude improvement in the limits on wrong-sign muon production to 5 x 10^{-5}.

either positively or negatively charged and the positive runs and negative runs are separate; the normalization of neutral-current neutrinos to neutral-current antineutrinos will then have flux-monitoring errors of at least $3-5\%$.[6] In the K_L tagged beam, we produce ν and $\bar{\nu}$ simultaneously in equal numbers[7] and the tagger allows us to distinguish ν from $\bar{\nu}$ event-by-event.

A systematic error in $\nu_\mu/\bar{\nu}_\mu$ separation would certainly affect the ratio and therefore must be controlled and understood. Recall that the tagger uses a dipole spectrometer to separate μ^+ from μ^- and therefore ν_μ from $\bar{\nu}_\mu$. Errors will then occur only for events where the tagger incorrectly identifies the charge of the lepton. Multiple scattering and chamber resolution effects will provide fewer than one misclassified event; the source would then be combinations of extra hits and inefficiencies creating spurious tracks. Here, the tagging scheme provides two methods to attack the problem. First, the K_L reconstruction from the tagger will give us a prediction of the neutrino impact point in the neutrino detector, with $\sigma \approx 10$ cm. A spurious track will lead to a misreconstructed K_L and a disagreement with the observed neutrino (note that we cannot use the energy determination for the neutral-current analysis because of the missing ν_μ) and we would then cut the event. Second, the charged-current data provides a *measurement* of the effect: a misclassification in charged-currents would have (for example) a μ^- in the tagger and *another* μ^- produced in the neutrino interaction. The size of the effect could then be determined as a function of analysis cuts in the charged-current sample. A study in the P-788 simulation tells us a factor of fifty suppression from cuts is likely; 5% of the events would have to be misclassified to produce an error of 0.001 in $\sin^2\theta_W$ after reconstruction cuts and then there would be 15K events[8] for study in the charged-current data. If we assume the size of the effect could be determined to 20% of itself, a 5% misclassification would result in an error a factor of twenty smaller than the statistical error (We also regard 5% misclassification to be a large overestimate. With three or more chambers upstream and downstream of the dipole, such spurious tracks would be eliminated in the normal course of track reconstruction and χ^2 cuts.) Acceptance asymmetries in the tagger could be studied in the same way; these problems have been attacked in K_L experiments in the past and many of the same techniques could be used.[9]

---

[6] Flux-monitoring uncertainties have been the limitation in the neutrino cross-section errors. For a discussion of the techniques and potential errors, see [9].

[7] Except for the small CP-violation correction.

[8] We know the limit on wrong-sign muon production[10] is 10^{-4} and so any excess over a few tens of events must be due to misclassification.

[9] Although this experiment differs from the K_L program at Fermilab, which used the double-beam method, many of the same techniques can still be applied (for example, reversing the polarity of the dipole on a regular basis will greatly reduce any such effect.) See W.R. Molson [11] or R.H. Bernstein [12] for details on two different K_L experiments.

We define R' to be the integral of $R'(y)$ over y; then Fig. 4 shows R' as a function of $\sin^2\theta_W$.[10] We note that in the Llewllyn-Smith approximation,

$$R' = r\left(\frac{R_{\bar{\nu}}}{R_\nu}\right) = \frac{{g_R}^2 + {g_L}^2 r}{{g_L}^2 + {g_R}^2 r} \tag{13}$$

Since $R_{\bar{\nu}}$ is insensitive to $\sin^2\theta_W$, we see that the dependence of R' on $\sin^2\theta_W$ is the same as the dependence of R_ν. In the region $\sin^2\theta_W = 0.25$, $dR'/d(\sin^2\theta_W) = 0.845$ and so $\Delta(\sin^2\theta_W) = 1.2\Delta R'$. In our calculation of the errors on R' we have used parameterizations of the structure functions along with measured distributions for the magnitude and shape of the u, d, and s sea from CCFR and calculated R' from the first-order diagrams.

Recall the sources of the theoretical errors in the determinations of $\sin^2\theta_W$ from R_ν: charm-production, θ_C, and sea effects. The first two vanish in R' since there is no excitation of charm (except from excitation of the charm sea, which is small) and no dependence on the Cabibbo angle. The ratio $s/\bar{d} = 0.53 \pm 0.14$[7] and $s/d = 0.06 \pm 0.015$. The values are important in R_ν because of the production of charm from s and d and because the d-quark mixing is suppressed by $\sin^2\theta_C$, making the small amount of s important. In neutral-current scattering, there is no θ_C suppression and charm production from s or d is forbidden.

The primary theoretical difficulty in the analysis of R' is the value of $\bar{Q}/Q$. We see from Eq. (5) that the ratio is sensitive to the value of $\bar{Q}/Q$; physically, the antineutrino numerator and the neutrino denominator reverse the roles of Q and $\bar{Q}$. The Amaldi *et al.* value is $(\bar{U}+\bar{D})/(U+D) = 0.125 \pm 0.020$; CCFR measures[13] $\bar{Q}/Q = 0.175 \pm 0.012$ and this error would produce a 6% error in $\sin^2\theta_W$. Hence we must find some way to measure $\bar{Q}/Q$ within the experiment. The tagged line provides *two* statistically independent determinations: one from the neutral-current data and one from the charged.

Let us first consider the neutral-current analysis. In any y-bin, we have a measured ratio of differential cross-sections and we know y from the measured shower energy (CCFR has a resolution of $\sigma_E = 0.8\sqrt{E}$)and the tagger determination of E_ν. The value of $\bar{Q}/Q$ is a constant independent of y up to scaling violations. We may then *fit* for $\sin^2\theta_W$ and $\bar{Q}/Q$ simultaneously within the data, and the internal calculation is then practically independent of Z/A, Λ_{QCD}, etc. Scaling violations may then be applied to the well-constrained value of $\bar{Q}/Q$. However, using the neutral-current data has two disadvantages: the statistical power of the determination is limited and a two-parameter fit will increase the error on the other unknown, $\sin^2\theta_W$.

The charged-current sample may be used to determine $\bar{Q}/Q$ as well. There is a small dependence on slow-rescaling here. If we write r in terms of the quark distributions we find:

[10]Here the effect of the strange sea, scaling violations, etc. have all been included.

(neglecting the charm-sea content)

$$r = \frac{\sigma^{cc}_{\bar{\nu}_\mu}}{\sigma^{cc}_{\nu_\mu}} = \frac{\frac{1}{3}U + (\cos^2\theta_C + \xi_c \sin^2\theta_C)\bar{D} + (\sin^2\theta_C + \xi_c \cos^2\theta_C)\bar{S}}{\frac{1}{3}\bar{U} + (\cos^2\theta_C + \xi_c \sin^2\theta_C)D + (\sin^2\theta_C + \xi_c \cos^2\theta_C)S} \tag{14}$$

where ξ_c is an operator[11] on the quark distributions that describes slow-rescaling. If ξ_c were unity, then for an isoscalar target we would find $\bar{Q}/Q$ directly from Eq. (9) above. We may rewrite the ratio, solving for $\bar{Q}/Q$ in a more transparent form[12]:

$$\frac{\bar{Q}}{Q} = \frac{r - \frac{1}{3}}{1 - \frac{1}{3}r} \tag{15}$$

The value of r we measure will be affected by slow-rescaling by an amount

$$\Delta_c \sim (1 - < \xi_c >) \tag{16}$$

$< \xi_c >$ is an "effective" slow-rescaling function and the term Δ_c describes the difference between full-strength $d, s \rightarrow c$ coupling and the actual coupling. We may use our measured value of r and correct it for slow-rescaling effects; r is only weakly dependent on m_c since more than half of the slow-rescaling effects cancel between the antineutrino numerator and neutrino denominator, and the induced error in $\bar{Q}/Q$ is small for the same reason: $\Delta(\bar{Q}/Q) \approx 1.2\Delta r$. The size of Δ_c and its error are also dependent on the neutrino energy spectrum; for sufficiently large energy, there is no penalty for making the heavy c-quark. Our energy spectrum is slightly harder than those of CCFR or the CDHS experiments, which helps reduce the error. For our particular spectrum within the slow-rescaling model we find varying $m_c = 1.5 \pm 0.5$ yields an error of ± 0.0015 in $\sin^2\theta_W$. This variation is almost twice as big as the standard $m_c = 1.5 \pm 0.3$ of Amaldi *et al.* yet produces an error down by a factor of nearly three. We will have $\approx 300K$ charged-current events with E_ν from the tagger and a momentum-analyzed muon, making the *statistical* error on $\bar{Q}/Q$ only ± 0.0018 and the resultant error on $\sin^2\theta_W$ only ± 0.0020. A precise determination of $\bar{Q}/Q$ is an important measurement on its own, since it tells us about the sea content of the nucleon; we will reduce the existing error on $\bar{Q}/Q$ by approximately a factor of three.[13]

Returning to the extraction of $\sin^2\theta_W$, the error from $\bar{Q}/Q$ is ± 0.008 for the determinations where ρ^2 and $\sin^2\theta_W$ are allowed to float and this measurement will reduce the old

[11] $\xi_c = \int\int (1 - y + \frac{xy}{\xi}) \xi q_i(\xi) \theta(\xi - 1)\, dx\, dy$ and q_i refers to the individual quarks. ξ is defined in Eq. (4).

[12] We have made a number of simplifying assumptions in deriving this form. The expression for $\bar{Q}/Q$ in Eq. (10) assumes an isoscalar target and no strange sea. We have also integrated over y and set $cos^2\theta_C = 1$ for simplicity. The numerical results quoted later do not make these approximations.

[13] The quoted error on $\bar{Q}/Q$ is for the application to the neutral-current data; the error on $\bar{Q}/Q$ as an absolute quantity *independent* of experiment involves scaling violation, etc. and is probably twice as big.

two-parameter fit errors significantly. The reason for the large error is again in part from flux normalization: determining the sea content from pure ν_μ data without the normalized $\bar{\nu}_\mu$ sample forces reliance on calculations of the structure functions instead of a measurement based on the data. The K_L beam and the event-by-event prediction of E_ν allow us to avoid these difficulties: if we measure $\bar{Q}/Q$ in the charged-current data with specific y-cuts, and apply the same cuts to the neutral-current data, we will have measured $\bar{Q}/Q$ for our data sample *including* scaling violation. The reliance on a Monte Carlo is greatly reduced; we would use it in $\bar{Q}/Q$ to calculate the effect of cuts instead of calculating $\bar{Q}/Q$ itself. We may systematically study the y-cuts in the charged-current data since there we have two ways of determining y for each event: first, from $y = 1 - E_\mu/E_\nu$ and second from $y = E_{had}/E_\nu$.

Although the error introduced from slow-rescaling is small ($\approx 0.5\%$ of $\sin^2\theta_W$) it would increase confidence in any result to have independent cross-checks. The K_L tagging scheme allows us to measure other functions of the cross-sections which will reduce the error as well. The Paschos-Wolfenstein relation[14]

$$R^- = \frac{\sigma^{nc}_{\nu_\mu} - \sigma^{nc}_{\bar{\nu}_\mu}}{\sigma^{cc}_{\nu_\mu} - \sigma^{cc}_{\bar{\nu}_\mu}} = \rho^2(\frac{1}{2} - \sin^2\theta_W) \tag{17}$$

provides a large reduction in the slow-rescaling errors; we see from Eq. (9) above that the strange-sea effects vanish when the difference is formed, leaving only $(d_V \sin^2\theta_C)\xi_c$. Numerically this reduces the slow-rescaling error by a factor of two ($d_V \sin^2\theta_C \approx s\cos^2\theta_C$ so the size of the slow-rescaling correction is reduced accordingly) relative to R_ν. In the absence of m_c effects, the Paschos-Wolfenstein test is almost independent of any details of the structure functions; both numerator and denominator contain the same combination of structure functions: $(d - \bar{d})$ (for an isoscalar target), which then cancels in forming the ratio. R^- is then independent of $\bar{Q}/Q$, unlike R'. The statistical error on $\sin^2\theta_W$ from the R^- determination will be only ± 0.0025, about 1%, better than that of R'. R^- has two disadvantages when compared to R'. First, it has a larger dependence on slow-rescaling effects. Second, since R^- uses a comparison between neutral and charged currents, it has a substantial error from charged-current to neutral-current cross-talk. The advantage of K_L tagging we wish to stress is that the four precisely determined cross-sections may be combined in several different ways, each with different systematic errors and each with different dependences on $\sin^2\theta_W$. We stress R' in this letter because it seems the most promising but there are a variety of other systematic controls which have been previously unavailable.

Let us next compare the errors in R_ν and R' from charged-current to neutral-current cross-talk. In R_ν we saw the correction was of order 20%; the precise size of the correction depends on the neutrino energy and detector. However, there is a critical difference between R_ν and R' in the nature of the correction. R_ν is a neutral-current to charged-current ratio;

hence any error is a direct correction to the ratio. In R' cross-talk from charged-current events affect *both* numerator and denominator and thus tends to cancel. The cancellation is not precise because νN scattering has a flat distribution in y while $\bar{\nu}N$ interactions follow $(1-y)^2$. The P-788 simulation at 900 GeV/c predicts an average E_ν of $\approx$ 70 GeV; if we assume muons with $p_\mu \leq 5$ GeV/c are missed, we find a correction in the numerator of 5% and in the ν denominator a correction of 12%. The actual corrections are about twice as big (22% for the ν_μ correction in CCFR and 18% in CDHS) because of wide-angle muons which escape out the side of the detector. The increase in numerator and denominator are then about 11% and 18% respectively. The ratio is thus only affected by 7%, about 1/3 of the previous correction. Here, a calculation of structure functions and the x distributions will be required in the subtraction and we will use the more-conservative CCFR analysis and errors scaled downward for the smaller correction.

We hope to improve the error further by using the features of the K_L tagged beam. We need to understand the ratio of charged-current $\nu_\mu N$ to $\bar{\nu}_\mu N$ scattering over a small range in y near $y = 1$ and proceed with the same method as in the analysis of R' but in the charged-current data instead. We write the differential cross-sections schematically as:

$$\frac{d\sigma_{CC}^{\nu N}}{dy} = Q(x,q^2) + (1-y)^2\bar{Q}(x,q^2) \tag{18}$$

$$\frac{d\sigma_{CC}^{\bar{\nu}N}}{dy} = \bar{Q}(x,q^2) + (1-y)^2 Q(x,q^2) \tag{19}$$

where $Q(x,q^2)$ and $\bar{Q}(x,q^2)$ are the quark and antiquark structure functions. We are interested in the error on this ratio near $y = 1$. We may *measure* the Q and $\bar{Q}$ structure functions at small y (recall that the tagging scheme provides us with a 7% measurement of E_ν and we may then measure y_{vis}) and use them to extrapolate into the high-y region. Since we have both ν_μ and $\bar{\nu}_\mu$ data we can measure the Q and $\bar{Q}$ contents separately and the extrapolation will be constrained by the data; of course, scaling violation and quasi-elastic scatters are important near $y = 0$; previous analyses (Auchincloss[9]) of the cross-sections excluded events with $y < 0.05$. A detailed calculation will be necessary to determine whether the method is sufficiently accurate. A further possibility for reducing the error comes from the nature of R'. CDHS and CCFR never used tracking since errors in the muon reconstruction efficiency do not cancel in R_ν; certainly for high-y the errors are worst. In R' the errors tend to cancel. If we cut on visible wide-angle muons we would reduce the correction by a factor of two; then the error would arise from the errors in the calculated differences in the ν_μ and $\bar{\nu}_\mu$ distributions in θ_μ. Again, only a detailed analysis will determine whether such a method is viable, but this argument shows that the tagging scheme has significant systematic advantages over previous experiments.

A better-understood and reliable tool in eliminating the charged-current to neutral-current cross-talk comes from the tagger: using the momentum prediction from the reconstructed K_L, we may make a cut in y from E_{vis}/E_ν and reduce the background by at least a factor of two, as in the CCFR analysis. However, with the energy resolution on E_ν from the tagger is better than that available in the dichromatic beam. The cut will remove at most 20% of the ν_μ data instead of half (as in E-616) , and at most a few percent of the $\bar{\nu}_\mu$ sample. Since the statistical power is dominated by the $\bar{\nu}_\mu$ data, the effect of the y-cut on the statistical error will be small; for a y-cut of 0.85, the error will only increase by 3% of itself.

Summarizing, (1) the level of the correction should be 1/3 as small as the CCFR or CDHS subtractions, since we have an extra cancellation in the purely neutral-current ratio, (2) the level of the correction may be set in exactly the same way as CCFR or CDHS and there is no reason to believe that a new experiment could not achieve a similar level of precision, (3) the error on the correction is reduced since the quark structure functions in the extrapolated region will have been *measured* in the same experiment, and (4) a y cut can be used to reduce the background to a further, negligible fraction with only a small loss in the data. We point out that before a y cut, the more-conservative error analysis of CCFR would produce an error in $\sin^2\theta_W$ of ± 0.003 in the R' determination. A calculation from the measured y-distributions indicates a y-cut of $y < 0.85$ will make residual errors from the muon subtraction less than 0.5% of $\sin^2\theta_W$.

This analysis of errors is far from complete: we have not attempted to calculate a variety of effects. For example, the y_{vis} distribution is different in charged-current and neutral-current events because we subtract the muon energy deposit in the charged-current data alone. We have not studied the effect of scaling violation and quasi-elastics on our determination of the structure-functions or calculated the momentum resolution on muons. Instead we have assumed we could do as well as the two similar detectors have done in the past and with that knowledge, searched for what we expect will be the limiting difficulties in a more precise determination. With the above arguments, we expect residual errors from theory and muon subtraction to be dominated by the error in $\bar{Q}/Q$, contributing an error of $\pm 0.0020(stat)$ to $\sin^2\theta_W$. Varying $m_c = 1.5 \pm 0.5$ changes $\sin^2\theta_W$ by ± 0.0015; the standard Amaldi *et al.* value of 1.5 ± 0.3 would produce an error of only ± 0.0009.

It is important to point out that the systematic cleanliness of the tagging method at this level of statistical accuracy provides a broad range of input to the Standard Model which has been previously unavailable. It will enable us to measure σ_{ν_μ} and $\sigma_{\bar{\nu}_\mu}$ for both charged- and neutral-current events with only small errors from flux normalization. The

cross-sections will be determined to $\approx$ 1–2%.[14] We also note that R' itself is insensitive to radiative corrections since it contains only neutral-current cross-sections, providing a direct comparison of $\nu_\mu N$ scattering at Q^2 of $\approx 10\ GeV^2$ to the collider results. Using the precisely determined cross-sections, we would then use all the standard ratios (such as R_ν,R^-) to perform fits to radiative corrections, ρ^2, etc.[15]

E. Conclusions

The Amaldi *et al.* world average for $\sin^2\theta_W$ from R_ν with $\rho^2 = 1$ fixed is (experimental error followed by theoretical):

$$\sin^2\theta_W \;=\; 0.233 \pm 0.0033 \pm 0.0054. \tag{20}$$

It is important to note that the determination of $\sin^2\theta_W$ from R_ν actually comes from a simultaneous fit to ρ^2 and $\sin^2\theta_W$, as is clear from Eq. (1). Unlike R_ν, R' is independent of ρ^2 since it cancels in forming a purely neutral-current ratio. Given that a precision measurement of $\sin^2\theta_W$ is largely motivated by searching for deviations from the Standard Model,[15] it is perhaps more appropriate to quote errors based on allowing ρ^2 to float. In that case, Amaldi *et al.* find a best fit of

$$\sin^2\theta_W \;=\; 0.232 \pm 0.014 \pm 0.008. \tag{21}$$

In contrast, the planned experiment at 900 GeV would provide a statistical error of 1.6% and would find (statistical errors on R' and $\bar{Q}/Q$ added in quadrature; it is followed by the systematic error for $m_c = 1.5 \pm 0.3$, and our estimated upper limits on the systematic error in $\bar{Q}/Q$ and the muon subtraction):

$$\delta(\sin^2\theta_W) \;=\; \pm 0.0040 \pm 0.0009 \pm 0.0005 \pm 0.0005. \tag{22}$$

With fixed-target upgrades to higher energy we may hope for an improved statistical error and lowered systematic error; an eventual error of $\pm 0.002 - 0.003$ should be achievable, since increased energy and increased statistical power will enable us to make cuts to reduce the

[14]The statistical power for the various channels will be better than 1%. We form the cross-section in two steps: first, only accept events in which the tagger predicts the neutrino passed through the detector, and second, form the ratio of neutrinos that interact to the number passing through. The systematic error on the quality of the prediction will then limit the cross-section determination. This systematic error would cancel in a ratio between cross-sections. Neutral-current to charged-current ratios will have an error from the cross-talk correction which both CCFR and CDHS have measured with $\Delta R_\nu/R_\nu \approx 1\%$.

[15]The CHARM II [16] measurement of $\sin^2\theta_W$ from $\sigma(\nu_\mu e)/\sigma(\bar{\nu}_\mu e)$ is expected to determine $\sin^2\theta_W$ to ± 0.005 in the purely leptonic process. LCD proposes[17] to measure $\sin^2\theta_W$ at low Q^2 to ± 0.002 in $\nu_\mu e$ scattering at LAMPF. A precise comparison of $\sin^2\theta_W$ measured leptonically to a measurement with quarks would be invaluable.

size of the muon subtraction and residual slow-rescaling corrections. The error quoted here is calculated using only the R' analysis; as we have pointed out, there are other ways of analyzing the data that can certainly be used to attack both the statistical and systematic errors.

The precise results for $\sin^2\theta_W$ so obtained could then be applied to constrain the value of ρ^2, from either this experiment or the sum of previous DIS experiments. For the two-parameter fit, the R' errors provide a factor of five improvement in the $\sin^2\theta_W$ error. In either case, the method provides a unique, precision DIS measurement of $\sin^2\theta_W$ largely free of slow-rescaling and other QCD corrections. Such a measurement is a critical part of a continuing program of detailed exploration of the Standard Model and is a logical continuation of neutrino physics at Fermilab into the 1990's.

References

[1] U. Amaldi *et al.*, Phys. Rev. D36, 1385 (1987) is a careful study of world data on $\sin^2\theta_W$ and we draw heavily from it throughout this Letter.

[2] An excellent review of DIS measurements of $\sin^2\theta_W$ and the systematic difficulties is R. Brock, "Deep-Inelastic Neutrino Measurements of $\sin^2\theta_W$," presented at *New Directions in Neutrino Physics at Fermilab*, September, 1988 (to be published).

[3] "A Proposal for a Neutrino Oscillation Experiment in a Tagged-Neutrino Line," R.H. Bernstein *et al.*, or "Neutrino Physics in a Tagged-Neutrino Beam," R.H. Bernstein, Fermilab-CONF-89/34.

[4] The most recent detailed description is B.A. Schumm, "Like Sign Dimuon Production in High Energy Neutrino Interactions," PhD Thesis, University of Chicago, August, 1988 (unpublished).

[5] M. Holder *et al.*, NIM148, 235 (1978).

[6] Here we rely heavily on three sources: P.G. Reutens, "Measurement of the Electroweak Parameters $\sin^2\theta_W$ and ρ^2 in Deep Inelastic Lepton-Nucleon Scattering," PhD Thesis, University of Chicago, June, 1988 (unpublished) (FNAL E-616), Amaldi *et al.*, and J. Kim *et al.*, RMP53, 211 (1981); the latter is a clear, informative, and useful paper which contains information hard to find elsewhere.

[7] C. Foudas *et al.*, to be published. Also see K. Lang *et al.*, "Neutrino Production of Dimuons," Z. Phys. C33, 483 (1987).

[8] Abramowicz *et al.*, Z. Phys. C28, 51 (1985) and Abramowicz *et al.*, Phys. Rev. Lett. 57, 298 (1986).

[9] H.E. Fisk and F.J. Sciulli, Ann. Rev. Nucl. and Part. Sci., 32, 499 (1982). Also see P.S. Auchincloss, "Measurement of the Total Cross-Section for Neutrino-Nucleon Interactions," PhD Thesis, Nevis Laboratories, Columbia University, 1987, Nevis Preprint 262.

[10] S.R. Mishra, "A Study of Wrong Sign Muon and Trimuon Events in Neutrino-Nucleon Scattering," PhD Thesis, Nevis Laboratories, Columbia University, 1986, Nevis Preprint 259.

[11] W.R. Molzon, "The Electromagnetic Interaction of the Neutral Kaon: A Measurement of the K^o Mean Square Charge Radius," PhD Thesis, University of Chicago, March 1979 (unpublished).

[12] R. H. Bernstein, "A Study of CP-Violation Through a Precision Measurement of η_{oo}/η_{+-}," PhD Thesis, University of Chicago, Dec. 1984 (unpublished).

[13] K. Lang *et al.*, Z. Phys. C33, 483 (1987).

[14] E.A. Paschos and L. Wolfenstein, Phys. Rev. D7, 91 (1973).

[15] See Amaldi *et al.* for a list of references on radiative corrections. Marciano and Sirlin have written several such articles (see Amaldi *et al.*, footnotes 13-14.) Also useful are E. Paschos and M. Wirbel, "Corrections to $\sin^2\theta_W$ in Neutrino Experiments," Nucl. Phys. B194, 189(1982) which discusses corrections to the Paschos-Wolfenstein relations and J.F. Wheater and C.H. Llewellyn-Smith, Nucl. Phys. B208, 27 (1982).

[16] "Proposal to Study Neutrino-Electron Scattering at the SPS," CERN/SPSC/83-24, SPSC/P186. A recent progress report and sketch of future plans were given by J. Panman and A. Capone, both presented at *New Directions in Neutrino Physics at Fermilab*, September, 1988 (to be published).

[17] "A Proposal for a Precision Test of the Standard Model by Neutrino-Electron Scattering," (Large Cerenkov Detector Project), LA-11300-P.

Fig. 1. A schematic of the Tagged-Neutrino Spectrometer and Neutrino Detector (not drawn to scale). A $K_L \to \pi^- \mu^+ \nu_\mu$ decay is pictured. The π and μ pass through drift chambers and a dipole which measure their momenta and determine the K_L decay point. They next pass through a TRD (useful for Ke_3 decays) and then into a muon filter. The π is absorbed and the μ continues downstream, first firing a bank of scintillators and then passing into a beam-dump. The ν_μ (dotted line) interacts in a neutrino detector downstream and a μ^- is observed in a charged-current interaction.

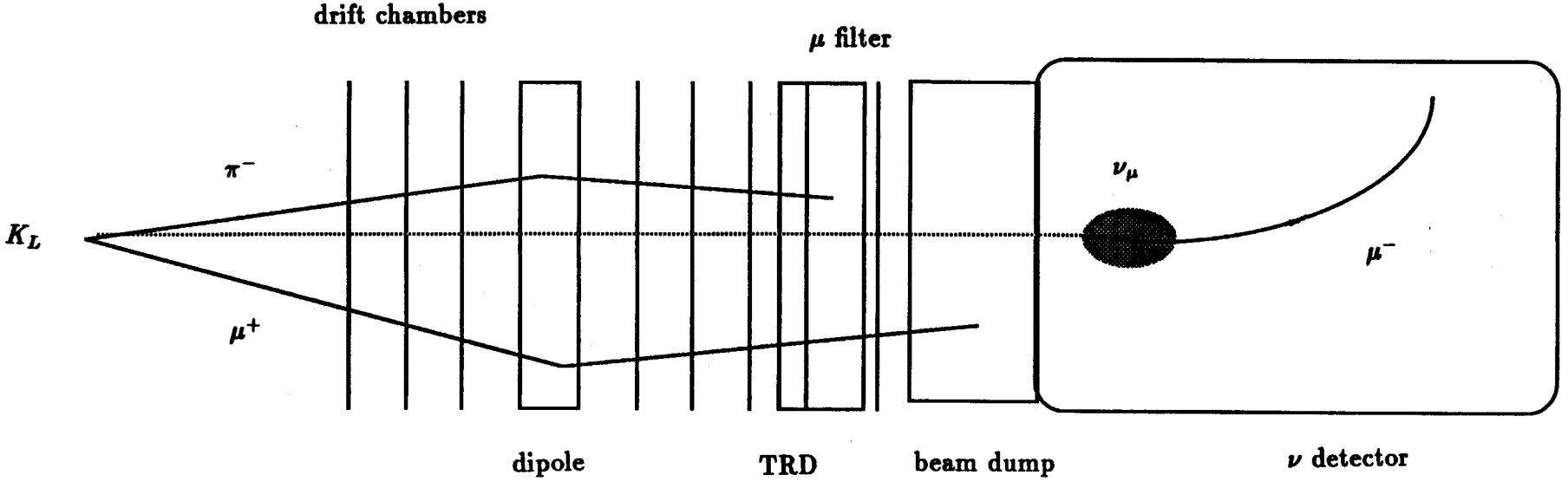

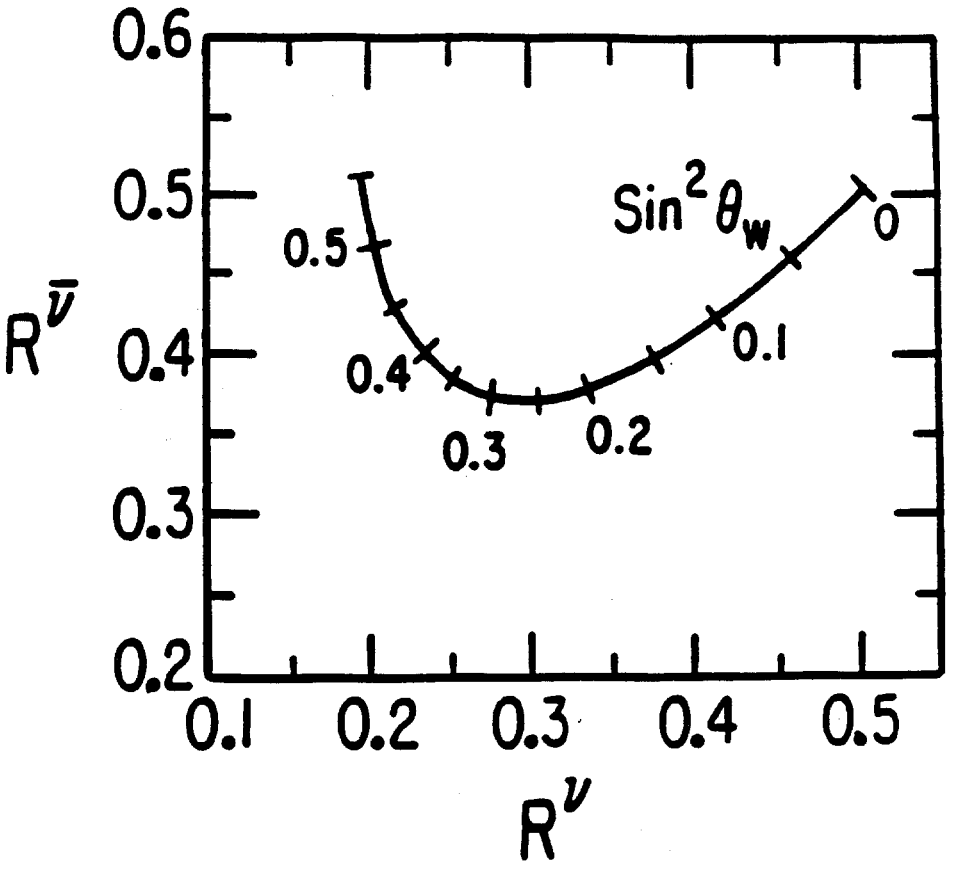

Figure 2 : $\sin^2\theta_W$ as a function of R^{ν} and $R^{\bar{\nu}}$

(from the thesis of P.G. Reutens)

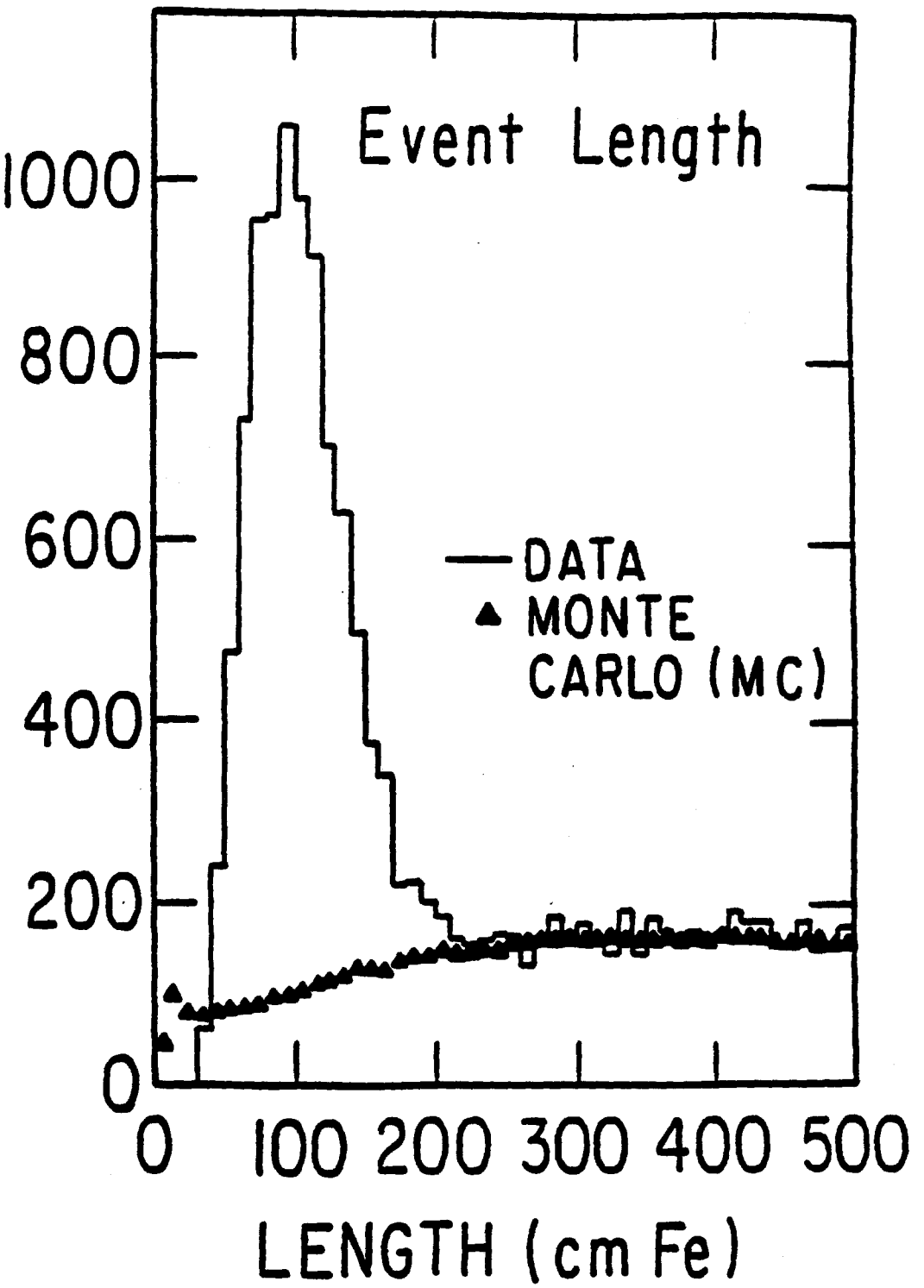

Figure 3 : Event length before application of radius dependent E_{HAD} cut, showing the large charged current background under the neutral current peak (total E616 neutrino sample)

(from the thesis of P.G. Reutens)

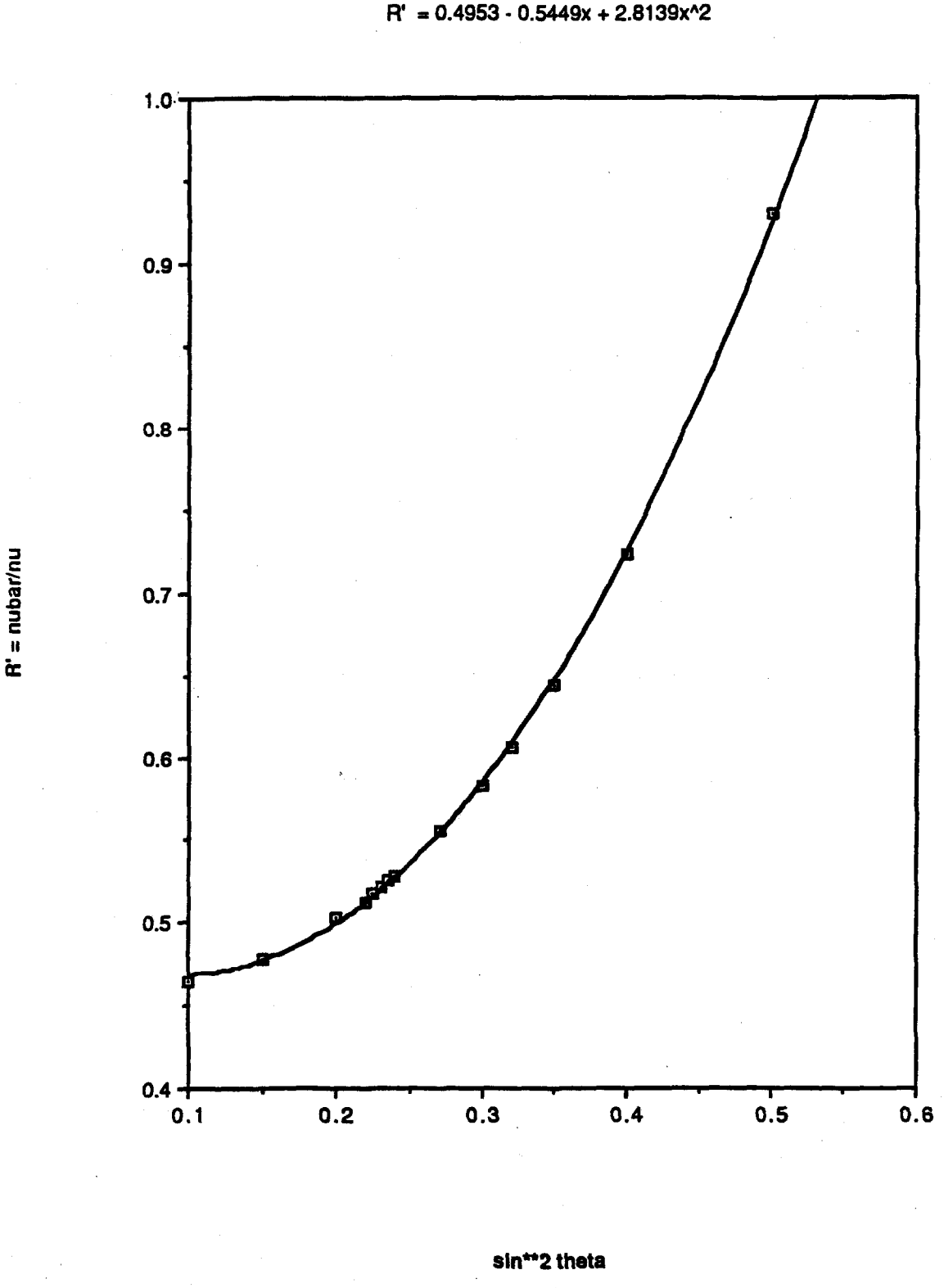

Fig. 4: R' vs. $\sin^2\theta_W$.

III. Rates and Acceptances

In this section we explicitly calculate the rates of ν-interactions expected in the experiment and the rates from interactions of neutrons and K_L in the beam; it is an amplification of the information outlined in earlier sections. We request 2.3×10^{18} protons, or 46 weeks of perfect beam time at 5×10^{12} protons per pulse in a 20 sec spill.

As stated earlier, we use the Malensek parameterization for K_L production; a comparison of the predicted spectrum to the E731 spectrum is given in Fig. 10;[24] the normalization is good to 20%. For neutrons, we use data from the ISR,[25] and for Λ^0 production we use a parameterization from the Fermilab hyperon experiments.[26] Figs. 11-14 show flux maps for neutrons, Λ^0, produced K_L and decaying K_L, into bins of 0.5 x 0.5 mr. The advantage of large targeting angle in the n/K ratio is clear: the neutron flux drops by two orders-of-magnitude from 0 to 5 mr while the K_L flux decreases by only a factor of two. However, choosing a large targeting angle has disadvantages as well: the K_L are at lower energy and (1) the hadron and lepton are produced at larger opening angle in the lab frame and have a lower geometric acceptance, and (2) the neutrinos are at lower energy and therefore have a smaller cross-section. We have chosen what we consider to be a reasonable compromise between n/K_L ratio and rate: we have tried to guarantee that rates per wire are under 1 MHz and the space charge for the hottest wire is under $10^3/\text{mm}^2/\text{sec}$, and moved to as small a targeting angle as possible consistent with these constraints.

[24] M. Woods, op. cit.
[25] J. Engler et al., Nucl Phys B84:70, 1985
[26] L. Pondrom, Phys. Rep. 122, 1985

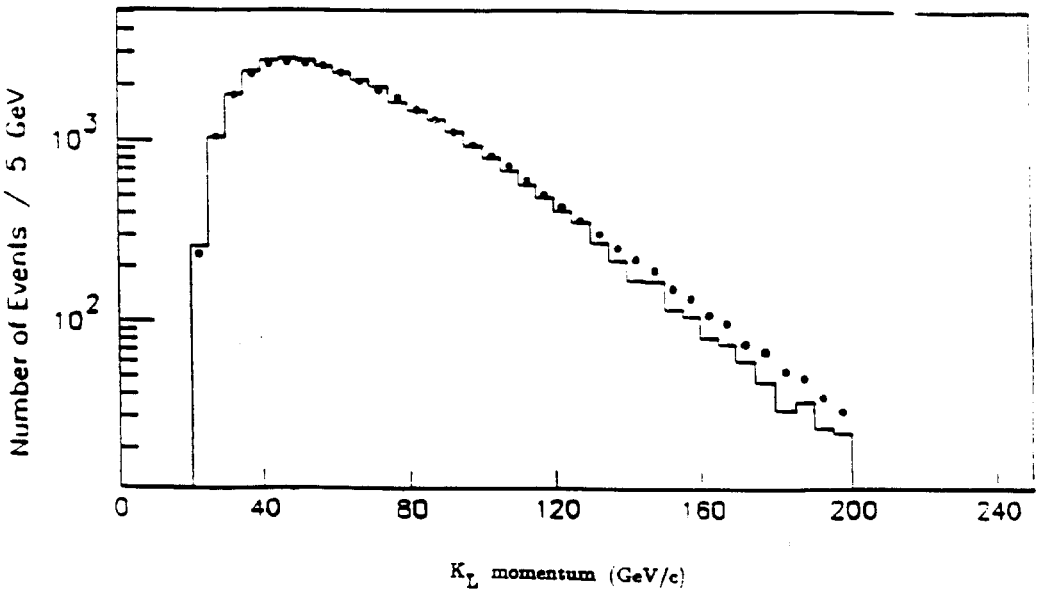

Fig. 10. A comparison of the observed K_L spectrum in E731 to that predicted by Malensek. The targeting angle for the E731 data was 5 mr, approximately in the center of our targeting. The normalization is checked to 20%; the agreement in shape is excellent.

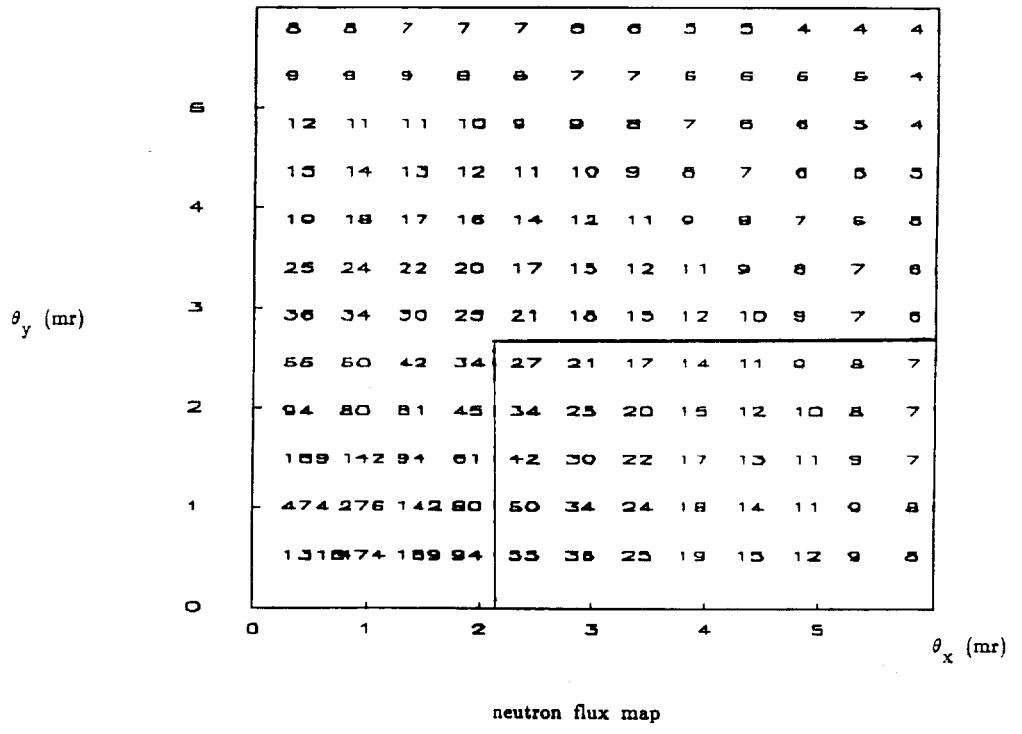

Fig. 11. A flux map for neutrons. The bin size is 0.5 x 0.5 mr, and the normalization is $10^8/5$ x 10^{12} protons. The upper half of the beam is shown. The preferred targeting is symmetric about the horizontal axis. The portion of the beam used is enclosed in the box.

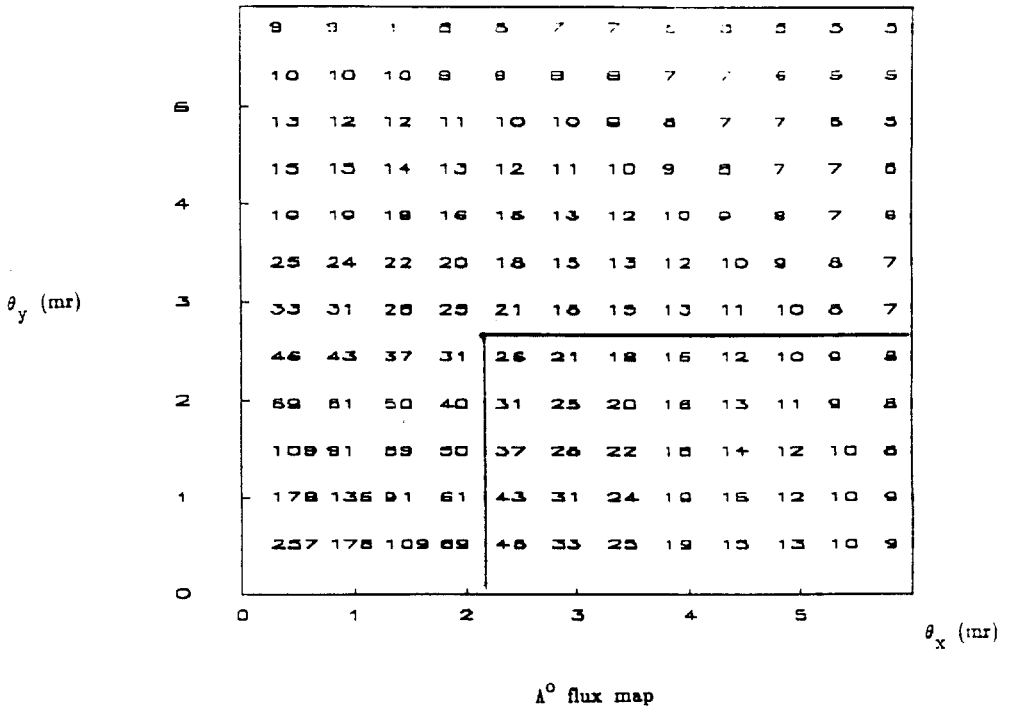

Fig. 12. A flux map for Λ^0, otherwise the same as Fig. 10.

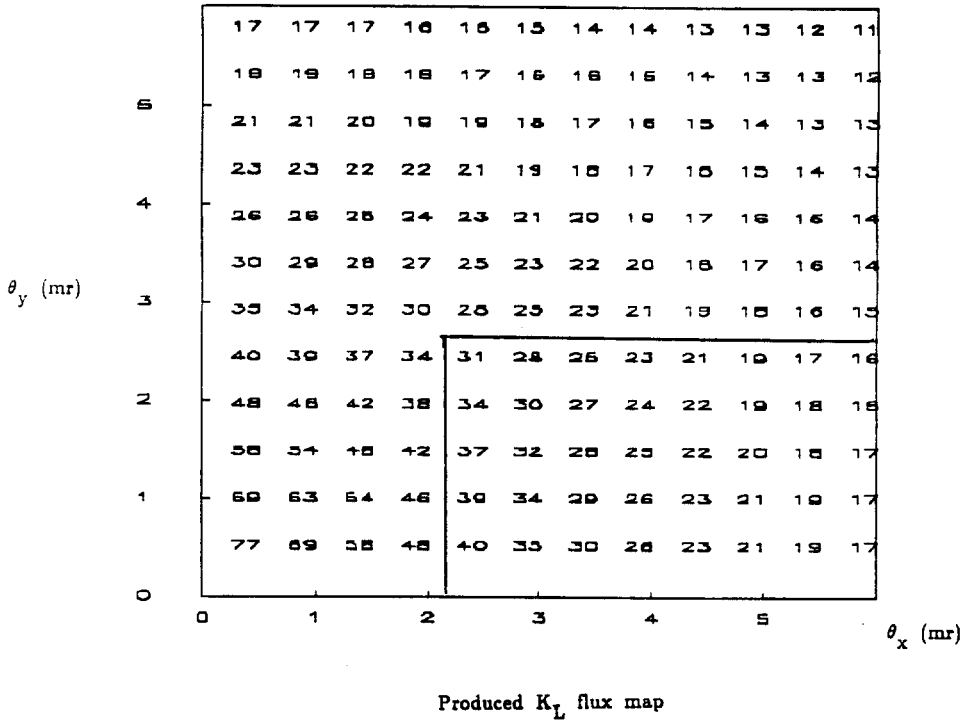

Fig. 13. A flux map for produced K_L, otherwise the same as Fig. 10.

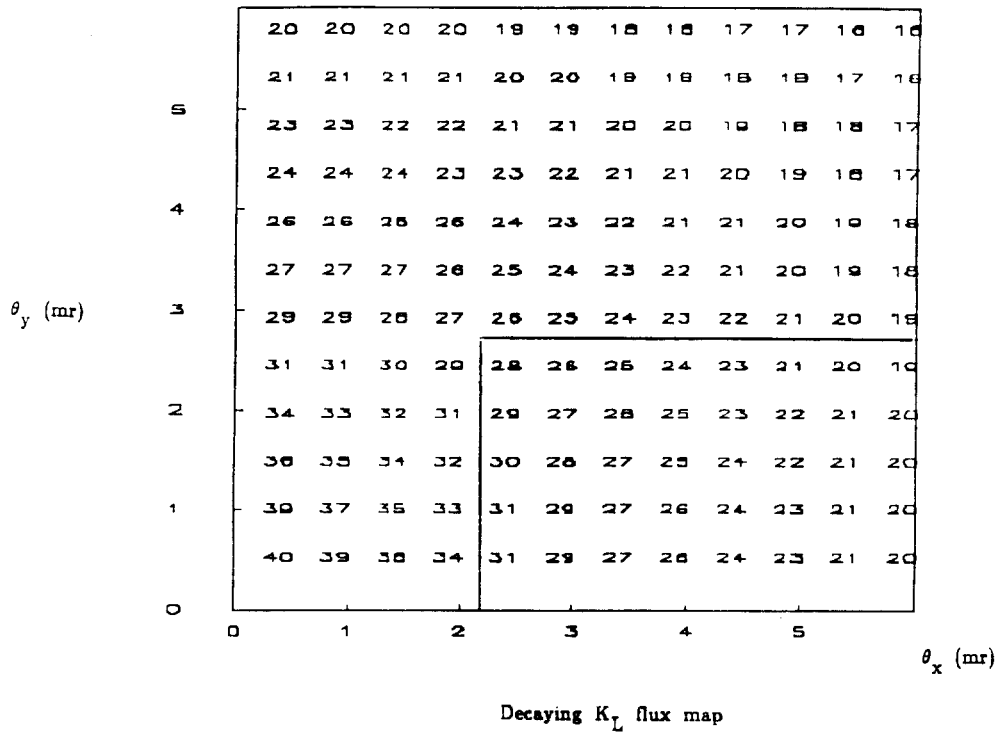

Fig. 14. A flux map for decaying K_L, with a normalization $10^6/5$ x 10^{12} protons.

The final chosen angle is -2 to +2 mr in θ_y and +2 to +6 mr in θ_x. We would like up to 2mr variability in θ_y to allow for errors in our estimates. We have placed 30 in. of Be and $10X_o$ of Pb in the beam to further moderate the n/K_L ratio and absorb photons in the beam; both these moderators will be variable to adjust to real conditions, but the rates are approximately correct and the choice of moderators and their lengths are consistent with previous choices in the M Center line. We then find, using our flux tables, 1.25×10^{10} neutrons, a similar 1.25×10^{10} K_L, and 1.5×10^9 decaying K_L per spill. The mean K_L energy is 70 GeV/c, with a spectrum similiar to that of Fig. 11. The ν energy spectrum, weighted for cross-section, is shown in Fig. 15.

We use the flux of K_L into each unit of solid angle, with the correct momentum spectrum

for that angle, to calculate a geometric acceptance of 14.8% for the tagger/neutrino detector pair (a hole for passage of the neutral beam would reduce this number by an order-of-magnitude). The mean neutrino energy is 47 GeV/c, and the probability of interaction in the CCFR detector is 2×10^{-11}/GeV. With the resultant spectrum of neutrinos and with standard CCFR fiducial cuts ($p_\mu > 9$ GeV/c at the vertex, and geometric acceptance), we have calculated an acceptance of 0.8 for muons from charged current ν_μ interactions. The lower energy muons from τ decay, from the chain $\nu_\tau N \rightarrow \tau X$, $\tau \rightarrow \mu\nu\nu$, have an acceptance of 0.67. Our total sample before cuts is then:

$$
\begin{aligned}
\#(\nu + \bar{\nu}) \; = \; & \\
& (1.5 \times 10^9 \; K_L/\text{spill}) \times \\
& (.148 \text{ acceptance}) \times \\
& (0.8 \text{ CCFR acceptance}) \times \\
& (47 \text{ GeV} \times 2 \times 10^{-11}/\text{GeV}) \times \\
& [0.39 \; BR(K_L \rightarrow \pi e \nu_e) \text{ or } 0.27 \; BR(K_L \rightarrow \pi \mu \nu_\mu)] \times \\
& 4.6 \times 10^5 \text{ spills} \\
\\
= \; & 30,000(\nu_e + \bar{\nu}_e)
\end{aligned}
$$

and

$$
= \; 20,800(\nu_\mu + \bar{\nu}_\mu)
$$

The application of cuts to eliminate background will be covered in the next section. The cross-section sample will be cut by only 20% but the $\nu_e \rightarrow \nu_\tau$ oscillation sample will be cut

in half.

The Λ^o flux is a potential problem, both from extra rate in the spectrometer and the decay chain $\Lambda \rightarrow p\pi^-$, $\pi \rightarrow \mu\nu_\mu$ where the ν_μ hits the neutrino detector. We have simulated the Λ^0 spectrum and determined that within our targeting region there are approximately 10 Λ^0 produced per bucket with a mean lifetime of 70-80 cm. The decay products can then be easily swept out of the beam. The background contribution of the ν_μ from the above decay chain with *no* sweeping and standard cuts (fiducial volume and $E_\nu > 30$ GeV) is $1/10^6$ events and is hence negligible. There are two Λ^0 rare decay modes which must be considered as well: $\Lambda^0 \rightarrow \pi e \nu_e (\mathrm{BR} = 8.3 \times 10^{-4})$ and $\Lambda^0 \rightarrow \pi\mu\nu_\mu$ ($\mathrm{BR} = 1.57 \times 10^{-4}$). The first decay, into ν_e, will not contribute background to the oscillation searches but only to the cross-section studies. The contribution to the cross-section after acceptance cuts will be under 10^{-5} of the signal. The second, which produces ν_μ, is a potential background. After acceptance and reconstruction cuts the background is at a similar, negligible level.

Similarly, production of π/K and background contribution from their decays are small. K_S decay has been modeled as well, and *before* sweeping, contributes 1 background event from $K_S \rightarrow \pi^+\pi^-$, $\pi \rightarrow \mu\nu_\mu$. However, 99% of the K_S decay in the first 50 meters and after sweeping we expect no background from K_S.

Finally, we consider "bare-target" production: production of charged π, K and their decays into $\mu\nu$. The neutrino trigger will require $E_\nu > 20$ GeV: for this energy, the π lifetime is 1.12 km and the K lifetime is 150 m. With enough sweeping to dump 900 GeV primary protons in the first ten meters, we do not expect a significant bare-target background, since higher-energy (longer-lived) particles will have progressively less chance to decay. A TURTLE simulation to systematically calculate the rates will be performed as part of a

detailed beam-line design.

IV. Triggering

The experiment will trigger on total energy deposit in the neutrino detector. Our data sample for simulations was cut at 30 GeV; we propose to have an E_H (hadronic energy) trigger of at least 20 GeV in the scintillation counters in coincidence with the RF. Cosmic ray air showers will dominate the trigger rate and from CCFR data with an E_H cut of 20 GeV we expect a trigger rate of 1-2 Hz.

We can generate an RF signal with scintillators near the target: they will see the beam bunches and we can then generate an RF signal which will be sent to the tagger and the neutrino detector. The trigger will then demand that the E_H trigger be in time with the upstream scintillator. The tagger, unlike the neutrino detector, will not be used in the trigger: the tagger readout will only encode the time of an interaction for each active channel of the spectrometer. In the 500-750 nsec that it will take for the neutrino to travel from the tagger to the neutrino detector, for the electronics to make a trigger decision, and then send a trigger back to the tagger, any channel will have less than 1.0 hit on average (since the rate per wire is only 0.5 MHz in the worst case). Each readout channel could store the time and location of any hits with a memory 1 μsec deep; fewer than 7500 hits would then need to be processed (at the highest rate of 0.5 MHz, in 1 μsec, half the wires would be hit). We could conceivably put mean-timing circuits on pairs of adjacent wires to only accept hits in time with the neutrino interaction, along with any unpaired hits, to reduce the amount of data to be processed.

V. Backgrounds and Systematic Errors

In this section we will discuss the backgrounds to the oscillation signals. First, we cover the physics of the sources; second, we will describe the reconstruction algorithm, and third, use the algorithm and predicted resolutions to set cuts and determine the contaminations. We conclude with a discussion of the systematics and backgrounds for the $\nu_\mu \rightarrow \bar{\nu}_\mu$ search and the cross-section sample.

A potentially serious background in $\nu_e \rightarrow \nu_\mu$ or $\nu_e \rightarrow \nu_\tau$ searches arises from mistags, depicted in Fig. 16. A mistag can occur whenever a Ke_3 and a $K\mu_3$ decay occur within the time resolution of the system; with 10 nsec time resolution, we only accept decays within the same RF bucket. Then if the $(\pi\mu)$ pair escapes detection and the (πe) pair is accepted, but the ν_μ interacts, we will have an oscillation signal. This background may be simulated in a straightforward way: generate Ke_3 and $K\mu_3$ decay pairs, look for the proper pattern, and then apply the reconstruction algorithm to accept or reject the event. The case in which all the tracks enter and the neutrino is associated with the incorrect (π-lepton) pair provides a negligible contribution and we ignore it.

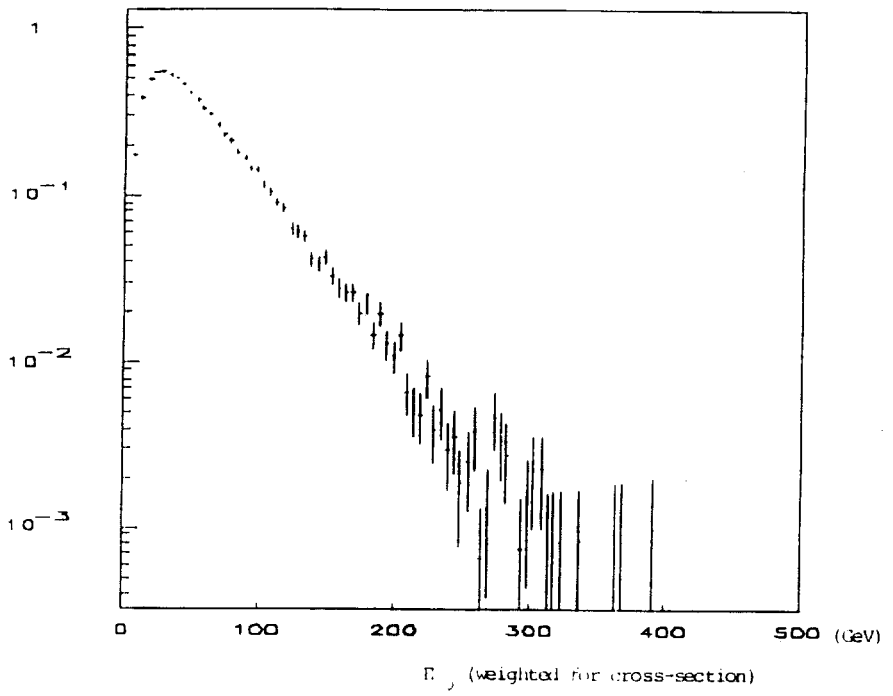

Fig. 15. The spectrum of ν incident on the detector, weighted for the energy dependence of the cross-section.

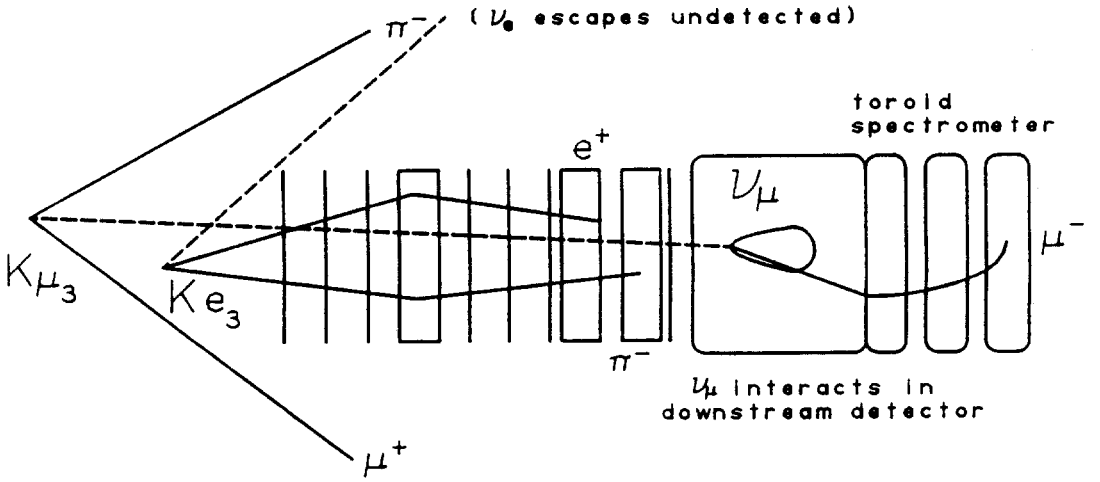

Fig. 16. A schematic of a mistag. A Ke_3 and a $K\mu_3$ decay occur simultaneously. The ν_μ from the $K\mu_3$ interacts, the ν_e escapes or does not interact in the neutrino detector. With the (πe) pair tagged as shown, the combination appears to be an oscillation.

The rejection factor has two terms: the first comes from the probability of two or more decays occurring in the same bucket. This is a straightforward calculation in Poisson statistics: at our rate of 1.5 K_L decays/bucket we find 8.4% for the overlap where both the electron from Ke_3 and the muon from $K\mu_3$ have the same charge. If they do not have the same charge, the "coincidence" with the neutrino detector will not be appear to be an oscillation.[27] The second, larger rejection, comes from the reconstruction of the K_L, which we now examine in detail.

The dipole spectrometer will reconstruct the momentum vectors of the pion and lepton. We then project the tracks back to a common vertex and determine a three-dimensional decay point for the K_L. The chambers are assumed to have a gaussian 250μ position resolution and we assume gaussian multiple coulomb scattering in the vacuum window (1% rl). The resultant deviations in the decay vertex are shown in Fig. 18 and Fig. 19; the first plot is the error in the x- or y- transverse position and the second shows the error in reconstructed position along the beamline. We then take the position of the target and draw a line from it to the decay vertex. This line provides the initial direction of the K_L.

[27]Except for a special case: Let us posit a $(\pi\mu^+)$ pair which escapes, a (πe^-) in the tagger, and a $\nu\mu$ neutral-current interaction in the neutrino detector which then produces an "opposite-sign" dimuon from charm decay. This background is suppressed by 1/3 for the neutral current cross-section and a factor of 400 for the "opposite-sign" rate *before* reconstruction and timing cuts.

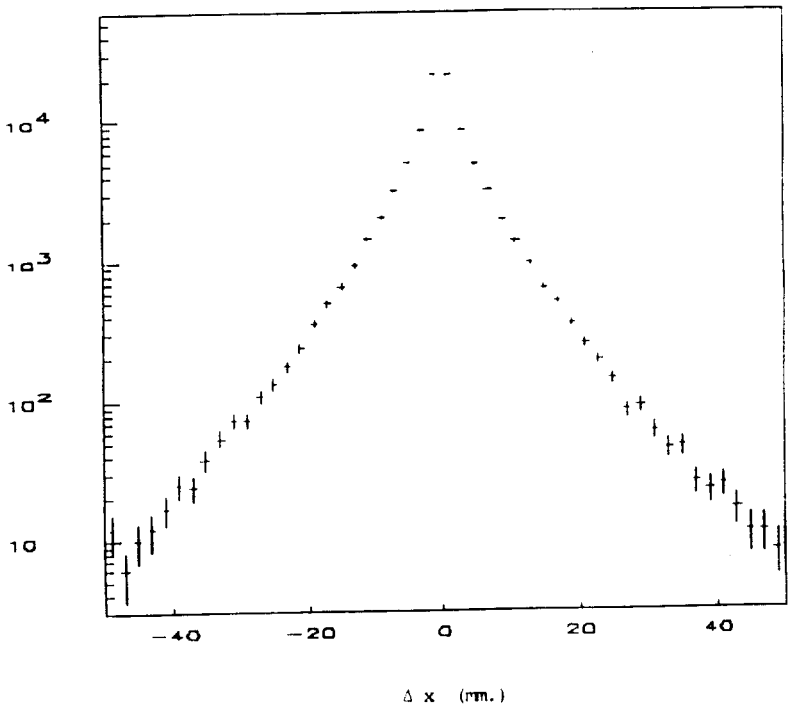

Fig. 17. The difference in the x-coordinate of the reconstructed vertex from the true value. The distance is given in mm.

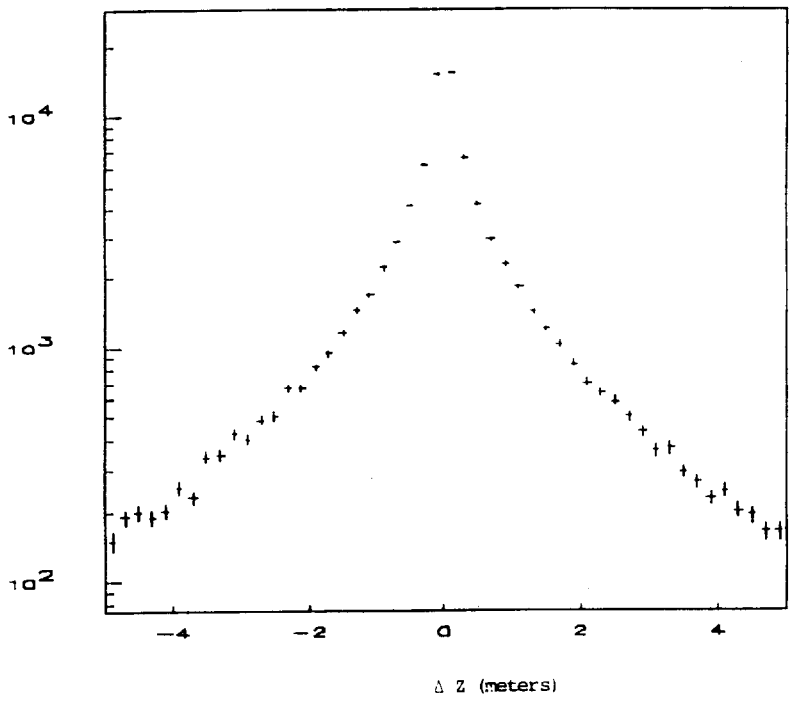

Fig. 18. The difference in the z-coordinate of the reconstruted vertex from the true value. The distance is given in meters.

At this point we have the momenta and trajectories of two of the daughter particles (but not the neutrino) and the initial trajectory of the K_L. We do *not* have the momentum of the K_L since that would require knowledge of the neutrino momentum vector. We may now reconstruct the K_L up to a two-fold ambiguity in its energy. Fig. 19 shows the difference of the two solutions divided by their sum; we see the difference is normally quite small but extends to large values. Taking each solution in turn allows us to predict two possible momentum vectors for the neutrino: two pairs of neutrino energy and transverse impact point in the neutrino detector. We then *compare* each pair to the measured values. Fig. 20 shows the smaller difference in transverse position $[\Delta r = (\Delta x^2 + \Delta y^2)^{\frac{1}{2}}]$ for each of the two pairs (the neutrino detector has a vertex resolution of 1.3 cm. for each of x,y). Having made this choice, we then plot the energy resolution $\Delta E_\nu / E_\nu = (E_{\nu,\ \text{measured}} - E_{\nu,\ \text{predicted}})/E_{\nu,\ \text{predicted}}$ (the energy resolution of the neutrino detector is given by $\Delta E/E = 0.89/\sqrt{E}$ for the hadronic shower and $\delta p_\mu / p_\mu = 0.11$) in Fig. 21. We see the position determination is reasonable but the energy resolution does not provide as stringent a test, largely because of the poor energy resolution of the neutrino detector.

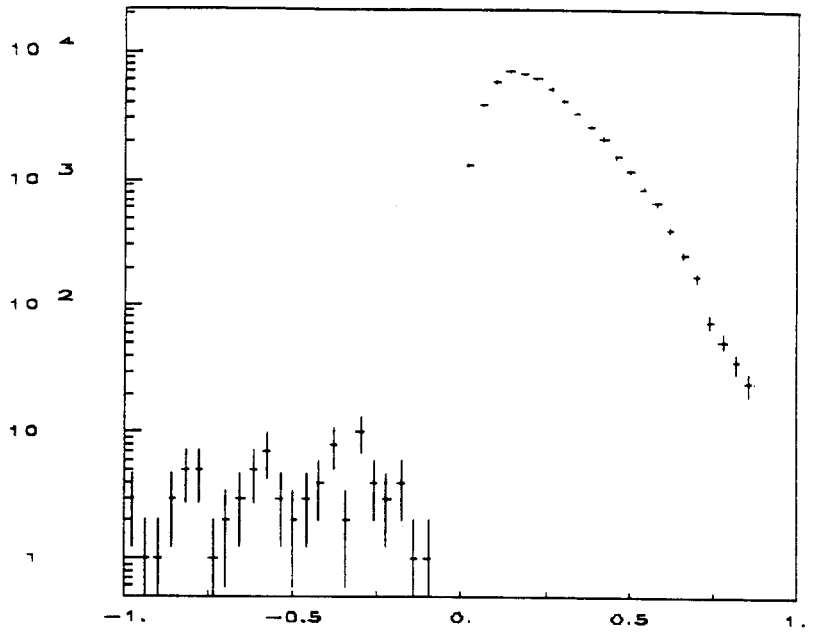

Fig. 19. The value of the K_L momentum is determined up to a two-fold ambiguity. Here we plot $(p_1 - p_2)/(p_1 + p_2)$; for physical events, we have chosen $p_1 > p_2$. The negative tail arises from resolution smearing.

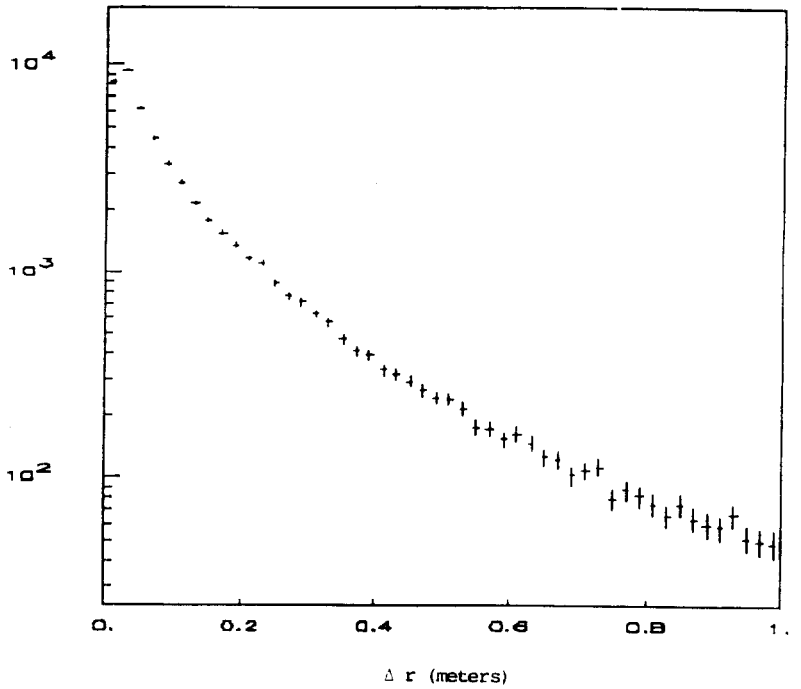

Fig. 20. The difference in distance from the reconstructed impact point in the neutrino detector to that predicted from the tagger. The distance is given in meters.

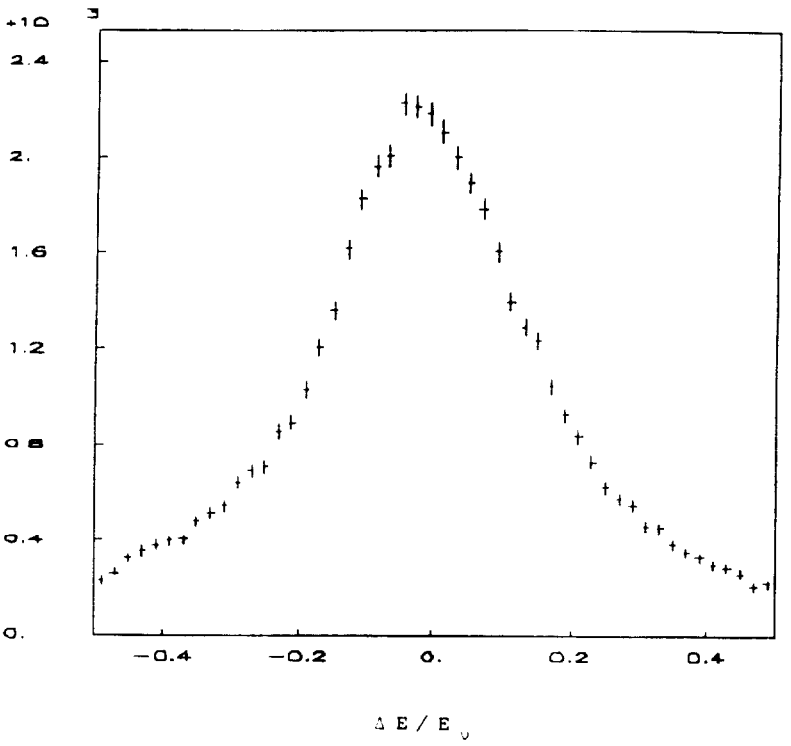

Fig. 21. The difference in neutrino energy predicted from the tagger from the measured value, divided by the predicted value.

There is an additional problem with the energy determination which we suspect makes it unusable for background rejection in the $\nu_e \rightarrow \nu_\tau$ search. There is normally approximately 5-10% "missing energy" - energy which escapes detection largely in the form of neutrinos created in the shower. The CCFR group has measured this in the Lab E detector and we could certainly apply a correction, which would be adequate for $\nu_e \rightarrow \nu_\mu$ and $\nu_\mu \rightarrow \bar{\nu}_\mu$ studies. However, for the $\nu_e \rightarrow \nu_\tau$ search, there are two missing neutrinos from $\tau \rightarrow \mu\nu\nu$. This will smear the energy resolution so as to be largely unusable (certainly we could cut on the visible energy being much *larger* than the predicted energy, and we will probably eventually use that). In order to avoid the resultant problems and complexities, for the $\nu_e \rightarrow \nu_\tau$ oscillation studies we will quote results using *only* the transverse agreement.

We see a long tail in the position resolution plot which extends to surprisingly large values

of Δr. The source of this tail is the ambiguity in the K_L reconstruction and arises from a mismeasurement of the initial K_L direction. The error occurs predominantly for decays at small distances from the target. If the vertex resolution (which worsens as the decay moves upstream) is large compared to the beam size, the initial K_L direction will have large errors and hence the reconstruction will be wrong. A second contribution comes from the finite target size, and again is worse for decays far upstream. This error in reconstruction is the reason we must lose approximately half the data in order to reduce the background to less than an event.

We first describe the background calculation for the $\nu_e \rightarrow \nu_\tau$ search. We may compare the plots of Δr for the correct Ke_3 pair to randomly generated $K\mu_3$ decays, both of which populate the neutrino detector evenly. We require Δr <15 cm. and find 0.3 background events after all cuts (acceptance, reconstruction, and timing; in addition we have placed a cut on the p_T of the μ with respect to the hadron shower direction, which will be discussed later and assumed 0.9 electron efficiency in the particle identifier). The $(\nu_e + \bar{\nu}_e)$ sample is reduced to 16K from 30K. The rejection factors break down as follows:

I.	Poisson statistics	
	@ 1.5 K_L decays/bucket	0.084
II.	Probability of $(\pi\mu)$ escaping,	
	ν_μ hitting	4.0×10^{-2}
III.	Probability of (πe)	
	acceptance in tagger	0.23
IV.	Probability that (πe)	
	matches ν_μ	4.2×10^{-3}

A final suppression arises because the ν_μ accepted in II. above have a mean energy of 27 GeV (the true matches have an mean E_ν of 47 GeV). We then calculate the number of background events exactly as we calculated the number of signal events at the end of section III. A more refined calculation is probably unjustified: for example, we have not simulated non-gaussian tails in the resolutions. However, the background is clearly small and the answer is approximately correct. We expect to measure the real resolutions from the data and only then will be we able to estimate the mistagged background more accurately.

The second source of background for $\nu_e \rightarrow \nu_\tau$ is the "same-sign" dimuon signal shown in Fig. 24. This occurs when a ν_e interacts and is correctly tagged, but a muon exits from the hadronic shower and survives the acceptance cuts in the neutrino detector. If the muon has the same charge as the muon expected at the vertex, then the event will pass the "charge-matching" requirement and appear to be an oscillation. This background is iden-

tical to the background in the "same-sign" dimuon search of E616 and E744/E770 and has been extensively studied in those experiments.[28] The overall scale is easily calculated: E744 observed approximately 115 same-sign dimuons with $p_\mu > 9$ GeV/c in a fiducial sample of 780K charged-current ν_μ events. We then expect 1.47 x 10^{-4} events with $p_\mu > 9$ GeV/c per charged-current neutrino interaction (neutral current ν_e interactions, which look the same topologically, will contribute another 1.2 events), or 3.5 events in our 16K sample. We may then apply kinematic cuts (for example, on the p_T of the muon with respect to the hadronic shower) and reduce this background by an order-of-magnitude without significant loss in the oscillation sample. We have used the CCFR Monte Carlo to calculate the measured p_T distribution for shower muons and for muons from τ decay: the distribution in p_T is shown in Fig. 25. With a cut on p_T of 1.0 GeV/c we find an order-of-magnitude loss in the background with a 15% loss in signal (the cut had been included in the 16K estimate).[29]

[28]B.A. Schumm et al., Phys. Rev. Lett. 60(1988), 1618. For more detail see B. A. Schumm, Like Sign Dimuon Production in High Energy Neutrino Interactions, PhD Thesis, University of Chicago (1988) unpublished.

[29]These cuts were not used by E744/E770; the distributions of p_T and other variables were compared to the simulations of π/K decay in the shower. Since the source of any dimuon excess was unknown, placing cuts could accidentally eliminate the signal and it was therefore safer to examine the entire distribution compared to the π/K background. In addition, the Lab E drift chambers were fitted with FADC's for E770 so that the energy flow of the hadronic shower can be accurately measured. We expect to use them in applying p_T cuts to eliminate the shower background; for this study, we have used the old analysis without the FADC's and will undoubtedly have greater background rejection with them.

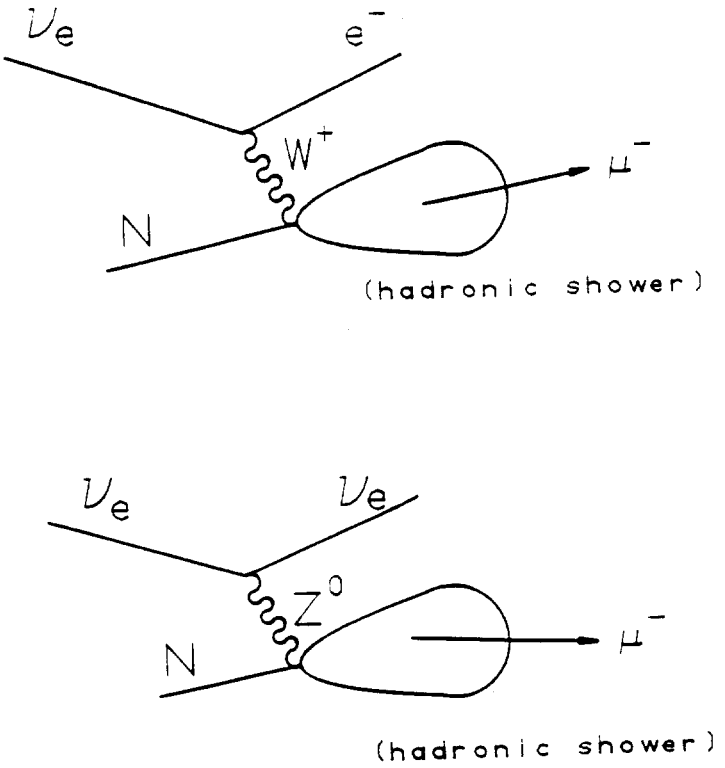

Fig. 22. The source of "same-sign" dimuons. A muon is produced in the hadronic shower. For ν_e, we cannot separate charged-current from neutral-current events and hence both diagrams contribute.

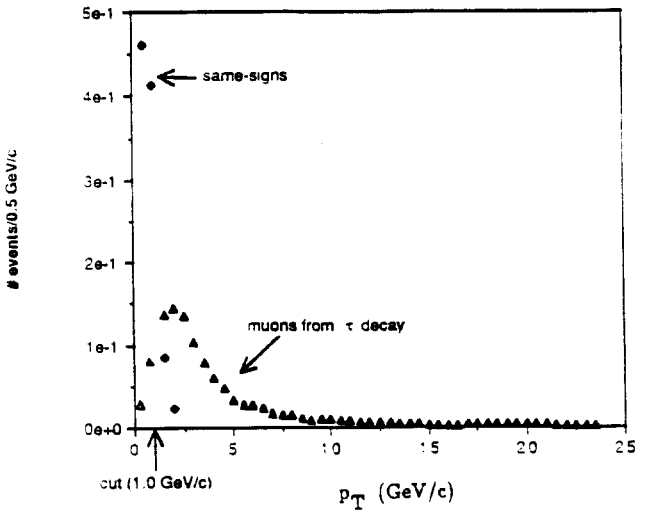

Fig. 23. The p_T of the muon with respect to the hadron shower. The sources are as shown: one from "same-sign" production, and the other from the final muon in $\nu_\tau N \to \tau X$, $\tau \to \mu\nu\nu$. The samples have been normalized to 1 event. The cut was placed at 1 GeV/c in the simulation.

The $\nu_\mu \rightarrow \bar{\nu}_\mu$ sample has, as explained earlier, a background from "opposite-sign" dimuon production. We estimate less than an event from the charged-current sample from the p_μ cuts described there. The neutral current background ($\nu_\mu N \rightarrow \nu_\mu X$) still remains, but the measured neutrino energy will be smaller than the predicted value because of the missing outgoing neutrino. The distribution of $\Delta E_\nu / E_\nu$ (tagger-to-neutrino-detector) can then be used; we cut on missing energy of >25% and lose 1/3 of the sample but eliminate this background.

Finally, we can think of no significant background in the cross-section determinations. The cross-section will be calculated by forming a ratio proportional to the cross-section:

$$R_\nu = \text{(observed } \nu \text{ with a tag)} \\ \text{/(random prescaled sample from the tagger)}$$

The dominant systematic error will be the error in predicting whether the neutrino will strike the detector for events in the denominator. By cutting away from the edges of the neutrino detector, we can increase the acceptance to 90% and are confident the systematic error on the acceptance will be 1% or less. We expect the final cross-section sample to be 25K for ν_e and 16K for ν_μ. In each, 2/3 will be neutrino and 1/3 antineutrino (from the relative neutrino/antineutrino cross-section) so the statistical errors will always be under 2%.

VI. Schedule

We are currently negotiating with other experimental groups and expect that the requisite

manpower will exist by Spring, 1989. Construction could begin in 1990 with a first run in 1991 which will "shake-down" the detector and provide our first data sample. The following fixed target run would provide our main sample. The experiment would then complete data-taking in approximately 1994.

VII. Long Term K_L Studies

The beam as planned could provide more than 10^{14} K_L per year. This is four to five orders of magnitude more K_L than have been seen in the best rare K_L decay experiments at Brookhaven. Triggering in such an environment is extremely difficult; furthermore, the detector is probably not optimized for the delicate background rejection required. However, with a lower rate and a better-defined decay region, we could think about a rare K_L decay search at the 10^{-13} level. We are discussing the long-term possibilities with the "Future of Kaon Physics" committee at Fermilab (B. Winstein, chair).

VIII. Summary

We have demonstrated the physics potential of the tagged neutrino line to significantly extend the $\nu_e \rightarrow \nu_\mu$ and $\nu_\mu \rightarrow \bar{\nu}_\mu$ limits, probe an important region of mixing in $\nu_e \rightarrow \nu_\tau$, and perform precision measurements of the ν_e and ν_μ cross-sections at the 1-2% level. The calculated fluxes are based on extensive experience at FNAL. The design of the tagging spectrometer, although obviously preliminary, is within standard practice. In two fixed target runs we can explore new neutrino oscillation physics and provide benchmark cross-section measurements that are perhaps uniquely accessible with tagged neutrinos.